Numerical studies of the critical behaviour of non-commutative field theories

Martin Petrov Vachovski
NUI Maynooth

October, 2013

Dissertation submitted to
The Department of Mathematical Physics, NUI Maynooth,
Head of the department Professor Danny Heffernan,
for the degree of Doctor of Philosophy
The research was conducted in Dublin Institute for Advanced Studies
under the supervision of Professor Denjoe O'Connor and Doctor Brian Dolan

Contents

Abstract

We study the critical behaviour of matrix models with built-in $SU(2)$ geometry by using Hybrid Monte Carlo (HMC) techniques.

The first system under study is a matrix regularization of the ϕ^4 theory defined on the sphere. We develop a HMC algorithm together with an $SU(2)$ gauge-fixing procedure in order to study the model. We extract the phase diagram of the model and give an estimation for the triple point for a system constructed of matrices of size $N = 7$. Our numerical results also suggest the existence of *stripe phases*- phases in which modes with higher momentum l have non-negligible contribution.

The second system under study is a matrix model realized via competing Yang-Mills and Myers terms. In its low-temperature phase the system has geometrical phase with $SO(3)$ symmetry: the ground state is represented by the $su(2)$ generators. This geometry disappears in the high-temperature phase the system. Our results suggest that there are three main types of fluctuations in the system close to the transition: fluctuations of the fuzzy sphere, fluctuations which drive the system between the two phases, and fluctuations of the high-temperature regime. The fluctuations of the fuzzy sphere show the properties of a second order phase transition. We establish the validity of the finite size scaling ansatz in that regime. The fluctuations which bring the system between the phases show the properties of a first order transition.

In the Appendix we provide in some detail the idea behind the HMC approach. We give some practical guidelines if one is to implement such an algorithm to study matrix models. We comment on the main sources for the phenomenon of *autocorrelation time*. As a final topic we present the basics of the *OpenCL* language which we used to port some of our algorithms for parallel computing architectures such as *GPU*'s.

Acknowledgements

First I would like to thank my supervisors Professor Denjoe O'Connor and Doctor Brian Dolan. The discussions with them were always helpful and inspiring. They were always patient and open to my opinion. They really helped my enthusiasm about non-commutative field theories. Also I would like to thank Xavier Martin for the interesting discussions and ideas.

The support my family gave me during the past four years was very important to me. Many thanks to my mother Reneta, my sister Tsvetelina, and my father Peter. Thanks for the support to my grandmother Tsvetanka, my aunt Maya, my cousin Velina, my uncle Ivo. Thanks for my family on my father's side: uncle Atanas, aunt Ginka, and my cousins Dimitar and Borislav.

My experience in Dublin would not have been the same without my fellow students and colleagues. I hope I've changed their stay in Dublin for better too. The order of appearance in the list is irrelevant: Thomas Kaltenbrunner, Matthew Agius, Andrew Schaeffer, Florian Le Pap, Anna Matheson, Marcin Kalecki, Olaf Smits, Nathalie Hinatea, Carlo Romoli, Rachael Ainsworth, Ruyman Azzollini, Alin Elena, Elisa Archilei, Andrea Licciardi, Veselin Filev, Joan Campanya, Duygu Kiyan, Sara Sihelnik, Grainne Costigan, and Lisa Fallon.

I would like to thank all my friends back in Bulgaria who stayed in touch with me the whole time. These include: Svetla Tsvetkova, Neno Todorov, Filip Dimitrov, Tsvetan Vasilev, Plamen Tanov, Emil Popov, Todor Petkov, Angelina Rimpova, Nikolai Penkov, Grisha Badhzakov, Galin Valchev, and Milena Ivanova.

As a final I would like to thank the staff in Dublin Institute for Advanced Studies for their help and hospitality.

Declaration

I declare that the material presented in this dissertation is a result of my own work under the supervision of Denjoe O'Connor[1] and Brian Dolan[2]. References to the best of my knowledge have been made for the source of the formulas and results which are not my own.

Martin Vachovski

[1]Dublin Institute For Advanced Studies, 10 Burlington Rd, Dublin 4, Ireland
[2]National University of Ireland Maynooth, Maynooth, Ireland

Chapter 1.

Introduction

Ever since the early days of quantum field theory (QFT) there have been problems associated with the ultra-violet (or short distance) divergences. Various strategies to overcome these problems have been devised. The most successful of which for practical purposes is the renormalization group approach. If a theory is re-normalizable (for example QED) then the divergences of the integrals can be absorbed into the parameters of the theory and the amplitude of the fields. This strategy produces numbers which are in very good agreement with the experiment. A physical picture that motivates the renormalization group approach by K. Wilson can be found in [83].

Almost parallel with the renormalization procedure approach there have been attempts to solve the problem of divergences on a fundamental level which involves the properties of the underlying space. There are plausible arguments that for distances smaller than a characteristic length the notion of point should not be well defined. This idea is borrowed from the original quantum mechanics where we have non-vanishing commutation relation between the coordinate and momentum operators (the usual Heisenberg uncertainty relation)

$$[x_i, p_j] = i\hbar\delta_{ij}. \tag{1.1}$$

The non-vanishing commutator between x and p implies that the phase space of the system does not have well defined points but rather cells with area $\propto \hbar$. Snyder [75] proposed that the same relations could be used on the coordinates of

a theory,

$$[x^\mu, x^\nu] = i\theta^{\mu\nu}, \tag{1.2}$$

where $\theta^{\mu\nu}$ is a real anti-symmetric matrix. That is one step further from the case of QM. In this setup we can not measure both coordinates of a particle simultaneously.[1] If we represent the coordinates in a theory with non-commuting objects according to (1.2) the configuration space of the theory does not possess points anymore, but only cells with area $\propto \theta_{ij}$. The spaces constructed that way are also known as *non-commutative Moyal spaces*. Another point of view on this idea is replacing the algebra of functions on the manifold (which is normally a infinite dimensional commutative) with a non-commutative but still infinite one.

Another class of non-commutative spaces are the *fuzzy spaces*. They are realized if we replace the infinite algebra on a given manifold by a finite algebra. As they are of special interest of us, we discuss their construction in more detail in §1.1.

In the context of this approach the question that naturally arises is what are the properties of the objects that replace the ones on the usual manifolds. To answer this an entirely new mathematical discipline, called *Non-commutative geometry*, was created as a generalization of differential geometry. Rigorous treatments of this subject is provided by [22, 52, 23]. A central problem in the theory of non-commutative geometry is the construction of non-commutative counterparts of already known spaces.

1.1. Fuzzy spaces

Following Connes [22] and Fröhlich and Krzysztof [36] a Riemann manifold $\mathcal{M}$ can be completely specified together with its geometry (or metric) by the so called

[1] In fact in QM in the presence of a magnetic field the commutator between two components of the momentum is non-zero which renders simultaneous measurement of its both components impossible.

spectral triple,

$$\{\mathcal{A}, \mathbb{H}, D\}. \tag{1.3}$$

In the above $\mathbb{H}$ is a Hilbert space of state vectors. $\mathcal{A}$ is the commutative algebra of smooth functions that are defined on $\mathcal{M}$. The algebra $\mathcal{A}$ can be used to recover the points of the manifold. And finally D is a bounded Dirac-type operator which can be used to determine the metric of $\mathcal{M}$. Instead of the Dirac operator one can use Laplace operator Δ. The difference is that the Dirac operator carries additional information about the spinor structure on the manifold.

One can use the above as a starting point for a construction of non-commutative (or fuzzy) manifold $\mathcal{M}_N$. The first step is to approximate the infinite-dimensional algebra $\mathcal{A}$ by some finite algebra $\mathcal{A}_N$. In this approximation we can not resolve each point on the manifold but only finite sets of patches on it, hence we get a fuzzy space. In order to keep the construction (1.3) consistent with the change of the algebra we need to find corresponding approximations for $\mathbb{H}$ and D as well. This way we arrive at a whole family of fuzzy approximations of $\mathcal{M}$

$$\{\mathcal{A}_N, \mathbb{H}_N, D_N\}. \tag{1.4}$$

This family is parametrized by the dimension of the algebra N and we expect in the formal limit $N \to \infty$ to be able to recover the initial smooth manifold $\mathcal{M}$. Very often $\mathcal{A}_N$ is implemented as a matrix algebra $\mathrm{Mat}_N(\mathbb{F})$ over some field $\mathbb{F}$. This gives us the possibility to translate many of the problems from non-commutative geometry to the language of matrix models. In the present work we would be mostly interested in fuzzy spaces realized via matrix algebras over $\mathbb{C}$. It is important that the dimension of $\mathbb{H}_N$ is such that it carries a faithful representation of D. If the $dim(\mathbb{H}_N)$ is too small then the only possible representation on D on $\mathbb{H}_N$ is the trivial one. That way the information about the geometry of the manifold which is encoded in D is lost. A typical example of this situation is the attempt to represent a manifold with $SU(3)$ isometry using $\mathrm{Mat}_2(\mathbb{C})$. The theory behind the construction of representations of matrix Lie algebras and their dimensions can be found in [38, 37, 40]. Another important and very restrictive requirement is that the space being approximated is compact.

The above program has been carried out successfully for numerous types of spaces. Without any claim for completeness here we mention some of the directions of research. The simplest non-trivial example of a fuzzy manifold, and perhaps one of the most celebrated, is the *fuzzy sphere* S_F^2[2] constructed by Madore [54]. In the literature also a deformed $su(2)$ fuzzy sphere [42] can be found. A supersymmetric version is described in [43]. In [30] a fuzzy S_F^1 has been constructed. The construction starts from S_F^2. Then the the non-circular modes are assigned to large eigenvalues. This effectively removes them from the spectrum. The construction of S_F^1 further makes it possible to construct *fuzzy tori*, by taking the product of different copies of S_F^1. General fuzzy S_F^N and $\mathbb{CP}_F^N$ have also been considered in [44, 1, 10, 59].

1.2. Matrix models and field theory

In parallel to the effort to construct fuzzy counterparts to known geometries, there has been work on constructing fuzzy versions of the known field theories. The formalism has been applied to a broad spectrum of physical problems. A comprehensive review that presents the applications can be found in [34]. In the literature there are constructions of ϕ^4 theory formulated on the fuzzy 4-sphere S_F^4 [84, 59, 58]. The limit $R \to \infty$ where R is the radius of the hyper-sphere corresponds to a scalar field theory on $4D$ flat space with *Euclidean* signature. Matrix models with Lorentz invariance have been considered in [7, 8]. In [28] a scalar field on a non-commutative black hole background have been studied. Every theory on a fuzzy space is inheritably *non-local* and therefore problems with *causality* are also to be expected. Besides scalar field theories, also gauge, and fermionic fields have been studied within the framework of matrix models and non-commutative geometry [20, 12, 77, 66, 58, 47].

A slightly different context where non-commutative spaces and matrix models arise comes from *string theory* and *quantum gravity* [27, 55]. As we mentioned earlier any theory of quantum gravity predicts that at small scales the notion of points disappears and non-locality is to be expected. This is consistent with the

[2] We will describe the fuzzy sphere in more detail in the chapters to follow since this fuzzy space is central to this work.

the picture in string theory where non-locality appears due to the finite length of the strings or with certain theories of quantum gravity. Moreover in the literature there are known examples where string theories can be reformulated in the language of matrix models as their low energy limits [4]. Perhaps the most prominent example is the *Ishibasi, Kawai, Kitazawa, Tsuchiya (IKKT)* Model [67, 2, 49]. The possibility of a matrix formulation of string theories allows one to easily apply non-perturbative methods such as *Monte Carlo* techniques to study string theory. One area which has more contact with the experiment where the language of matrix models and non-commutative geometry are used is the *fractional quantum Hall effect* [71, 62, 19].

The above applications of matrix models in the studies of field theories makes the framework an interesting alternative to lattice QFT when it comes to field theory regularization. The main focus of this work will be on the aspects of numerical studies of matrix approximations to field theories.

1.3. Lattice vs. matrix regularization

Without any doubt lattice QFT is the most widely used method when it comes to numerical studies of field theories. As we mentioned before matrix regularization can be seen as an alternative approach. Here we note some of the crucial differences between the two regularization procedures.

1.3.1. Lattice regularization

We start with a few remarks on the lattice approach. In this context the underlying manifold of the theory is represented by a set of points Λ, most often a hypercube of dimension D and size L of the form

$$\Lambda = a\mathbb{Z}^D = \{x | x_\mu / a \in \mathbb{Z}^D\}. \tag{1.5}$$

The number of degrees of freedom of the theory is in the order of $N_d \sim (L/a)^D$. Usually the time direction of the theory has been subject to *Wick-rotation* so the signature of Λ is Euclidean. One should take care of the boundary conditions

for the field. Possible choices are *periodic*, *anti-periodic* and *free*. Each of them has its advantage in certain situations. The theory is still divergent at the naive $a \to 0$ limit. But some continuum limit properties of the system can be extracted from a second order phase transition. Continuous symmetries and the topological features of theory on a lattice are not preserved for a finite a. In particular this causes the famous *fermion doubling* problem when one considers theories with fermions.

1.3.2. Matrix regularization

On the other hand, the regularization via matrix models is done by replacing the algebra of the functions $\mathcal{A}$ with $\mathcal{A}_N$ according to the scheme described in §1.1. The number of degrees of freedom of the theory is usually a multiple of the dimension of $\mathcal{A}_N$ as a vector space. When we have the matrix algebra $Mat_N(\mathbb{C})$ which represents a single complex scalar field it is $N_d = 2N^2$. Of course the difference in numbers of the degrees of freedom between the lattice and matrix regularization is deceiving. If we want to describe the field ϕ in D dimensions on a lattice and as a matrix model with the same detail, we usually need to provide the same number of degrees of freedom in both cases, which means that we need to increase the size of the matrices accordingly.

The notion of *non-commutative time* is still poorly understood. Non- commutative time leads inevitably to problems related to causality. One way to work with time-dependent matrix actions is to treat the time direction as in the lattice case [57]. The issue of the boundary conditions is more complicated in this case. The boundary of the system is not defined simply as the outermost elements of the matrices due to the non-local interaction terms.

The naive limit $N \to \infty$ does not always work. The reason is the so called *UV-IR* mixing which is a feature specific to non-commutative field theories. The phenomenon of UV-IR mixing is responsible for low momentum singularities at high energies. Therefore even in the $N \to \infty$ limit some matrix models show features that are not present in the original theories. See for example [59, 39]. The solutions to this problem are non-trivial and model-dependent as demonstrated in [31, 32]. There the diagrams which are responsible for UV-IR mixing are

identified and removed by hand by the so called *normal ordering*. Perhaps the most important advantage of the matrix regularization is that by construction it preserves the topological features and the symmetries of the initial theory exactly. As another important result we point out the construction of a Dirac operator which preserves chiral symmetry while avoiding the fermion doubling [12, 11].

1.4. Outline

The goal of the present work is to study in detail some aspects of numerical simulations of matrix models and non-commutative geometry. We demonstrate in detail the explicit implementation of the simulations. The thesis can be used as a guide for people with interest in writing their first Hybrid Monte Carlo simulation of matrix models and/or lattice QFT. The structure the present work is as follows.

In §2 we give the construction of the fuzzy sphere S_F^2. We describe the main properties of derivations on that space and give the properties of the polarization tensors T_{lm} and of $SU(2)$ coherent states. Using the coherent states we discuss how a matrix model with S_F^2 geometry can be interpreted as a theory on a spherical lattice.

In §3 we give a formulation of a scalar field theory on the sphere in the language of matrix models. We develop Hybrid Monte Carlo algorithm which can be used for numerical studies of the theory. We use our algorithm to study the phase diagram of the model. At the end of the chapter we demonstrate the existence of the so called *stripe* phases of the model for finite sized matrices.

In §4 we describe the properties of a matrix model which has two phases with different geometry properties in its phase diagram. We develop two numerical algorithms which are suitable for the study of the transition and also comment on the difficulties which we encounter when we try to apply our algorithms in the critical regime.

In §5 we present the results of our studies on the phase transition of matrix model from the previous chapter. We identify the different types of fluctuations

in the system near the phase transition and study their influence on observables of the theory. At the end of the chapter we make some final remarks and present our conclusions.

As most of the results in this thesis are numerical, we give some guidelines with regard to applying Monte Carlo techniques in the Appendix. In §A we describe the method in details and in §B we comment on the basics of *OpenCL* implementation for GPU.

Chapter 2.

Fuzzy Sphere

A big part of this work is based on the concept of the fuzzy sphere S_F^2. In this chapter we will describe at an intuitive level its construction following the work of Madore [54] in §2.2. Another important question concerning the formulation of field theories onto S_F^2 is the definition of derivations on this space. It is covered in §2.3. We briefly mention the basis of polarization tensors T_{lm} and their explicit construction. In the end of the chapter we describe the construction of the $SU(2)$ coherent states and their symbols. We discuss how the later could be used for localization on the fuzzy sphere.

2.1. Smooth 2-sphere

The sphere S^2 is a compact smooth simply-connected manifold. The symmetry of the round sphere is described by the group of the rotations in 3 dimensions $SO(3)$. Here we will rather work with its double- cover $SU(2)$. These properties make it an ideal candidate for approximation by fuzzy spaces using the scheme described in §1.1.

Let us consider $\mathbb{R}^3$ with Euclidean metric $g_{ab} = \delta_{ab}$ and $a, b = 1, 2, 3$. A round sphere with radius R is defined by the equation

$$g_{ab}\tilde{x}^a\tilde{x}^b = R^2, \tag{2.1}$$

with $\tilde{x}^a$ Cartesian coordinates on $\mathbb{R}^3$.

The algebra of complex-valued functions on the sphere $\mathrm{C}(S^2)$ plays the role of $\mathcal{A}$ in our description of the manifold. Every sufficiently well-behaved function $f(\tilde{x}^a) \in \mathrm{C}(S^2)$ can be expanded in the form

$$f(x^a) = f_0 + f_a \tilde{x}^a + \frac{1}{2} f_{ab} \tilde{x}^a \tilde{x}^b + \dots \tag{2.2}$$

These functions form an infinite dimensional algebra which can be used to separate every two points on the sphere. As basis for $\mathrm{C}(S^2)$ we can use the spherical harmonics Y_{lm}. Let us consider the operator $\hat{\vec{L}} = -i\hat{r} \times \vec{\nabla}$ [1]. In spherical coordinates its components can be written as

$$\begin{aligned} L_x &= i \left(\sin\varphi \frac{\partial}{\partial\theta} + \cot\theta \cos\varphi \frac{\partial}{\partial\varphi} \right) \\ L_y &= i \left(-\cos\varphi \frac{\partial}{\partial\theta} + \cot\theta \sin\varphi \frac{\partial}{\partial\varphi} \right) \\ L_z &= -i \frac{\partial}{\partial\varphi}. \end{aligned} \tag{2.3}$$

The operator $\hat{L^2}$ is the angular part of the Laplacian in $\mathbb{R}^3$ written in spherical coordinates. Thus the Laplacian Δ_{S^2} on a sphere with radius R in spherical coordinates is given by

$$\Delta_{S^2} = \frac{1}{R^2} \left[\frac{1}{\sin\theta} \frac{\partial}{\partial\theta} \Big(\sin\theta \frac{\partial}{\partial\theta} \Big) + \frac{1}{\sin^2\theta} \frac{\partial^2}{\partial\varphi^2} \right]. \tag{2.4}$$

The eigenfunctions Δ_{S^2} are the spherical harmonics

$$\Delta_{S^2} Y_{lm} = l(l+1) Y_{lm}. \tag{2.5}$$

More detailed discussion can be found in [50].

[1] This is the angular momentum operator from quantum mechanics with $\hbar = 1$.

2.2. Constructing the fuzzy approximations of the sphere

In order to construct S_F^2 we need to define the algebra $\mathcal{A}_N$ as an approximation to $\mathrm{C}(S^2)$. The most obvious way to do so is to leave only a finite number of terms into the series (2.2). We begin with the simplest case where we leave only the constant term. This gives us the approximation $\mathcal{A}_1 = \mathbb{C}$. This is the algebra of the constant complex-valued functions on the sphere. This approximation can not distinguish any two points on the sphere- it represents the sphere as only one point. The multiplication of the algebra $\mathcal{A}_1$ is given by the usual multiplication on $\mathbb{C}$ and it is closed.

Let us consider now keeping the linear term in (2.2). By counting the degrees of freedom associated with the coefficients f_0 and f_a, we see that this is a 4 dimensional complex vector space. Now we need to equip the vector space with multiplication in order to turn it into an algebra. If we take the usual term-by-term product of two functions we get

$$\begin{aligned} f(\tilde{x}^a)g(\tilde{y}^a) &= (f_0 + f_a\tilde{x}^a)(g_0 + g_b\tilde{x}^b) \\ &= f_0g_0 + f_0g_b\tilde{x}^b + f_a\tilde{x}^ag_0 + \underbrace{f_a\tilde{x}^ag_b\tilde{x}^b}_{\text{quadratic term}} . \end{aligned} \tag{2.6}$$

From (2.6) we can see that under this multiplication the vector space does not form an algebra because of the quadratic term that occurs. In order to close the algebra we need to modify the multiplication in such way that the expansion contains only constant and linear terms in $\tilde{x}^a$. One obvious solution is to truncate all higher order terms. This would lead to a non-associative algebra. The approach that Madore adopted is to replace the coordinates $\tilde{x}^a$ with the Pauli matrices

$$\tilde{x}^a \longrightarrow x^a = \kappa\sigma^a. \tag{2.7}$$

In the above κ should be fixed in such a way that

$$\sum_a (x^a)^2 = \mathbf{1}R^2. \tag{2.8}$$

This gives $3\kappa^2 = R^2$. The Pauli matrices together with the identity matrix form closed algebra under matrix multiplication. This promotes the vector space to the algebra $\mathcal{A}_2 = \mathrm{Mat}_2(\mathbb{C})$. This approximation allows us to distinguish between the two poles of the sphere and it is the lowest dimensional representation of the fuzzy sphere.

We can apply the same construction if we wish to keep the quadratic term in the expansion (2.2). The only difference is that instead of the Pauli matrices we will need to use the 3 dimensional irreducible representations of $su(2)$- i.e. the spin-1 angular momentum operators L_a. Here we note that in this work unless specified otherwise we choose the operators L_a to be the hermitian irreducible representations of $su(2)$ and satisfy the algebraic relations

$$[L_a, L_b] = i\epsilon_{abc}L_c. \tag{2.9}$$

Further we choose a basis in which the operator L_3 is diagonal. By the requirement that the tensor f_{ab} in (2.6) is traceless we get $8\kappa^2 = R^2$. Thus $\mathcal{A}_3 = \mathrm{Mat}_3(\mathbb{C})$ and we have a 9-dimensional complex vector space. Again this is a finer approximation of the sphere- now we can distinguish three zones around the south and north poles together with the equator.

Using the above scheme we can construct a fuzzy S^2 using irreducible representations of $su(2)$ of arbitrary dimension N. This will lead us to the algebra $\mathrm{Mat}_N(\mathbb{C})$ which has N^2 complex degrees of freedom. With $X_a = \kappa L_a$, the parameter κ is fixed by $\frac{1}{4}(N^2-1)\kappa^2 = R^2$. Spaces with larger N describe the sphere better. The parameter κ is a measure of the non-commutativity of the space and decreases with N. We recover the commutative space when $N \to \infty$ since $\lim_{N\to\infty} \kappa = 0$. As basis vectors for the algebra $\mathcal{A}_N = \mathrm{Mat}_N(\mathbb{C})$ we can use the polarization tensors ${T_{lm}}^2$ with $0 \leq l < N$ and $-l \leq m \leq l$.

From the above sequence of algebras $\{\mathrm{Mat}_1(\mathbb{C}), \mathrm{Mat}_2(\mathbb{C}), \ldots, \mathrm{Mat}_N(\mathbb{C})\}$ we exclude the first one $\mathrm{Mat}_1(\mathbb{C})$. The reason is that the matrix space (which is essentially $\mathbb{C}$) does not carry any non-trivial representations of $su(2)$ so the information about the geometry of the sphere is not preserved as commented in §1.1.

[2]The polarization tensors will be defined in §2.4

2.3. Derivations and Laplace-Beltrami operator

Now that we have defined the fuzzy sphere space, important question is can we define differential operators or some kind of analogues to them? A derivation X over an algebra $\mathcal{A}$ is an endomorphism $X : \mathcal{A} \to \mathcal{A}$ which obeys the Leibniz rule for $\forall f, g \in \mathcal{A}$

$$X(fg) = X(f)g + fX(g). \tag{2.10}$$

In our case $\mathcal{A} = \mathrm{Mat}_N(\mathbb{C})$. A linear map with the above properties is provided by the adjoint action of $\mathrm{Mat}_N(\mathbb{C})$ on itself. The commutator is a linear map by construction. The Leibniz rule can be demonstrated easily. For $x, f, g \in \mathrm{Mat}_N(\mathbb{C})$ we have

$$[x, f]g + f[x, g] = xfg - fxg + fxg - fgx = [x, fg]. \tag{2.11}$$

Thus $X = \mathrm{ad}\ x$ is a derivation for arbitrary fixed x. However there are special elements in the algebra which resemble better the properties of the usual derivation. We would like analogues of the differential operators (2.3) which are used in the construction of the Laplacian on the smooth sphere. These are elements of the form iL_a where L_a are the aforementioned N-dimensional irreducible representations of $su(2)$. For $f \in \mathrm{Mat}_N(\mathbb{C})$ the commutators $-i[L_a, f]$ for $a = 1, 2, 3$ simultaneously vanish only if f is proportional to the identity element. This suggests that the identity matrix is the analogue of the constant function in the framework of $\mathrm{Mat}_N(\mathbb{C})$.

Now the Laplace-Beltrami operator acting on an element $f \in \mathrm{Mat}_N(\mathbb{C})$ can be defined as

$$\Delta f = \sum_a [L_a, [L_a, f]]. \tag{2.12}$$

Its eigenvectors are the polarization tensors T_{lm} [46]

$$\sum_a [L_a, [L_a, T_{lm}]] = l(l+1)T_{lm}. \tag{2.13}$$

We provide more details about the objects T_{lm} together with their explicit construction in §2.4.

2.4. Polarization tensors. Explicit construction and properties

The polarization tensors[3] mentioned in §2.3 have similar algebraic structure to the spherical harmonics Y_{lm}— their product is described in terms of *Clebsch-Gordan coefficients*. In this section we give the formula for their explicit construction following [46] and mention some of their properties which are of importance for us.

We start with the explicit form of the matrix entries of the tensors T_{lm}. Let us denote by $T_{lm}^{(N)}$ the tensor T_{lm} in the space $\mathrm{Mat}_N(\mathbb{C})$. We define $s = \frac{N-1}{2}$. Then $T_{lm}^{(N)}$ can be expressed in terms of *Wigner-3j symbols*[4] [5]

$$(T_{lm}^{(N)})_{s+1+M_2,\, s+1+M_1} = (-1)^{s-M_1}\sqrt{2l+1}\begin{pmatrix} s & l & s \\ -M_1 & m & M_2 \end{pmatrix}. \tag{2.14}$$

The above expression is to be taken for all *physical* values of M_1 and M_2 where $-M_1 + m - M_2 = 0$. Otherwise the corresponding matrix element is zero. The polarization tensors defined this way have only real entries.

In addition to the explicit formula (2.14) one can obtain tensors with higher m via ladder operators. We need the matrix irreducible representations of the generators L_1, L_2, L_3 of $su(2)$. If not stated otherwise everywhere in the present work we will use a basis in which the generator L_3 has a diagonal form and L_1 has real entries unless specified otherwise. Using L_1 and L_2 we can define ladder

[3] In the context of the present work by polarization tensors we understand a certain set of basis vectors of $\mathrm{Mat}_N(\mathbb{C})$ rather than the polarization tensor which characterizes the electric properties of matter in condensed matter physics.

[4] The Wigner-3j symbols and Clebsch-Gordan coefficients arise when one needs to represent the tensor product of two irreducible representations into a direct sum of irreducible representations. More details can be found in [18, 80, 82].

[5] We denote the Wigner $3j$ symbols by $\begin{pmatrix} a & b & c \\ d & e & f \end{pmatrix}$, and Wigner $6j$ symbols by $\begin{Bmatrix} a & c & e \\ b & d & f \end{Bmatrix}$.

operators

$$\begin{aligned} L_+ &= L_1 + iL_2 \\ L_- &= L_1 - iL_2. \end{aligned} \tag{2.15}$$

Using the ladder operators from (2.15), from each diagonal tensor T_{l0} we can obtain $2l$ off-diagonal tensors T_{lm}, $-l \leq m \leq l$

$$[L_\pm, T_{lm}] = \mp\sqrt{l(l+1) - m(m \pm 1)}T_{l,m\pm1}. \tag{2.16}$$

And by the use of the above described procedure we can construct N^2 polarization tensors. They form an orthonormal basis for $\mathrm{Mat}_N(\mathbb{R})$ or for $\mathrm{Mat}_N(\mathbb{C})$ with respect to the inner product

$$(T_{l_1,m_1}, T_{l_2,m_2}) = \mathrm{Tr}(T_{l_1,m_1}T^\dagger_{l_2,m_2}) = \delta_{l_1,l_2}\delta_{m_1,m_2}. \tag{2.17}$$

Every vector $f \in \mathrm{Mat}_N(\mathbb{C})$ can be expressed in terms of the polarization tensors T_{lm}.

$$f = \sum_{l=0}^{N-1}\sum_{m=-l}^{l} c_{lm}T_{lm} \quad \text{where} \quad c_{lm} = \mathrm{Tr}(T^\dagger_{lm}f). \tag{2.18}$$

The element f can be described either in terms of its matrix entries f_{ij} or in terms of the coefficients c_{lm}. The second is analogous to momentum representation of f. Because the tensors $\{T_{lm}\}$ form an orthonormal basis the inner product (2.17) is extended to all elements of $\mathrm{Mat}_N(\mathbb{C})$ by linearity.

Under hermitian conjugation the polarization tensors transform as

$$T^\dagger_{lm} = (-1)^m T_{l,-m}. \tag{2.19}$$

The polarization tensors are eigenvectors of the adjoint action of L_3 and the Laplacian defined in (2.12).

$$\begin{aligned} &[T_{lm}, L_3] = mT_{lm} \\ &\sum_a [L_a, [L_a, T_{lm}]] = l(l+1)T_{lm}. \end{aligned} \tag{2.20}$$

The property that the polarization tensors T_{lm} are eigenvectors of L_3 determines their behaviour under rotation around the axis along L_3. For elements $U(\phi) \in SU(2)$ of the form $U(\phi) = \exp(i\phi L_3)$ we have

$$U^{-1}(\phi) T_{lm} U(\phi) = e^{im\phi} T_{lm}. \tag{2.21}$$

Thus we can perform rotations around the axis of L_3 without even computing the explicit form of the unitary matrix $U(\phi)$. This property is useful when one wants to change the basis of a matrix. The polarization tensor T_{lm} has non-zero entries of the form $t_i \delta_{i,i+m}$ (no summation over i). In other words the tensors T_{l0} have only diagonal entries, T_{l1} have only entries next to the main diagonal and so on. The above formula also shows the reason why the spinors with $m = 1/2$ need rotation of 4π instead of 2π in order to return to their origin.

Finally the algebra of the polarization tensors is understood in terms of *Wigner-3j* and *Wigner-6j* symbols.

$$\begin{aligned} T^{(N)}_{l_1,m_1} T^{(N)}_{l_2,m_2} &= \sqrt{(2l_1+1)(2l_2+1)} \sum_{l,m} (-1)^l \times \\ &\begin{Bmatrix} l_1 & l_2 & l \\ s & s & s \end{Bmatrix} (-1)^{l_1 - l_2 + m} \sqrt{2l+1} \begin{pmatrix} l_1 & l_2 & l \\ m_1 & m_2 & -m \end{pmatrix}. \end{aligned} \tag{2.22}$$

The sum in the above expression extends over values of m for which $m_1 + m_2 = m$ and all values of l for which $|l_1 - l_2| \leq l \leq l_1 + l_2$.

2.5. Coherent states

In §2.2 we argued that the fuzzy sphere provides an alternative approximation to the lattice approach to S^2. However there is one crucial difference between the two. In the most physically interesting cases the interaction in lattice theory is local. This means that each lattice point interacts only with its closest neighbors or the force drops as some power of the distance between them. Each lattice point describes a lattice site with characteristic size a and can be localized given its lattice coordinates.

This is not the case any more if we replace the algebra on the space in question by a non-commutative algebra such as a matrix algebra. The interaction on fuzzy spaces and matrix models by construction is *non-local*. Let us consider two elements $f, g \in \mathrm{Mat}_N(\mathbb{C})$. Their product is given in terms of the usual matrix multiplication

$$(f.g)_{ij} = \sum_k f_{ik} g_{kj}. \tag{2.23}$$

From the above we see for example that the element f_{ik} contributes to the values of every element of the i-th row of the product $f.g$. This suggests that we can not directly assign coordinates on the sphere to the entry f_{ij}.

In order to map the matrix entries to coordinates on the sphere we use the apparatus of the $SU(2)$ coherent states (CS). More about construction of coherent states associated to arbitrary lie groups can be found in [69, 70, 29] etc. Here following [70] we give a sketch of their construction.

An element $g \in G = SU(2)$ is in the form

$$g = \begin{pmatrix} \alpha & \beta \\ -\bar{\beta} & \bar{\alpha} \end{pmatrix} \quad \text{where } |\alpha|^2 + |\beta|^2 = 1,\ \alpha, \beta \in \mathbb{C}. \tag{2.24}$$

The form of g allows for three independent real parameters which correspond to the three Euler angles. Let us denote these degrees of freedom as the triple (ψ, ϕ, θ). They parametrize points on the three-sphere S^3.

The group G is not complex, but it can be embedded in the complex group $G^c = SL(2, \mathbb{C})$. Every element $g^c \in G^c$ is in the form

$$g^c = \begin{pmatrix} \alpha & \beta \\ \gamma & \delta \end{pmatrix} \quad \text{where } \alpha\delta - \beta\gamma = 1;\ \alpha, \beta,\ \gamma,\ \delta \in \mathbb{C}. \tag{2.25}$$

The bigger group G^c is interesting to us because it contains the images of the exponentiated elements of the ladder operators (2.15). The group can be decomposed into subgroups in a few different ways. The one that is of interest to us is

the following decomposition

$$\begin{pmatrix} \alpha & \beta \\ \gamma & \delta \end{pmatrix} = \underbrace{\begin{pmatrix} 1 & \xi(g^c) \\ 0 & 1 \end{pmatrix}}_{z_+(g^c)} \underbrace{\begin{pmatrix} \epsilon^{-1}(g^c) & 0 \\ 0 & \epsilon(g^c) \end{pmatrix}}_{h(g^c)} \underbrace{\begin{pmatrix} 1 & 0 \\ z(g^c) & 1 \end{pmatrix}}_{z_-(g^c)}. \tag{2.26}$$

For our needs it is convenient to use the so-called z-representation of SU(2). It acts on the space of the polynomials in the complex variable z of degree up to $2l$. The basis vectors of the space are denoted by $|l, m\rangle$ where $m \in -l, -l+1 \ldots l$. They can be constructed in the form

$$\langle z|l, m\rangle = \sqrt{\frac{(2l)!}{(l-m)!(l+m)!}} z^{l+m}. \tag{2.27}$$

For a fixed l we can obtain different vectors through the ladder operators L_- and L_+. The action of these operators on the space is given by

$$L_- |l, -l\rangle = 0 \qquad (L_+) |l, m\rangle = \sqrt{\frac{(l-m)!}{(l+m)!(2l)!}} L_+^{l+m} |l, -l\rangle . \tag{2.28}$$

Next we need to specify the group action in this space. Let $f(z)$ be a polynomial of degree $2j$ in z and $T^j(g)$ a z-representation, i.e. a representation of g^c and g acting in the space of the polynomials in z. Then the action of $T^j(g)$ is given by [69]

$$T^l(g^c) f(z) = (\beta z + \delta)^{2l} f\left(\frac{\alpha z z(g^c) + \gamma}{\beta z + \delta}\right). \tag{2.29}$$

For the special case of $h = \begin{pmatrix} e^{i\psi/2} & 0 \\ 0 & e^{-i\psi/2} \end{pmatrix}$ they have the property

$$T^l(h) |l, m\rangle = e^{im\psi} |l, m\rangle . \tag{2.30}$$

In other words rotations around the x_3 affect the vector $|l,m\rangle$ only with a phase change. Also

$$L_3 |l,m\rangle = m |l,m\rangle , \tag{2.31}$$

where L_3 is the infinitesimal operator corresponding to h.

We build the coherent states by applying an element g^c on an initial vector $|\Psi_0\rangle = |l,-l\rangle$. The explicit action of an arbitrary group element onto a vector can be written in terms of the decomposition (2.26).

$$T(g^c) |\Psi_0\rangle = T(z_+)T(h(g^c))T(z_-) |\Psi_0\rangle = e^{im\psi}(1+|\xi|^2)^{-l}T(z_+) |\Psi_0\rangle . \tag{2.32}$$

Because $h \in \mathrm{U}(1) \subseteq \mathrm{SU}(2)$ we can factorize out the ψ dependence thus arriving to SU(2) / U(1). By assigning the vectors $|l,m\rangle$ and $e^{im\psi} |l,m\rangle$ to the same equivalence class we effectively remove the degree of freedom associated to ψ and what is left is S^2. A point on the unit sphere can be parametrized by the unit vector $\mathbf{n} = (\cos(\phi)\sin(\theta), \sin(\phi)\sin(\theta), \cos(\theta))$. Let $g(\mathbf{n})$ be a group element which represents rotation around the unit vector $\mathbf{n}$ and $T^l(g(\mathbf{n}))$ be its z-representation. Then we can create a family of vectors which are parametrized by the points of S^2. This is the system of coherent states associated with the factor space $SU(2)/U(1)$. Now if we represent the operator $T(z_+)$ as exponentiation of the generator L_+ we get

$$|\xi\rangle = (1+|\xi|^2)^{-l} \exp(\xi L_+) |l,-l\rangle . \tag{2.33}$$

Now we Taylor- expand the exponential of the operator L_+ and use (2.28). This way we arrive at the explicit form of the vector $|\xi\rangle$.

$$|\xi\rangle = \sum_{m=-l}^{m} \sqrt{\frac{(2l)!}{(l+m)!(l-m)!}} (1+|\xi|^2)^{-l} \xi^{l+m} |l,m\rangle . \tag{2.34}$$

Through stereographic projection we can parametrize the above states with complex numbers $\xi = \cot(\frac{\theta}{2}) e^{i\frac{\phi}{2}}$.

Let us define the projector $\rho(\xi) = |\xi\rangle\langle\xi|$ with $Tr\rho(\xi) = 1$. Its matrix elements can be written as

$$\rho(\theta,\,\phi)_{m_1+l+1,\,m_2+l+1} = \sqrt{\frac{(2l)!(2l)!}{(l+m_1)!(l-m_1)!(l+m_2)!(l-m_2)!}}\frac{\xi^{l+m_1}(\xi^*)^{l+m_2}}{(1+|\xi|^2)^{2l}}. \tag{2.35}$$

We note that $\xi(\theta = 0, \phi)$ is not well defined because of the divergence of $\cot(\theta)$ at $\theta = 0$. However $\rho(\theta = 0,\,\phi)$ can be defined as $\rho(0,\,\phi) = \lim_{\theta\to 0}\rho(\theta,\,\phi) < \infty$. Let us consider the angular part of matrix elements of (2.35). We also ignore the ϕ-dependent part because it is oscillatory and thus finite for every ϕ. Thus we get

$$\lim_{\theta\to 0}\frac{\cot^{l+m_1}(\frac{\theta}{2})\cot^{l+m_2}(\frac{\theta}{2})}{(1+\cot^2(\frac{\theta}{2}))^{2l}} = \lim_{\theta\to 0}\frac{\cot^{l+m_1}(\frac{\theta}{2})\cot^{l+m_2}(\frac{\theta}{2})}{\sum_{k=0}^{2l}\binom{2l}{k}(\cot^2(\frac{\theta}{2}))^{2l-k}}.$$

From comparison of the powers of $\cot(\frac{\theta}{2})$ in the numerator and the denominator we can see that the above limit is zero except for the case $m_1 = m_2 = l$— then we have $\rho(0,\,\phi)_{l,l} = \lim_{\theta\to 0}\rho(\theta,\,\phi)_{l,l} = 1$. The matrix can be written down in compact form $\rho(0,\phi)_{m_1+l+1,m_2+l+1} = \delta_{m_1,l}\delta_{m_2,l}$.

Now we consider $f \in \mathrm{Mat}_N(\mathbb{C})$. The object

$$\tilde{f}(\theta,\phi) = \mathrm{Tr}(\rho f) = \langle\xi|f|\xi\rangle \tag{2.36}$$

is a complex-valued periodic function of the coordinates θ and ϕ and it is called symbol of f. The expression (2.36) provides a linear map between the elements of $\mathrm{Mat}_N(\mathbb{C})$ and complex-valued functions on the sphere. This technique allows one to translate problems related to the operators f in the language of functions $\tilde{f}(\theta,\phi)$ and vice versa. Here we give a list of the images of some important operators taken from [70]

$$\begin{aligned}
\mathrm{Tr}(\rho(\theta,\phi)\mathbf{1}) &= 1\\
\mathrm{Tr}(\rho(\theta,\phi)L_1) &= (N-1)\sin\theta\cos\phi\\
\mathrm{Tr}(\rho(\theta,\phi)L_2) &= (N-1)\sin\theta\sin\phi\\
\mathrm{Tr}(\rho(\theta,\phi)L_3) &= (N-1)\cos\theta.
\end{aligned} \tag{2.37}$$

The images of the group elements $g(\tau,\nu) = \exp\{i\tau(\nu L)\} \in SU(2)$ are given by the formula

$$\mathrm{Tr}\left(\rho(\theta,\phi)g(\tau,\nu)\right) = \left(\cos\frac{\tau}{2} + i\sin\frac{\tau}{2}\cos\theta\right)^{2(N-1)}, \tag{2.38}$$

where $\nu^2 = 1$ is a unit vector along the axis of rotation of the element g and τ is the angle.

This map is consistent with our choice of derivatives in §2.3. From (2.37) we see that the identity matrix is mapped to a constant function on the sphere and the three $su(2)$ generators to the coordinate functions x, y, z.

2.6. From matrices to lattice

In this section we comment on a simple application of the coherent states that we described in §2.5. Let $X \in \mathrm{Mat}_N(\mathbb{C})$ be a hermitian matrix. Then the symbol $\tilde{X}(\theta,\phi) = \mathrm{Tr}(X\rho)$ from (2.36) is a real valued function. We can see that if we take its complex conjugate[6] [7]

$$(\mathrm{Tr}(\rho X))^* \sim \left((\xi)^i(\xi^*)^j X_{ij}\right)^* \sim \left((\xi^*)^i(\xi)^j X_{ji}\right) \sim \mathrm{Tr}(\rho X).$$

We can now project the matrix elements of X onto a grid on the sphere consisting of K real points. Let $N = 2M$. We can define a grid (or lattice) consisting of points on the sphere with coordinates

$$\Lambda = \left\{\theta_j = \frac{j\pi}{N-1}\right\}, \tag{2.39}$$

where

$$j \in \{0,\ldots,N-1\} \quad \text{and } k \in \begin{cases} \{1,\ \ldots,\ j+1\} & \text{if } j < M \\ \{1,\ \ldots,\ 2M-j+1\} & \text{if } j \geq M. \end{cases}$$

[6] We omit the normalization factors and the denominator from (2.35) as they are real by construction.

[7] In the above calculations the variables i and j denote the indices of the matrix X but also denote power of the variable ξ.

There is a freedom in the definition of the grid. We chose our grid of that form for two main reasons: First the number of degrees of freedom of the grid agrees with the number of degrees of freedom of our underlying (matrix) model. And second reason is that we want more degrees of freedom around the equator of the sphere.

If we study the fluctuations around the ground state of the degrees of freedom on the grid and their decay rate, we can define geometrical objects like *correlation angle* or *correlation length* in a way which is consistent with the usual lattice definition.

Using the above tools, we can project out any matrix model to degrees of freedom defined on the sphere. Of course such a correspondence makes sense only if the underlying theory has a notion of S^2 geometry built-in it. The matrix models that we study in the next chapters have S^2 geometry therefore are suitable for representation as degrees of freedom on the sphere.

Important is the question whether or not the same idea can be applied to manifolds with different geometries? Coherent states can be constructed for the groups- Heisenberg-Weyl group, $SU(2)$, $SU(1,1)$, $SO(3,1)$, $SO(n,1)$ etc [70]. Complications arise when the groups are non-compact or non-simply connected. In the case of non-compact groups (like $SU(1,1)$) there are no finite- dimensional unitary representations, which prevents us from construction of the analogue of the projector from (2.35) as a finite size matrix.

Chapter 3.

Scalar field theory on the fuzzy sphere

In this chapter we discuss the fuzzy approximation to ϕ^4 theory. We begin with an overview of the usual scalar field theory in §3.1. Using the construction of S_F^2 from Chapter 2 we give two equivalent formulations of the theory in the language of the matrix models in §3.2 and §3.3. Next in §3.4 and §3.5 we show how the Hybrid Monte Carlo method can be applied to the theory and discuss the properties of our algorithm. Our method is based on Hamiltonian dynamics and allows us to simulate systems with relatively big size. In §3.6 we make some remarks on a model with higher order kinetic term. In §3.7 we discuss a gauge—fixing of the global $SO(3)$ symmetry. In the rest of the chapter we present the numerical results from our studies and make some comments.

3.1. Scalar field

Because of its relative simplicity in comparison with gauge and fermion fields, the scalar field theory is one of the most extensively studied. Studies of the phase diagram can be found in [53, 61, 78, 3]. The action of the theory is given by

$$S[\phi] = \int d\Omega \left(\frac{1}{2}\phi\Delta\phi + r\phi^2 + \lambda\phi^4 \right), \tag{3.1}$$

where $d\Omega$ is a measure over the space where the theory is defined. In most cases it is $\mathbb{R}^d$. The expectation value of a generic observable of the system A which is a function of ϕ is computed with the path integral

$$\langle A \rangle = Z^{-1} \int A[\phi] e^{-S[\phi]} d\mu. \tag{3.2}$$

The measure $d\mu$ is infinite dimensional and Z is the partition function of the system

$$Z = \int e^{-S[\phi]} d\mu. \tag{3.3}$$

For $\lambda > 0$ the action is bounded from below and the field-theory is well-defined. In the limit $\lambda \to 0$ and $r > 0$ it corresponds to pure Gaussian model. In the large λ limit it resembles the Ising model. And it is in the same universality class — it has the same static critical exponents. The model has two phases in the (r, λ) parameter space. For $-r$ large enough the system is in the so called disordered phase. In this regime the symmetry $\phi \to -\phi$ of the Lagrangian from (3.1) is manifest and $\langle \phi \rangle = 0$. In the ordered phase the field has $\langle \phi \rangle \neq 0$ which is an indication of spontaneous symmetry breaking. The two phases are separated by a critical line [53].

3.2. Matrix regularization

Now as we have the formulation of the fuzzy sphere in §2.2 we can formulate the matrix regularization of the system (3.1) by formal application of the scheme described in Chapter 1. This regularization has been studied in [56, 39] etc. We represent the real scalar field ϕ by an Hermitian $N \times N$ matrix Φ

$$\phi \to \Phi \in \mathrm{Mat}_N(\mathbb{C}), \quad \Phi = \Phi^\dagger. \tag{3.4}$$

The inner product of Φ with itself is given by the usual matrix multiplication. The Hermitian property of the field Φ is important for our formulation because it makes the action of the theory real-valued. The kinetic term is replaced by the

adjoint action of the $su(2)$ generators, as discussed in §2.3

$$\int \phi\Delta\phi \to \mathrm{Tr}\sum_a \Phi[L_a,[L_a,\Phi]]. \tag{3.5}$$

The kinetic term (3.5) also defines the geometry of the space where Φ is defined—in our case the fuzzy sphere. If we want to define a scalar model on a different space, we need to replace it with a suitable generalization of the Laplacian for the new space. A simple example would be replacing the spherical Laplacian by a Laplacian on the ellipsoid. This can be achieved if we substitute $L_a \to \frac{1}{C_a^2}L_a$ with C_a three real constants.

We return to our theory on a sphere. We replace the integral over the sphere with a trace. Thus the matrix regularized version the action 3.1 reads

$$S[\Phi] = \frac{4\pi}{N}\,\mathrm{Tr}(\sum_a \Phi[L_a,[L_a,\Phi]] + rR^2\Phi^2 + \lambda R^2\Phi^4). \tag{3.6}$$

While there are three parameters in the above action r, λ and R^2 and each of them has its interpretation, they are not fully independent. We can redefine $\tilde{r} = rR^2$ and $\tilde{\lambda} = \lambda R^2$ and work with those without any loss of generality. Moreover, all properties of the system should be expressible solely as functions of $\tilde{r}$ and $\tilde{\lambda}$.

The potential terms $\mathrm{Tr}(\Phi^2)$ and $\mathrm{Tr}(\Phi^4)$ have full $SU(N)$ symmetry with N being the size of the matrix Φ. The kinetic term on the other hand is constructed with the $su(2)$ generators. It breaks the symmetry of the whole action down to $SU(2)$. This is how the Laplacian defines the geometry of the system in our case.

Before we are able to compute observables in the theory we need to define the measure $d\mu$. As Φ is a Hermitian matrix, $d\mu$ must extend over the space of all Hermitian matrices. It is given by

$$d\mu = \prod_{i=1}^{N}\prod_{j=1}^{i} d\mathfrak{Re}(\Phi_{ij})d\mathfrak{Im}(\Phi_{ij}). \tag{3.7}$$

The measure extends over $\mathbb{R}^{N^2}$ — this corresponds to the number of independent degrees of freedom in a Hermitian N by N matrix. As was mentioned in §1.3 the number of degrees of freedom of the model (and the volume of the measure $d\mu$)

do not depend on the physical dimensions of the system. By analogy with (3.2) the observables of the theory are defined to be

$$\langle A \rangle = Z^{-1} \int A[\Phi] e^{-S[\Phi]} d\mu, \tag{3.8}$$

and the partition function is

$$Z = \int e^{-S[\Phi]} d\mu. \tag{3.9}$$

Now we have a well-defined non-commutative field theory realized as a matrix model. In the next section we give a formulation of the theory in different basis and compare the two. In the rest of this chapter we will investigate the phase diagram of the above system using Hybrid Monte Carlo simulation techniques.

3.3. Matrix regularization II

In §3.2 we regularized the scalar field Φ in terms of a matrix degrees of freedom Φ_{ij}. We can rewrite the action (3.6) in momentum representation. In order to do that we expand the field Φ in the basis of the polarization tensors. It is convenient to define the *spin* $s = \frac{N-1}{2}$ of the field

$$\Phi = \sum_{l=0}^{N-1} \sum_{m=-l}^{l} c_{lm} T_{lm}. \tag{3.10}$$

The coefficients c_{lm} are complex. They are determined from the inner product (2.17)

$$c_{lm} = \mathrm{Tr}(\Phi . T_{lm}^{\dagger}). \tag{3.11}$$

From the hermicity of Φ it follows that

$$\begin{aligned} \Phi^{\dagger} &= \Big(\sum_{lm} c_{l,m} T_{l,m} \Big)^{\dagger} \\ &= (-1)^m c^{*}_{l,-m} T_{l,-m} = \Phi. \end{aligned} \tag{3.12}$$

This imposes constraints on the coefficients $c_{lm} = (-1)^m c^*_{l,-m}$ and $\mathfrak{Im}(c_{l0}) = 0$ for $\forall l$. The first few terms of the expansion (3.10) have the form

$$\begin{aligned}\Phi &= \mathrm{Tr}(\Phi.T_{00}^\dagger)T_{00} + \sum_{m=-1}^{1} \mathrm{Tr}(\Phi.T_{1m})T_{1m} + \dots \\ &= \frac{1}{N}\,\mathrm{Tr}(\Phi.\mathbf{1})\mathbf{1} + \frac{4}{N^2-1}\sum_{a=1}^{3}\mathrm{Tr}(\Phi.L_a)L_a + \dots\end{aligned} \tag{3.13}$$

Now we can proceed and rewrite (3.6) in momentum representation.

We begin with the mass term

$$\begin{aligned}\frac{4\pi}{N}\,\mathrm{Tr}(rR^2\Phi^2) &= \frac{4\pi r R^2}{N}\,\mathrm{Tr}(\Phi\Phi^\dagger) \\ &= \frac{4\pi r R^2}{N}\,\mathrm{Tr}\Big(\sum_{l=0}^{N-1}\sum_{m=-l}^{l} c_{lm}T_{lm}\sum_{l_1=0}^{N-1}\sum_{m_1=-l_1}^{l_1} c^*_{l_1m_1}T^\dagger_{l_1m_1}\Big) \\ &= \frac{4\pi}{N} rR^2\sum_{l=0}^{N-1}\sum_{m=-l}^{l}|c_{lm}|^2.\end{aligned} \tag{3.14}$$

In the above we have used the orthogonality relation (2.17) and the hermitian conjugation (2.19). Next we consider the kinetic term in (3.6)

$$\begin{aligned}&\frac{4\pi}{N}\,\mathrm{Tr}\Big(\sum_a \Phi[L_a,[L_a,\Phi]]\Big) = \frac{4\pi}{N}\,\mathrm{Tr}\Big(\sum_a \Phi[L_a,[L_a,\Phi^\dagger]]\Big) \\ &= \frac{4\pi}{N}\,\mathrm{Tr}\Big(\sum_a\Big(\sum_{l=0}^{N-1}\sum_{m=-l}^{l} c_{lm}T_{lm}\Big[L_a,\Big[L_a,\sum_{l_1=0}^{N-1}\sum_{m_1=-l_1}^{l_1} c^*_{l_1m_1}T^\dagger_{l_1m_1}\Big]\Big]\Big)\Big).\end{aligned}$$

Now we can use the property that the spherical harmonics T_{lm} are eigenvectors of the Laplacian (2.13) with eigenvalues $l(l+1)$

$$\begin{aligned}&\frac{4\pi}{N}\sum_{l=0}^{N-1}\sum_{m=-l}^{l}\sum_{l_1=0}^{N-1}\sum_{m_1=-l_1}^{l_1} c_{lm}c^*_{l_1m_1}\,\mathrm{Tr}\Big(T_{lm}l_1(l_1+1)T^\dagger_{l_1m_1}\Big) \\ &= \frac{4\pi}{N}\sum_{l=0}^{N-1}\sum_{m=-l}^{l} l(l+1)|c_{lm}|^2.\end{aligned} \tag{3.15}$$

A comparison between the expression for the kinetic term (3.15) and the mass term (3.14) shows that in momentum representation the two terms have similar structure. The only difference is that in the kinetic term each mode T_{lm} has assigned weight $l(l+1)$.

Next we work on the self-interaction term. In the following calculation we will replace the double sum $\sum_{l=0}^{N-1}\sum_{m=-l}^{l}$ with $\sum_{l,m}$ if it is possible to do so without the introduction of ambiguity

$$\begin{aligned}\frac{4\pi}{N}\operatorname{Tr}(\lambda R^2\Phi^4) &= \frac{4\pi\lambda R^2}{N}\operatorname{Tr}(\Phi\Phi\Phi\Phi)\\ &= \frac{4\pi\lambda R^2}{N}\operatorname{Tr}\Big(\sum_{l,m}\sum_{l_1,m_1}\sum_{l_2,m_2}\sum_{l_3,m_3} c_{lm}c_{l_1m_1}c_{l_2m_2}c_{l_3m_3}\times\\ &T_{lm}T_{l_1m_1}T_{l_2m_2}T_{l_3m_3}\Big).\end{aligned} \tag{3.16}$$

We compute $\Theta = \Phi^2 = \sum_{l,\,m} t_{l,\,m}T_{l,\,m}$. The matrix multiplication in terms of polarization tensors has the form

$$\sum_{l,\,m} t_{l,\,m}T_{l,\,m} = \sum_{l_1,\,m_1}\sum_{l_2,\,m_2} c_{l_1,\,m_1}c_{l_2,\,m_2}T_{l_1,\,m_1}T_{l_2,\,m_2}. \tag{3.17}$$

The algebra of polarization tensors is given in terms of Wigner's $3j$ and $6j$ symbols. A detailed description of the theory of angular momentum and polarization tensors is provided in [15, 82, 18, 46, 80]. With the help of (2.4.16) and (8.1.13) from [80] for the coefficients $t_{l,\,m}$ we have

$$\begin{aligned}t_{l,\,m} = \sum_{l_1,\,m_1}\sum_{l_2,\,m_2}(-1)^{2s+1+l_1+l_2-m}\sqrt{(2l_1+1)(2l_2+1)(2l+1)}\times\\ \begin{Bmatrix} l_1 & l_2 & l_l\\ s & s & s\end{Bmatrix}\begin{pmatrix} l_1 & l_2 & l_l\\ m_1 & m_2 & -m\end{pmatrix} c_{l_1,\,m_1}c_{l_2,\,m_2}.\end{aligned}$$

Now the quartic term can be computed similarly to (3.14)

$$\frac{4\pi\lambda R^2}{N}\operatorname{Tr}(\Phi^4) = \frac{4\pi\lambda R^2}{N}\sum_{l,\,m}|t_{l,\,m}|^2. \tag{3.18}$$

Each of the above terms is invariant under the exchange of $l_1 \leftrightarrow l_2$. Odd- permutation of columns of the Wigner $3j$ symbols in the above expression brings a phase $(-1)^{l+l_1+l_2}$, after we take the square the phase factor always equals 1. Also the Wigner $6j$ symbols are invariant under any permutation of its columns. By using this invariance we can reduce the number of terms by a factor of 2. The sum over l and m is further restricted by the selection rules of the vector coupling coefficients {} and (). Wigner $3j$ symbols are zero unless the following requirements are fulfilled $m_1 + m_2 + m = 0$ and $|l_1 - l_2| \leq l \leq l_1 + l_2$ (triangular rule). These selection rules are consequences of the angular momentum conservation. It is easy to see that the expression (3.18) is real-valued as each of the multipliers in the sum itself is real.

And finally we define the measure for the path integral

$$d\mu = \prod_{l=0}^{N-1} \prod_{m=-l}^{l} d\mathfrak{Re}(c_{lm}) d\mathfrak{Im}(c_{lm}). \tag{3.19}$$

As required it has the same size as (3.7).

The above expressions (3.14), (3.15) and (3.18) provide an equivalent formulation of the theory (3.6) in momentum representation and give us further insight into the the structure of the theory. However because the first matrix formulation has simpler form, we will use it in our numerical studies.

3.4. Hybrid Monte Carlo approach

As we have the matrix action of the theory (3.6) we can apply the recipe described in §A.2 in order to implement a Hybrid Monte Carlo simulation algorithm.

First we rewrite the kinetic term in a form which is easier to work with

$$\begin{aligned} &\frac{4\pi}{N} \operatorname{Tr}\Big(\sum_a \Phi[L_a,[L_a,\Phi]]\Big) = \frac{4\pi}{N} Tr\Big(\Phi[L_a, L_a\Phi - \Phi L_a]\Big) \\ &= \frac{8\pi}{N} \operatorname{Tr}\Big(L_a L_a \Phi\Phi\Big) - \frac{8\pi}{N} Tr\Big(L_a \Phi L_a \Phi\Big) \\ &= \frac{8\pi c_2}{N} \operatorname{Tr}\Big(\Phi\Phi\Big) - \frac{8\pi}{N} Tr\Big(L_a \Phi L_a \Phi\Big). \end{aligned} \tag{3.20}$$

In the above we have used the cyclic property of the trace. The factor $c_2 = \sum_a L_a L_a = \frac{N^2-1}{4}$ is the second order Casimir operator of $su(2)$. We see that effectively the kinetic term brings a correction to the mass Φ^2 term with factor of $2c_2$. The contribution specific to the kinetic term comes from $L_a \Phi L_a \Phi$. The simplified form of (3.6) reads

$$S[\Phi, N, r, R, \lambda] = \frac{4\pi}{N} \operatorname{Tr}\Big((2c_2 + rR^2)\Phi^2 - 2\sum_a L_a \Phi L_a \Phi + \lambda R^2 \Phi^4\Big). \tag{3.21}$$

The first step towards implementation of the HMC algorithm is to define momenta P which are conjugate to the degrees of freedom of the field Φ. In order to fulfill the requirement of ergodicity from §A.1 and to have phase volume element preservation, P must have the same number of degrees of freedom as Φ. Thus we define $P \in \mathrm{Mat}_N(\mathbb{C})$ to be hermitian. Now we define the Hamiltonian of our extended system

$$\mathbf{H}[\Phi, P] = \frac{1}{2} \operatorname{Tr}(P^2) + \mathbf{S}[\Phi]. \tag{3.22}$$

The above Hamiltonian is also real-valued for every Hermitian Φ and P. In order to obtain the Hamiltonian equations (A.6) we need to take the derivatives with respect to the single entries Φ_{ij} and P_{ij}. We formally define them by

$$\frac{\partial}{\partial \Phi_{i_1 j_1}} \Phi_{i_2 j_2} = \delta_{i_1 i_2} \delta_{j_1 j_2} \quad \frac{\partial}{\partial P_{i_1 j_1}} P_{i_2 j_2} = \delta_{i_1 i_2} \delta_{j_1 j_2}. \tag{3.23}$$

Now compute the derivative of $\mathbf{H}[\Phi, P]$ with respect to an arbitrary component P_{ij} of the momentum. It enters the equations of motion for the Φ_{ij}

$$\begin{aligned} &\frac{\partial}{\partial P_{ij}} \frac{1}{2} \operatorname{Tr}(P_{i_1 j_1} P_{j_1 i_1}) \\ &= \frac{1}{2}\big(\delta_{i i_1} \delta_{j j_1} P_{j_1 i_1} + \delta_{i j_1} \delta_{j i_1} P_{i_1 j_1}\big) \quad = P_{ji}. \end{aligned} \tag{3.24}$$

The above derivative is model-independent. If we define the conjugate momenta P the same way we did, the derivative $\frac{\partial \mathbf{H}}{\partial P}$ has always the same form for any matrix model. An important peculiarity that shows in (3.24) is that it turns out that the conjugate momentum to Φ_{ij} is P_{ji} rather than P_{ij}.

Next we compute the derivatives of the action. The derivative of the $\mathrm{Tr}(\Phi^2)$ term is the same as the one computed above

$$\frac{\partial}{\partial\Phi_{ij}}\frac{4\pi}{N}\,\mathrm{Tr}\left((2c_2+rR^2)\Phi^2\right)=\frac{8\pi}{N}(2c_2+rR^2)\Phi_{ji}. \tag{3.25}$$

The derivative of the second part of the kinetic term reads

$$\begin{aligned}&-\frac{\partial}{\partial\Phi_{ij}}\frac{4\pi}{N}\,\mathrm{Tr}\left(2\sum_a L_a\Phi L_a\Phi\right)\\&=-\frac{8\pi}{N}\sum_a\Big((L_a)_{i_1j_1}\delta_{ij_1}\delta_{ji_2}(L_a)_{i_2j_3}\Phi_{j_3i_1}+(L_a)_{i_1j_1}\Phi_{j_1i_2}(L_a)_{i_2j_3}\delta_{ij_3}\delta_{ji_1}\Big).\end{aligned} \tag{3.26}$$

After reordering of the summands and summing over the Kronecker δ-symbols we get

$$\begin{aligned}&=-\frac{8\pi}{N}\sum_a\Big((L_a)_{jj_3}\Phi_{j_3i_1}(L_a)_{i_1i}+(L_a)_{jj_1}\Phi_{j_1i_2}(L_a)_{i_2i}\Big)\\&=-\frac{16\pi}{N}(L_a\Phi L_a)_{ji}.\end{aligned} \tag{3.27}$$

The last piece is the derivative of the self-interacting Φ^4 term

$$\begin{aligned}&\frac{\partial}{\partial\Phi_{ij}}\frac{4\pi}{N}\,\mathrm{Tr}\left(\lambda R^2\Phi^4\right)=\frac{4\pi\lambda R^2}{N}\frac{\partial}{\partial\Phi_{ij}}\Phi_{i_1j_1}\Phi_{j_1i_2}\Phi_{i_2j_2}\Phi_{j_2i_1}\\&=\frac{16\pi\lambda R^2}{N}\Phi_{jj_1}\Phi_{j_1i_2}\Phi_{i_2i}=\frac{16\pi\lambda R^2}{N}\left(\Phi^3\right)_{ji}.\end{aligned} \tag{3.28}$$

Now with the use of (3.25), (3.27) and (3.28) we can write down the explicit form of the Hamiltonian equations of motion for the extended system

$$\begin{aligned}\dot\Phi_{ij}&=P_{ji}\\\dot P_{ij}&=\frac{8\pi}{N}\Big(\left(rR^2\Phi+2c_2\Phi\right)-2\sum_a(L_a\Phi L_a)+2\lambda R^2\Phi^3\Big)_{ji}.\end{aligned} \tag{3.29}$$

Every Monte Carlo simulation works by generating different configurations of Φ and P as function of discretized time $t=0,1,\dots N_s$. In our simulations the time interval length between two consecutive configurations is ϵ. We will denote by $\Phi(t)$ and $P(t)$ the values of the fields and momenta in a particular time step t.

Now we can write a discretized in time first order approximation to (3.29)

$$\begin{aligned}\Phi_{ij}(t) &= \Phi_{ij}(t-1) + P_{ji}(t-1)\epsilon \\ P_{ij}(t) &= P_{ij}(t-1) - \frac{8\pi}{N}\Big(\big(rR^2\Phi(t-1) \\ &+ 2c_2\Phi(t-1)\big) - 2\sum_a (L_a\Phi(t-1)L_a) + 2\lambda R^2(\Phi(t-1))^3\Big)_{ji}\epsilon\end{aligned} \tag{3.30}$$

The above equations allow us to generate the configuration $(\Phi(t), P(t))$ from the configuration $(\Phi(t-1), P(t-1))$. The momentum P is generated according to a normal distribution for Monte Carlo every step. The initial value of the field $\Phi(0)$ in principle can be chosen arbitrary. In this work rather than (3.30) the equations (3.29) are solved with the Omelyan integrator (A.12). It provides analogous but finer approximation which preserves the Hamiltonian conservation better.

3.5. HMC algorithm properties

In this section we briefly describe the properties of the algorithm and discuss them with regard of the requirements stated in §A.1.

For small enough values of the parameters and matrix size the algorithm prescribed in the previous paragraph is ergodic. From every configuration Φ' the simulation can bring the system to an arbitrary configuration Φ'' provided the algorithm is run long enough. This is fulfilled because the space of hermitian matrices is connected. In other words there always exists a momentum $P = \Phi'' - \Phi'$. However the profile of (3.6) has lots of local minima and their number and height in each phase grows with N and the magnitude of the parameters of the model. Thus for some values of the parameters the system becomes trapped into the local minima of the action- this phenomenon is known as *ergodicity breaking*. Due to the ergodicity breaking the result of the simulation is not independent of the initial state of the system and we should take special care in this situation.

The third requirement of detailed balance is automatically fulfilled because of the definition of the momentum P and the Metropolis accept/reject decision which is built into the HMC algorithm.

The system dynamics as described by (3.30) preserve the phase volume element as discussed in (A.14). This holds to a high precision in our simulations.

Another check which can be made comes from the *Schwinger-Dyson* type analysis of (3.6). Let us consider the integral

$$\int d\mu(\Phi) \frac{d}{d\Phi_{ij}} \Big(\Phi_{ij} e^{-S[\Phi]} \Big) = 0. \tag{3.31}$$

The above integral vanishes identically being an integral over a full differential. After simplifying the above we get

$$N^2 = \frac{4\pi}{N} \Big(2(2c_2 + rR^2) \left\langle \mathrm{Tr}\, \Phi^2 \right\rangle - 2 \sum_a \langle \mathrm{Tr}(L_a \Phi L_a \Phi) \rangle + 4\lambda R^2 \left\langle \mathrm{Tr}(\Phi^4) \right\rangle \Big). \tag{3.32}$$

Further we make the substitutions $\left\langle \frac{4\pi}{N}(2c_c + rR^2)\, \mathrm{Tr}\, \Phi^2 \right\rangle \equiv \langle S_2 \rangle$ and $\langle 4\lambda R^2\, \mathrm{Tr}\, \Phi^4 \rangle \equiv \langle S_4 \rangle$. We get

$$2 \langle S_2 \rangle + 4 \langle S_4 \rangle = N^2. \tag{3.33}$$

In the above we have denoted the expectation values of terms quadratic in Φ with $\langle S_2 \rangle$ and the expectation values of terms quartic in Φ with $\langle S_4 \rangle$. We can also use this identity to check our code.

The last comment in this section is about the complexity of the algorithm. As we point out in §A.3 as the action (3.21) is expressed in terms of a matrix polynomial, it leads to equations of motion also expressed in polynomials. Thus the complexity of generating a new configuration of Φ using (3.30) is $\sim \mathcal{O}(N^3)$. This is a major advantage of this algorithm when compared to the Metropolis update scheme. In the case of Metropolis the computation of δS for monomial with power higher than 4 cannot be computed in time $\sim \mathcal{O}(N)$ which makes the complexity of the whole update algorithm $\gtrsim \mathcal{O}(N^4)$ [56]. However the complexity of the HMC equations of motion derived from the action in §3.3 which is in terms of the modes c_{lm} is higher $\sim \mathcal{O}(N^6)$[1]. This can be easily seen if we take a closer look at (3.3) and assign complexity of $\mathcal{O}(N^2)$ to every loop over l, m indeces on

[1] Actually the complexity of the algorithm is even higher because of the presence of Wigner $6j$ symbols in (3.18).

the left and right side of the equation. The higher complexity is mainly due to the fact that in contrast to the entries Φ_{ij} the modes c_{lm} are no longer matrix degrees of freedom but modes with more complicated interactions between them. This is another reason for us to prefer the first formulation of the theory for our numerical studies.

3.6. Fourth order derivative

Actions with higher order derivatives are considered in the context of perturbation theory of gravity. A construction of fourth order derivative model is given in [13] together with discussion of the problems of higher order kinetic term theory and ways to treat them. In the context of matrix models, the higher order kinetic term is of interest because it suppresses the modes with higher momentum l and is expected to help with the problem of UV-IR mixing.

In this section we present matrix realization of higher order kinetic term on the fuzzy sphere. Then we derive the equations of motion of such a model and make some remarks.The action of the theory is completely symmetric with respect to the coordinate and velocity

$$\begin{aligned} S_{4d}[\Phi] = \frac{4\pi}{N}\,\mathrm{Tr}\Big(\sum_{a}^{1}\Phi[L_a,[L_a,\Phi]] + rR^2\Phi^2 + \\ \lambda R^2\Phi^4 + z\sum_{a,b=1}^{3}\Phi[L_a,[L_a,[L_b,[L_b,\Phi]]]]\Big), \end{aligned} \tag{3.34}$$

where $z \in \mathbb{R}$. The Hamiltonian of the extended system is constructed in a similar way to (3.22). The derivatives with respect to the momentum P are the same. The only change is the derivative with respect to Φ of the higher order kinetic term. Before we find it we simplify the z-term. After expanding the commutators

and some reordering, we can rewrite the higher order term in the form

$$\begin{aligned}&\sum_{a,b} \operatorname{Tr} \Phi[L_a,[L_a,[L_b,[L_b,\Phi]]]] = \\ &4c_2^2 \operatorname{Tr} \Phi^2 - 8c_2 \sum_{a=1}^{3} \operatorname{Tr} \Phi L_a \Phi L_a + 4 \sum_{a,b=1}^{3} \operatorname{Tr} \Phi L_a L_b \Phi L_b L_a.\end{aligned} \tag{3.35}$$

We see that terms analogous to the first two terms are already present in the expansion of the kinetic term and the piece that carries the higher order derivative specific behaviour is the third part. We note that for matrix size $N = 2$ the higher order kinetic term behaves exactly like the kinetic term. The reason is: for that matrix size the $su(2)$ generators are proportional to the Pauli matrices which form a closed algebra with respect to matrix multiplication (if we allow for complex coefficients). In then $N = 2$ case we have $\sigma_a \sigma_b = \delta_{ab} + i\epsilon_{abc}\sigma_c$. For $N \geq 3$ we compute the derivative of the last part of the expansion (3.35)

$$\frac{\partial}{\partial \Phi_{ij}} 4 \sum_{a,b=1}^{3} \operatorname{Tr} \Phi L_a L_b \Phi L_b L_a = 8 \sum_{a,b=1}^{3} (L_a L_b \Phi L_b L_a)_{ji}. \tag{3.36}$$

The derivative of the the higher order kinetic term can be written as

$$\begin{aligned}&\frac{\partial}{\partial \Phi_{ij}} \sum_{a,b} \operatorname{Tr} \Phi[L_a,[L_a,[L_b,[L_b,\Phi]]]] = \\ &8c_2^2 \Phi_{ji} - 16c_2 \sum_{a=1}^{3} (L_a \Phi L_a)_{ji} + 8 \sum_{a,b=1}^{3} (L_a L_b \Phi L_b L_a)_{ji}.\end{aligned} \tag{3.37}$$

With the help of (3.34) and (3.37) we can simulate the model with higher order kinetic term.

As a final remark we would like to comment on the structure of the term in the basis of polarization tensors T_{lm}. As we mentioned before the polarization tensors are eigenvectors of the Laplacian. Thus if we expand our field according

to (3.10) we get

$$\begin{aligned}
&\sum_{a,b} \mathrm{Tr} \sum_{l_1 m_1} c_{l_1 m_1} T_{l_1 m_1} [L_a, [L_a, [L_b, [L_b, \sum_{lm} c_{lm} T_{lm}]]]] = \\
&\mathrm{Tr} \sum_{l_1 m_1} \sum_{lm} l^2 (l+1)^2 c^*_{l_1, -m_1} c_{lm} T^\dagger_{l_1 m_1} T_{lm} = \\
&\sum_{l_1 m_1} \sum_{lm} l^2 (l+1)^2 c^*_{l_1, -m_1} c_{lm} \delta_{l,l_1} \delta_{m,m_1} = \sum_{lm} l^2 (l+1)^2 |c_{lm}|^2.
\end{aligned} \tag{3.38}$$

In the above we have used the orthogonality relation (2.17). That expression shows that the higher order derivative term is real-valued and positive definite for $z > 0$. Therefore we don't expect any problems with stability. As we expected, this kinetic term strongly suppresses terms with higher momentum l. Those modes have relative contribution $\sim l^4$.

3.7. Gauge fixing of SO(3) symmetry

We would like to note that the idea for the $SO(3)$ gauge-fixing was provided to us by Xavier Martin.

3.7.1. SO(3) invariant vs. non-invariant quantities

As we pointed out the matrix action has a full $SO(3) \times \mathbb{Z}_2$ symmetry. The action involves only terms which are quadratic and quartic in Φ thus the change $\Phi \to -\Phi$ leaves it invariant. Also any two configurations Φ and Φ', where

$$\Phi' = U^{-1} \Phi U \tag{3.39}$$

and U is a unitary representation of $SU(2)$ produce the same value of the action. In other words the path integral of the theory (3.8) can be split into angular and non-angular parts

$$\langle A \rangle = Z^{-1} \int_{S^2} \int A[\Phi] e^{-S[\Phi]} d\mu' d\Omega. \tag{3.40}$$

From the above integral it is evident that every quantity which is a function of the field Φ is averaged over the *Haar measure* of $SO(3) \times \mathbb{Z}_2$. We note that the symmetry groups $SO(3)$ and $\mathbb{Z}_2$ do not build up to the $SU(2)$ group. The reason is that the two symmetries are implemented via different actions. The $SO(3)$ group acts via its adjoint action (3.39). However there is no unitary matrix U which transforms $\mathbf{1} \to -\mathbf{1}$ via its adjoint action. For invariant quantities the angular part can be integrated out as an overall factor of the integral

$$\langle A \rangle = Z^{-1} \int_{S^3} d\Omega \int A[\Phi] e^{-S[\Phi]} d\mu'. \tag{3.41}$$

The quantities that have this property are functions of the trace of Φ of the form $Tr(P(\Phi))$. However there are quantities which are of interest for us and which are not necessary invariant under the action of $SO(3) \times \mathbb{Z}_2$. Examples of such quantities are the expectation values of the entries Φ_{ij} and the coefficients c_{lm} in the expansion of Φ (3.10). Without gauge fixing the quantities $\langle c_{lm} \rangle$ or $\langle \Phi_{ij} \rangle$ average to zero. But if we fix the gauge degrees of freedom the expectation values of the modes of Φ can be used as order parameters in order to distinguish between different phases of the theory.

3.7.2. Gauge fixing

During a simulation the configurations that are generated possess the aforementioned $SO(3) \times \mathbb{Z}_2$ freedom. We fix this freedom in steps. First we fix the $\mathbb{Z}_2$ part of the symmetry. To do so we check if $\mathrm{Tr}(\Phi) < 0$ and if so we change $\Phi \to -\Phi$. This way the $\mathbb{Z}_2$ symmetry is fixed and configurations of Φ which differ by sign would produce the same result. We note that $\langle \mathrm{Tr}\, \Phi \rangle$ can still be used as an order parameter.

In order to fix the $SO(3)$ symmetry we can rotate the field Φ into a particular basis before making measurements. The full rotation symmetry in $\mathbb{R}^3$ has three parameters. Usually they are chosen to be the Euler angles (ϕ, θ, ψ).[2]

[2] In this context the variable ϕ is a spherical coordinate and should not be mixed with the scalar field from (3.1)

First we find the coordinates of Φ in the coordinate system spanned by the three $su(2)$ generators. We do that by projecting Φ onto L_a using the inner product (2.17)

$$c_{1a} = \frac{4\pi}{N} \operatorname{Tr}(L_a \Phi^\dagger). \tag{3.42}$$

We form a vector $\vec{r} \in \mathbb{R}^3$ out of the coefficients c_{1a}. Now we can switch to spherical coordinates $(\rho_1, \phi_1, \theta_1)$ using the standard coordinate transformation. The angles ϕ_1 and θ_1 correspond to ϕ and θ in our $SO(3)$ symmetry. Our aim is to change the basis of Φ in such a way that it has only component along the L_3 direction.

First we gauge out the ϕ dependence. This angle corresponds to rotation around the z-direction which is parallel L_3. We can gauge-fix $\phi = 0$ or $\phi = \frac{\pi}{2}$ by applying the unitary transformation $U(-\phi, 0)$ or $U(\frac{\pi}{2} - \phi, 0)$ from (2.21). The first choice eliminates the component along L_2 and the second eliminates the component along L_1. We use the second transformation. We obtain

$$\Phi' = U^\dagger(\frac{\pi}{2} - \phi, 0)\Phi U(\frac{\pi}{2} - \phi, 0), \tag{3.43}$$

which does not have component along the direction of L_1.

Now we need to gauge-fix the second degree of freedom to $\theta = 0$. In order to rotate around L_1 we need to perform a unitary transformation $V(0, -\theta) = \exp(-iL_1\theta)$ on Φ'. There is a complication coming from the fact that L_1 is not diagonal in this basis and as a consequence the action of $V(0, -\theta)$ is not as simple as (2.21). We can either compute $V(0, -\theta)$ explicitly by exponentiation of L_1 or we can rotate into a basis in which L_1 is diagonal. In this basis $V(0, -\theta)$ will have a simple action. We choose the second option. We construct a unitary transformation $W^\dagger W = \mathbf{1}$ such that $W^\dagger L_1 W = L_3$. The generator L_1 is irreducible representation of $su(2)$. Thus it has N non-degenerate eigenvalues and eigenvectors. The transformation matrix W is constructed from the eigenvectors of L_1 as columns but normalized to 1 with respect to the usual complex Euclidean vectors dot product. Now we can perform the transformation on Φ' as follows

$$\Phi'' = W[V^\dagger(W^\dagger \Phi' W)V]W^\dagger. \tag{3.44}$$

After we perform the rotation around L_3 in the new basis, we return to the initial one by applying the inverse transformation. That way we produce the field Φ'' which has component only along L_3. For $\theta = 0$ the angle ϕ is undefined. At this point we have rotated the system in such way that the vector $\vec{r}$ has only c_{3a} non-zero component but its length is preserved. This can be used as a consistency check for the gauge-fixing code.

There is one more gauge degree of freedom left in Φ''[3] that we can fix associated with the third Euler angle ψ. This phase can be computed in different ways. Similarly to the first gauge degree of freedom we can compute the coefficient c_{21} (if we prefer we might work with $c_{2,-1}$ instead) and we can fix the direction of Φ'' in the 2-dimensional space spanned by $\mathfrak{Re}(c_{21})$ and $\mathfrak{Im}(c_{21})$. The angle ϕ is defined to be $\tan\psi = \frac{\mathfrak{Re}(c_{21})}{\mathfrak{Im}(c_{21})}$. We define ψ to be the phase of the element Φ_{21}. We set $\psi = 0$ by applying

$$\Phi''' = \exp(i\psi L_3)\Phi''\exp(-i\psi L_3). \tag{3.45}$$

Finally the field Φ''' has no $SO(3)$-associated freedom left. We can now measure the expectation values of the form $\langle c_{lm}\rangle$. We note that the gauge-fixing procedure is done after the Hybrid Monte Carlo update process thus it does not affect the equations of motion (3.30). It leaves $|\operatorname{Tr}\Phi|$, the value of the action S and C_v invariant.

3.8. Phase diagram

There are three known phases of the model in the parameter space $(\frac{rR^2}{N}, \lambda R^2)$. Two of them, disordered and uniform phase, correspond to the disordered and magnetized phases in the usual ϕ^4 field theory. The last one, which is known as matrix phase, is specific only to the matrix Φ^4 theory. The quantities that identify those phases and which are of interest to us are the specific heat $C_{\mathrm{v}} = \frac{\langle S^2\rangle - \langle S\rangle^2}{N^2}$, magnetic susceptibility defined as $\chi = \langle(\operatorname{Tr}(\phi))^2\rangle - \langle|\operatorname{Tr}(\phi)|\rangle^2$ [4] and the expectation value of the action S. Other quantities which are evaluated are

[3] In the case $N = 2$ the field does not have this degree of freedom.

[4] The usual definition of susceptibility is $\chi = \langle(\operatorname{Tr}(\phi))^2\rangle - \langle\operatorname{Tr}(\phi)\rangle^2$, but for finite size systems $\langle\operatorname{Tr}(\phi)\rangle = 0$, so we use the version with modulus, which has the desired properties.

eigenvalue distribution of the field and the modes with the biggest contribution (relative weight of coefficients c_{lm} in (3.11). In this section we describe the basic properties of Φ in each phase.

3.8.1. Disordered phase

For large enough λR^2 the contribution of the kinetic term is negligible in comparison to the potential terms of the action. The classical ground state is represented by $\Phi = 0$. This can be verified by a numerical measurement of the leading order terms in the expansion of Φ from (3.11). We have $\langle c_{00} \rangle \sim \langle c_{1i} \rangle \sim 0$. In this regime the system does not feel the $su(2)$ nature of the Laplacian and can be approximated by a pure potential model. The pure potential model is studied in [16]. An explicit form for the eigenvalue distribution of Φ is obtained which is symmetric around zero. It has the form

$$p(x) = \frac{1}{\pi}(b_0 + b_2 x^2)\sqrt{a^2 - x^2}, \tag{3.46}$$

with

$$\begin{aligned} a &= \sqrt{\frac{-\pi r R^2 + \sqrt{\pi^2 r^2 R^4 + 3\pi\lambda R^2 N^2}}{3\pi\lambda R^2}} \\ b_0 &= \frac{4}{3N^2}\left(2\pi r R^2 + \sqrt{\pi^2 r^2 R^4 + 3\pi\lambda R^2 N^2}\right) \\ b_2 &= \frac{8\pi\lambda R^2}{N^2}. \end{aligned} \tag{3.47}$$

The eigenvalue spectrum as obtained from a simulation and plotted along with the curve (3.46) are presented in Figure 3.1.

We plot the expectation values of the matrix entries $\langle \Phi_{ij} \rangle$ for $N = 7$ matrix in this phase in Fig. 3.2. We see that the contribution comes mainly from the diagonal entries which correspond to modes $c_{l,0}$ and from modes $c_{l,\pm 1}$. The rest of the entries of the matrix are essentially zero.

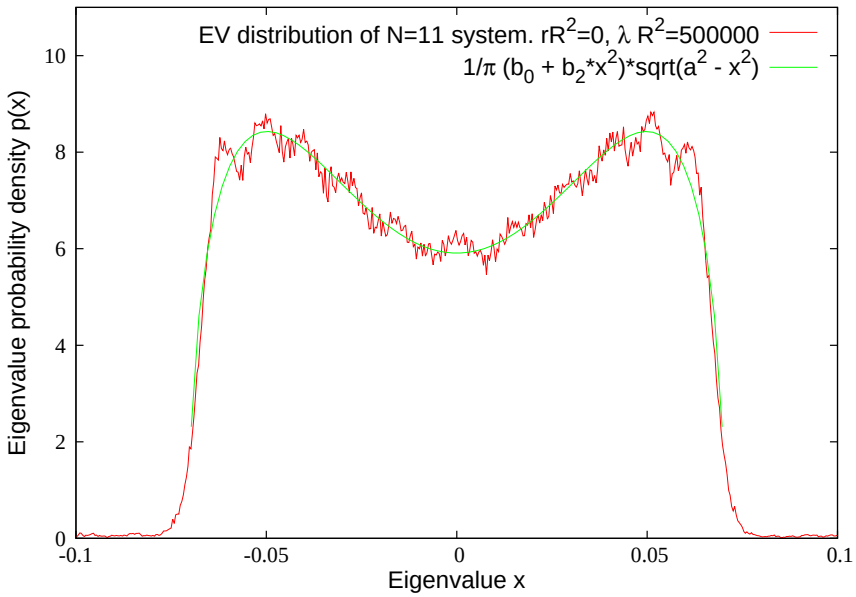

Figure 3.1.: Eigenvalue spectrum of $N = 11$ field obtained from simulation and the curve (3.46). A least squares fit produces for the parameters of the distribution $a = 0.07 \pm 0.001$, $b_0 = 264 \pm 2$ and $b_2 = 111 \times 10^3 \pm 1 \times 10^3$. These values are in a good agreement with the pure potential model prediction ($a \approx 0.071$, $b_0 \approx 263.12$, $b_2 = 104 \times 10^3$). This suggests that the pure potential model is a good approximation in this part of the phase diagram of the theory. The fluctuations around the theory prediction are mainly due to finite-size effects.

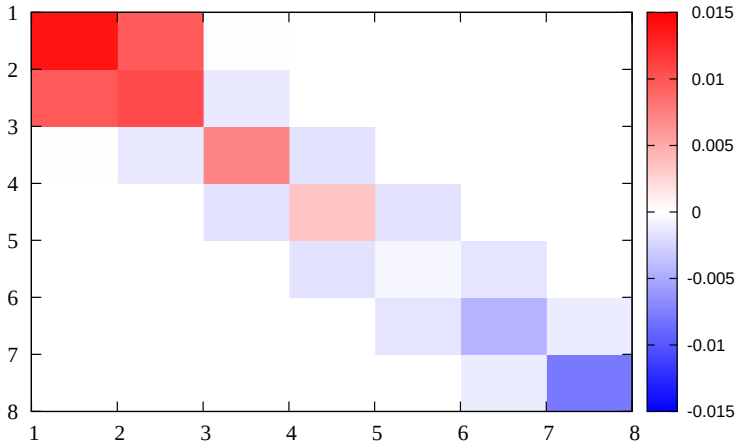

Figure 3.2.: Matrix entries of $N = 7$ matrix in disordered phase. $rR^2 = -10$, $\lambda R^2 = 545000$.

3.8.2. Matrix (ordered non-uniform) phase

As $-rR^2$ grows for a fixed λR^2 , the system enters a new phase. The configuration $\Phi = 0$ is no longer the ground state. The action is minimized for fields of the form $\Phi \sim \pm\sqrt{\frac{-r}{2\lambda}}U^\dagger(1_{N/2} \oplus -1_{N/2})U$ for $N = 2s$ and $\Phi \sim \pm\sqrt{\frac{-r}{2\lambda}}U^\dagger(1_{(N-1)/2} \oplus -1_{(N+1)/2})U$ for $N = 2s + 1$. What is typical for this phase is that $\langle c_{00}^2 \rangle < \langle \sum_m |c_{1m}|^2 \rangle$, i.e. the biggest contribution in the expansion of Φ comes from the higher order terms. Moreover because of the kinetic term, the modes c_{1m} have the biggest contribution. We have plotted the distributions of $|\operatorname{Tr}\Phi|$ and $|\operatorname{Tr}\Phi^2|$ for a system in the Matrix phase in Fig. 3.3.

The support of eigenvalue distribution consists of two separated domains. It is given by

$$p(x) = \frac{1}{\pi}c_0|x|\sqrt{(c^2 - x^2)(x^2 - d^2)}, \tag{3.48}$$

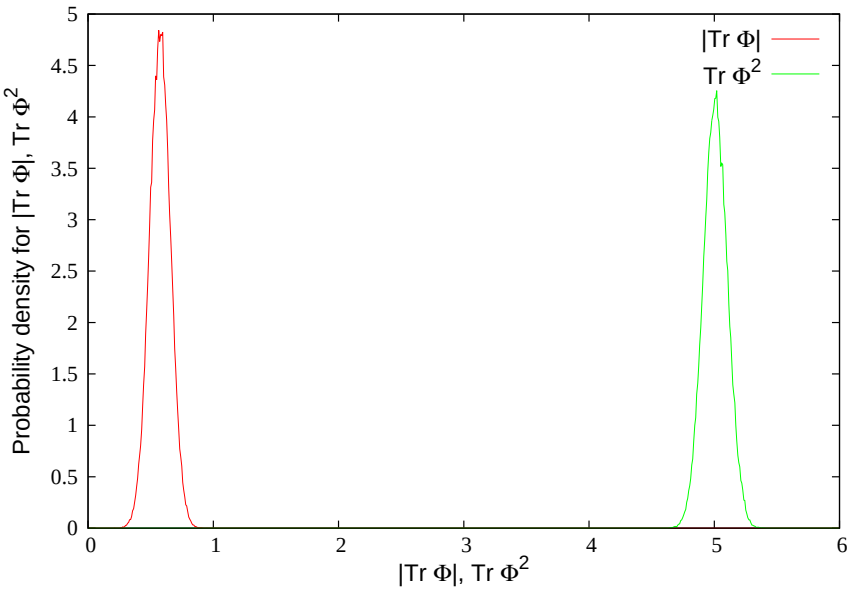

Figure 3.3.: Distribution for $|\operatorname{Tr}\Phi|$ and $|\operatorname{Tr}\Phi^2|$ for $N = 15$ system, $\tilde{r} = -728280.0$, $\lambda R^2 = 1020$, in matrix phase.

with

$$c_0 = \frac{8\pi\lambda R^2}{N}$$
$$c = \sqrt{\frac{\sqrt{\pi N\lambda R^2} - \pi r R^2}{4\pi\lambda R^2}}$$
$$d = \sqrt{\frac{-\sqrt{\pi N\lambda R^2} - \pi r R^2}{4\pi\lambda R^2}}.$$

The eigenvalue spectrum as obtained from a simulation is presented in Fig. 3.4.

We can further extend the matrix phase by configurations in which the biggest contribution comes from $\langle \sum_m |c_{km}|^2 \rangle$ with $m \geq 1$. For a system with size N the matrix phase is split in $\frac{N-1}{2}$ such sub-regions. We expect those configurations to play a role when the kinetic term is strongly suppressed. In order to detect those we need to gauge-fix Φ using the method described in §3.7. In Fig. 3.5 we present the matrix entries of Φ as averaged over a Monte Carlo run in that regime. The map of the matrix elements looks qualitatively similar to the entries in the

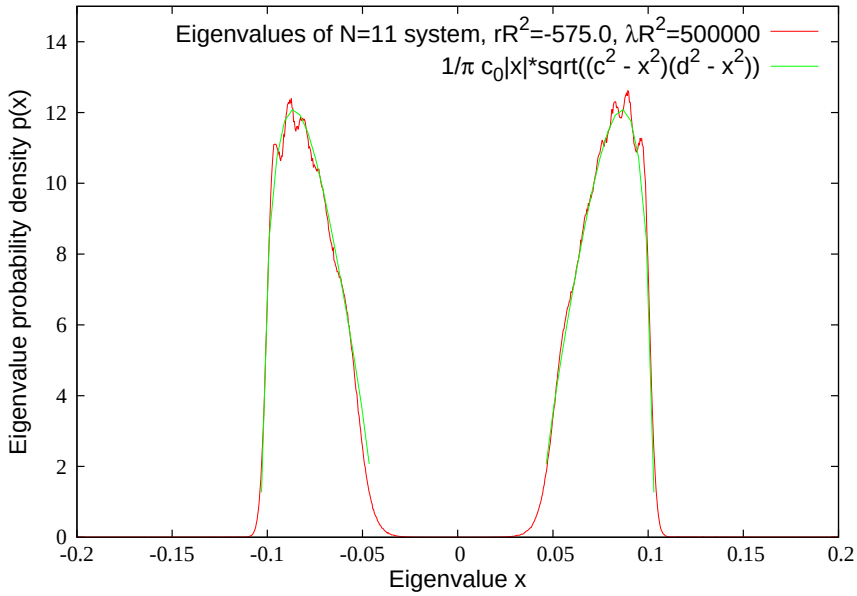

Figure 3.4.: Eigenvalue spectrum of 11x11 field obtained from simulation and the curve (3.48). Least squares fit produces for the parameters of the distribution $c_0 = 105{\times}10^3{\pm}0.2{\times}10^3$, $c = 0.103{\pm}3{\times}10^{-5}$ and $d = 0.044{\pm}5{\times}10^{-5}$.

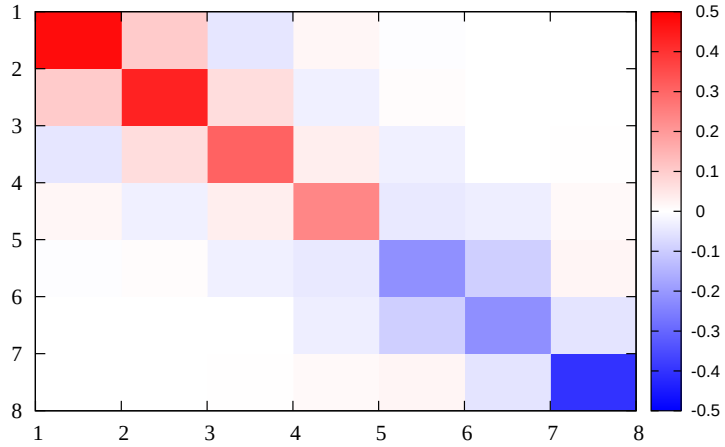

Figure 3.5.: Matrix entries of $N = 7$ matrix in ordered non-uniform phase. $rR^2 = -4100$, $\lambda R^2 = 5460$.

disordered phase 3.2. The major difference is that the amplitudes of the main—diagonal modes are bigger and there is a small contribution of the $c_{l,\pm 3}$ modes.

3.8.3. Disordered/Matrix phase transition

Deep into the disordered matrix phase the kinetic term is negligible. Therefore a reasonable approximation to the action is provided by the pure potential model

$$S[\Phi, N, r, R, \lambda] = \frac{4\pi}{N} \operatorname{Tr}\left(rR^2\Phi^2 + \lambda R^2\Phi^4\right). \tag{3.49}$$

The critical line between the two phases is defined as $(r_c R^2, \lambda R^2)$. It is a curve which consists of the points where distribution (3.46) transforms into (3.48). In the case of the commutative ϕ^4 theory the phase transition is known to be of second order [53]. Explicitly the curve in the pure potential approximation is

$$r_{\mathrm{c}} R^2 = -N\sqrt{\frac{\lambda R^2}{\pi}}. \tag{3.50}$$

In fact the presence of the kinetic term slightly changes the coefficient, but preserves the behavior of (3.50) as it becomes apparent from the numerical studies. As first order correction for large R in the case with kinetic term, we can try to replace (3.50) with

$$r_{\mathrm{c}} R^2 = -N\sqrt{\frac{\lambda R^2}{\pi}}\left(1 + \frac{B}{(\lambda R^2)^{\alpha}} + \cdots\right) \tag{3.51}$$

where B and α are constants which would be subject of our measurement.

3.8.4. Uniform phase

There exists one more phase of the system— the uniform ordered phase. It emerges for small $R^2 > 0$ and large enough $-r$. In this regime the kinetic term plays an important role. The classical background configuration is characterized by the property that the biggest contribution in the expansion of (3.10) comes from the constant term. In this case we can search for the minima of the action

by minimizing the potential and the kinetic term separately. From (3.15) it is evident that the kinetic term being positive definite penalizes modes with higher l. Therefore its minima $\mathrm{Tr}(\Phi[L_a,[L_a,\Phi]])=0$ are realized when $\Phi\sim T_{00}$ or $\Phi\sim 0$. Let us parametrize this solution as $\Phi = x\mathbf{1}$ and plug it into the pure potential part of the action (3.49). The classical solution for the action is obtained when

$$\frac{d}{dx}S[x\mathbf{1},N,r,R,\lambda]=0, \tag{3.52}$$

which has the form

$$x(2R^2\lambda x^2+rR^2)=0.$$

There are three solutions for the above equation

$$\Phi_\pm = \pm\sqrt{\frac{-r}{2\lambda}}\mathbf{1}_N \quad \text{or} \quad \Phi=0. \tag{3.53}$$

The trivial solution corresponds to a local maximum. If we look into the other two solutions we can see that the eigenvalues of Φ are distributed around $\pm\sqrt{\frac{-r}{2\lambda}}$. For the quantity $\langle|\,\mathrm{Tr}(\Phi)|\rangle$ classically we have

$$\left\langle\left|\,\mathrm{Tr}\left(\Phi\right)\right|\right\rangle = N\sqrt{\frac{-r}{2\lambda}}. \tag{3.54}$$

Numerical measurement of the eigenvalues of Φ and $|\,\mathrm{Tr}\left(\Phi\right)|$ is presented in Fig.3.6 and Fig.3.7. As it is evident from the simulations the peaks in the eigenvalues and $|\,\mathrm{Tr}\left(\Phi\right)|$ depend weakly on R^2. This is because R^2 essentially controls the relative importance of the kinetic term with respect to the potential terms. When R^2 grows the contribution of the kinetic term becomes negligible. In the limit $R^2\to\infty$ the model is expected to behave as the pure potential model.

The action of the classical solution is given by

$$S[\Phi,N,r,R,\lambda] = -\frac{\pi r^2R^2}{\lambda}. \tag{3.55}$$

The expectation value is thus $\langle S\rangle = -\frac{\pi r^2R^2}{\lambda}+\langle S_{fl}\rangle$, where $\langle S_{fl}\rangle$ represents the fluctuations of the system around the classical solution. Note that there are two

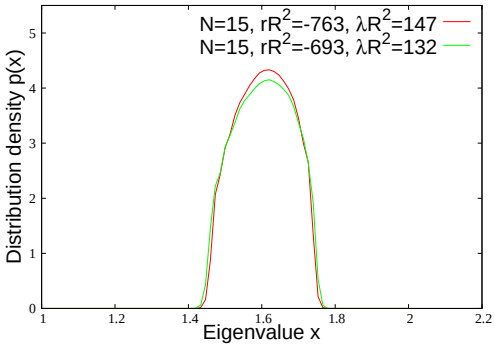

Figure 3.6.: Distribution of the eigenvalues of $N = 15$ system in uniform phase

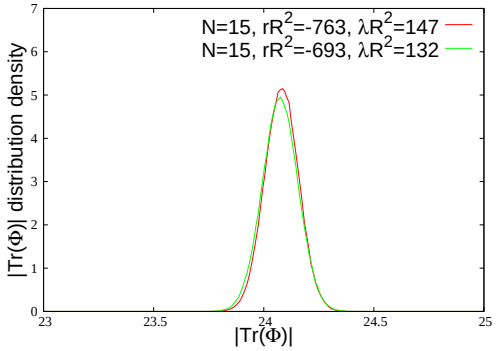

Figure 3.7.: Distribution of $|\operatorname{Tr}(\Phi)|$ of $N = 15$ system in uniform phase. The peak is dependent of R^2

local minima of the action, but they are related to each other by the discrete symmetry $\Phi \to -\Phi$. However the $SU(2)$ symmetry of the action is formally preserved as the identity element is invariant under the action of $SU(2)$. Thus the two solutions from (3.53) are stationary under the action of the group.

The non-zero modes of the system are suppressed as $\frac{1}{-r}$. In Fig. (3.8) we present the real part of the matrix elements Φ_{ij} of the field averaged over the Monte Carlo time. We can clearly see that the biggest contribution comes from the diagonal elements and moreover from the c_{00} mode of the matrix. We note that the action of the theory is invariant under the change $\Phi \to -\Phi$ and thus in this phase there are two local minima. Also c_{00} is invariant under the action of any unitary transformation being an $SU(N)$ scalar.

The transition between matrix and uniform phase is numerically found in [39], using a different parametrization, to be the straight line for each matrix size N defined by:

$$\lambda R^2 = krR^2 N^{-1/2} + NC, \tag{3.56}$$

where k and C are constants independent of N, subject to numerical measurement. Our simulations of small systems $N = 2, 3$ suggest that there is a coexistence of the phases near the transition line which is an indication of a first order phase transition.

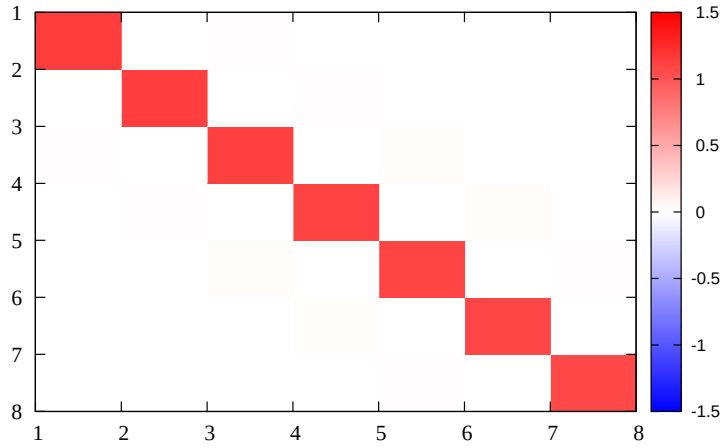

Figure 3.8.: The real part of $\langle \Phi_{ij} \rangle$ of matrix of size $N = 7$ into the uniform ordered phase. $rR^2 = -103$ and $\lambda R^2 = 40.6$.

3.8.5. Triple Point

We have defined two critical curves for the different phase namely (3.50) and (3.56). Naturally comes the question is there a triple point? A place in the diagram where all the three possible phases coexist. To answer this question we need to solve a system of 2 equations in the variables λR^2 and rR^2

$$\left| \begin{array}{l} rR^2 = -\sqrt{\frac{N^2 \lambda R^2}{\pi}} - \sqrt{\frac{N^2 \lambda R^2}{\pi}} \frac{B}{(\lambda R^2)^\alpha} \\ rR^2 = -\frac{(\lambda R^2 - CN) N^{1/2}}{k}. \end{array} \right. \tag{3.57}$$

The above system is a transcendental system of equations with parameters B, C, k and α. A closed form solution is not possible to obtain for arbitrary α. However if we simply assume $\alpha = 1/2$, we can write down an explicit formula for the coordinates of the triple point in the $(rR^2, \lambda R^2)$ plane. The simplified system has the form:

$$\left| \begin{array}{l} rR^2 = -\sqrt{\frac{N^2 \lambda R^2}{\pi}} - B\sqrt{\frac{N^2}{\pi}} \\ rR^2 = -\frac{(\lambda R^2 - CN) N^{1/2}}{k}. \end{array} \right. \tag{3.58}$$

The solutions of the system in that case are given by

$$\left| \begin{array}{l} rR^2 = -\frac{BN+CN^2}{kN^{1/2}+\pi^{1/2}} \\ \sqrt{\lambda R^2} = -\frac{N(Bk-CN^{1/2}\pi^{1/2})}{kN^{1/2}+\pi^{1/2}}. \end{array} \right. \tag{3.59}$$

If we know the parameters B, C, and k, the above solutions specify the coordinates of the triple point in the case of $\alpha = 1/2$ and also give a hint of where to search for it in case of $\alpha \approx 1/2$.

3.9. Eigenvalue separation criterion

The critical line between disordered and matrix phase consists of points $r_c = r_c(R)$, where the eigenvalue distribution changes from (3.46) to (3.48). In the large N limit when the system is at a critical point the eigenvalue distribution of Φ satisfies

$$p(x) \neq 0 \quad for \quad x \in [-a, a]/\{0\}$$

i.e. $p(x)$ is non-zero in some finite interval symmetric around zero and $p(0) = 0$. When we are dealing with a finite system, this is not the case as there are fluctuations, which would smooth out the distribution leading to $p(0) \neq 0$. In fact for a finite ensemble (number of configurations as produced from our simulation), the $p(0) \neq 0$ will appear even when the system is deep into the non-uniform ordered phase. So in order to use the eigenvalue distribution to pinpoint a phase transition in a reproducible manner, we need to define an objective algorithmic criteria which could be described and later reused. There are a few ways we can proceed.

1. One can try to extract the analytical properties of $\partial_x p(r, R, x)|_{r=r_c(R),x=0}$. We see that one should expect a change in the analytical properties of the function. However, dealing with numerical derivatives is unstable and leads to very big errors, not to mention the additional complication coming from the fluctuations around the ground state, which will render the method useless.

2. The approach used in this work is based on a different idea. We count the number of eigenvalues generated during the simulation which fall into some finite interval $[-q, q]$ around the origin. Then we compute the ratio of those situated in the interval with respect to the whole number of all generated eigenvalues which is given by $N \times N_s$. Here N is the matrix size (which corresponds to the number of eigenvalues of the matrix Φ per configuration) and N_s is the number of generated configurations of Φ. This gives us the probability $P(x \in [-q, q])$. If $P(x \in [-q, q])$ is smaller or greater then a predefined small number δ, we say that the system is either in the matrix phase or in the disordered phase. And if $\delta - \eta < P(x \in [-q, q]) < \delta + \eta$, with $\eta \ll \delta$, we say that the system is within the neighborhood of the phase transition. This means that instead of a critical point we talk about an interval in which the transition occurs. The parameter 2η then could be used as error estimation.

The weakest point of the employed method is that one should choose the parameters of the algorithm (q, δ, η) by hand. On the other hand once we have fixed them, the same algorithm/method can be used by others to check if the results are reproducible. The only argument for choosing the values of the parameters comes from the fact that the domain where the probability (3.46) is not zero depends on the parameters $(R^2 r, \lambda R^2)$. Basically the domain of interest is given by a from (3.47). In this work, we rely on an algorithmic evaluation of the width of the distribution[5]. In Fig.3.9 we have shown schematically the non-zero domain $[-a, a]$ of a distribution of a system deep into the disordered phase. The parameter p of our algorithm is chosen as $q = a/10$, corresponding to the smaller region. In this way we always examine a region around the origin, which is 1/10 part of the domain of interest, irrelevant of matrix size and system parameters. For the other two parameters of the algorithm δ and η, we don't have any objective guide, so we will fix them at some particular values and try to check if the algorithm shows agreement with the theoretical predictions for the system. In this work we have chosen $\delta = 0.003$, which corresponds to 3σ, i.e. for a system close to the

[5]The reason we don't use the analytic expression is because equations (3.46) and (3.48) strictly speaking only hold for the pure potential model. And we want to study the full system for which we don't have analytical expressions, but which we expect to behave in a similar way in this region of the phase diagram.

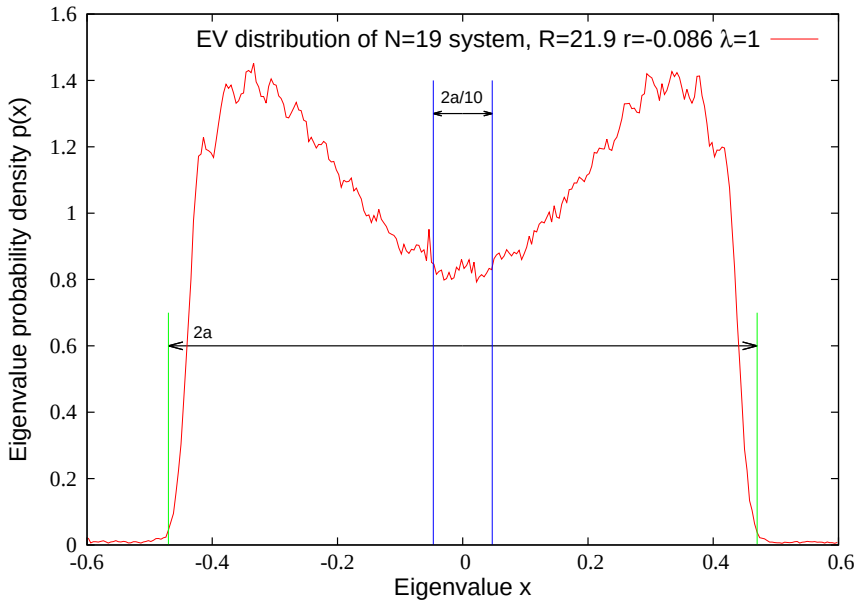

Figure 3.9.: Eigenvalue spectrum of $N = 19$ system in Disordered phase.

phase transition eigenvalues in the interval $[-q, q]$ are essentially "3σ" events.[6] The parameter which describes the uncertainty η is set to 0.0005.

3.10. Simulation results and comparison with theoretical predictions

As we have defined the methods we are using, we can now turn to comparison with the theory predictions. Before we proceed we switch to the alternative parametrization of the theory used in [39]

$$\kappa = \frac{4\pi}{N} \quad \bar{b} = \frac{4\pi r R^2}{N} \quad \bar{c} = \frac{4\pi\lambda R^2}{N}. \tag{3.60}$$

Again only two of the three parameters are independent. In the new parametrization the action has the form

$$S[\Phi] = Tr\left(\kappa \sum_a \Phi[L_a, [L_a, \Phi]] + \bar{b}\Phi^2 + \bar{c}\Phi^4\right). \tag{3.61}$$

[6] By σ we denote standard deviation.

The reason for the change is that while the parameters from (3.6) have a natural physical interpretation, the new set of parameters appears to be more convenient if our goal is to study the phase diagram of the model. In [39] it was found that the transition curve between disordered and matrix regimes is independent of N in terms of the scaled variables

$$b = \frac{\overline{b}}{\kappa N^{3/2}} \quad c = \frac{\overline{c}}{\kappa^2 N^2}. \tag{3.62}$$

As the theory predictions are obtained in the $N \to \infty$ limit our numerical results should converge to the theoretical estimation as the matrix size grows. That is why we perform our measurements with different matrix sizes.

3.10.1. Simulating the pure potential model

First we start with the pure potential model, (3.49) as we have more analytical control over it, also we can use it to calibrate the parameters of our eigenvalue separation criteria from §3.9. In the new parametrization the transition curve has the form

$$c_{dm} = \frac{(-b)^2}{4}. \tag{3.63}$$

We have identified the critical point between the disordered and ordered phase for different matrix sizes and superimposed them with the curve from (3.63). The numerical data are presented in Fig. 3.10. We can see from the data that as the system size N increases the data converge to the theoretical prediction. This demonstrates, that we have an algorithmic method to detect the phase transition which agrees with the known results for the pure potential model, and we can rely on it for the more complex model (3.6).

3.10.2. Disordered to non-uniform phase transition. Full system

In the previous section we demonstrated that the transition between the disordered and matrix phases of the pure potential model is described by the analytical

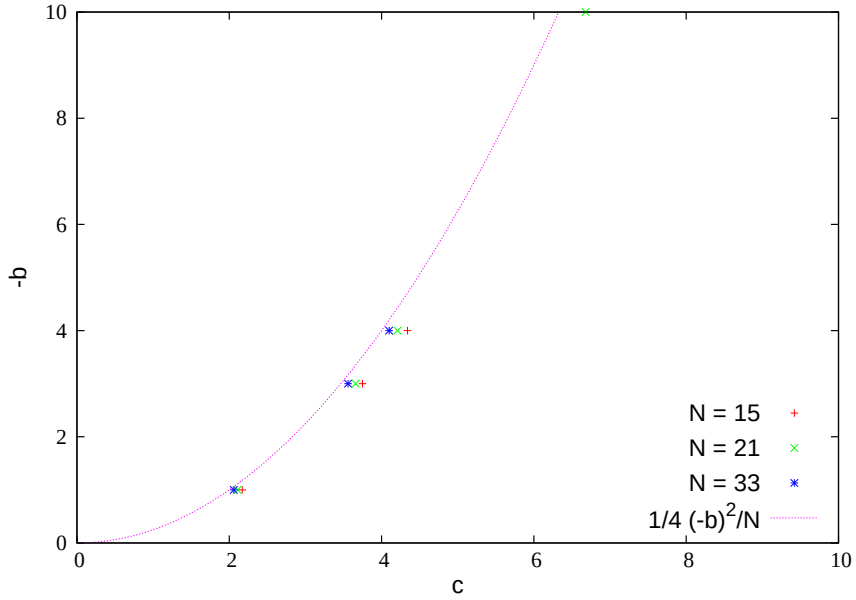

Figure 3.10.: Pure potential model. The uncertainties are small in comparison to the symbol size and therefore omitted.

result (3.63). However we expect deviations from the above curve if we include the kinetic term. In Fig. 3.11 we present transition points for the $N = 15$ system with $\kappa = 0$ and $\kappa = \frac{4\pi}{N}$. From the figure we can see that the kinetic term brings corrections to the transition curve as expected. The model with the kinetic term included has not been solved exactly. Therefore we resort to our numerical studies of the transition. In Fig. 3.12 we present the transition curve as obtained for different matrix sizes. From the data we can see that the corrections due to the kinetic term are dependent on N. Our strategy is to use the data from our biggest matrix size simulation ($N = 45$) as it is our best estimation of the transition in the large N limit. Our three parameter fit produces

$$c_{dm} = (12 \pm 2) - (2 \pm 0.17)(-b) + (0.254 \pm 0.002)(-b)^2. \tag{3.64}$$

3.10.3. Non-uniform to uniform phase transition

We proceed with our study of the transition between the matrix phase and the uniform phase. The uniform phase is defined in §3.8.4 to be a phase where the biggest contribution to Φ comes from the constant term or $\langle |Tr\Phi| \rangle \gg \sqrt{\left\langle \sum_{l=1}^{N-1} |c_{lm}|^2 \right\rangle}$.

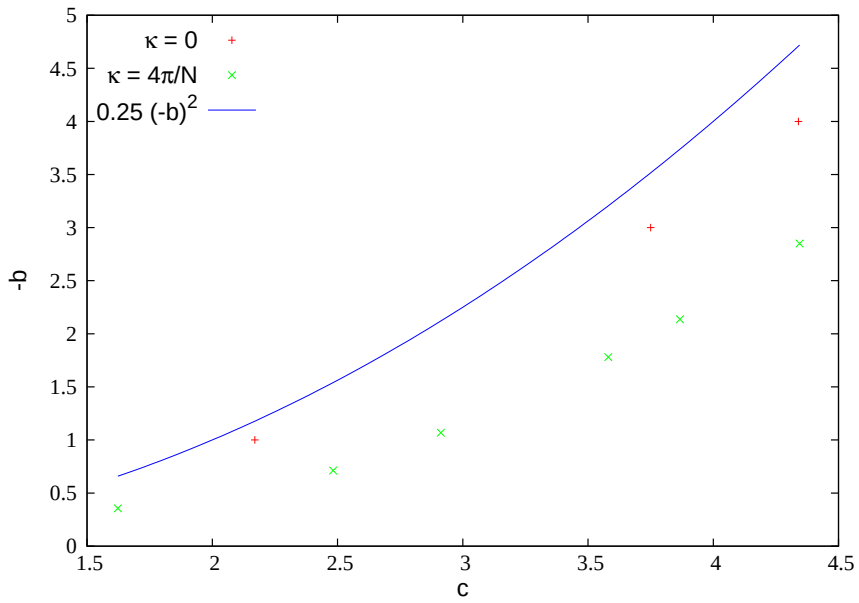

Figure 3.11.: Comparison between the transition curve for $N = 15$ system with or without kinetic term included. The uncertainties are small in comparison to the symbol size and therefore omitted.

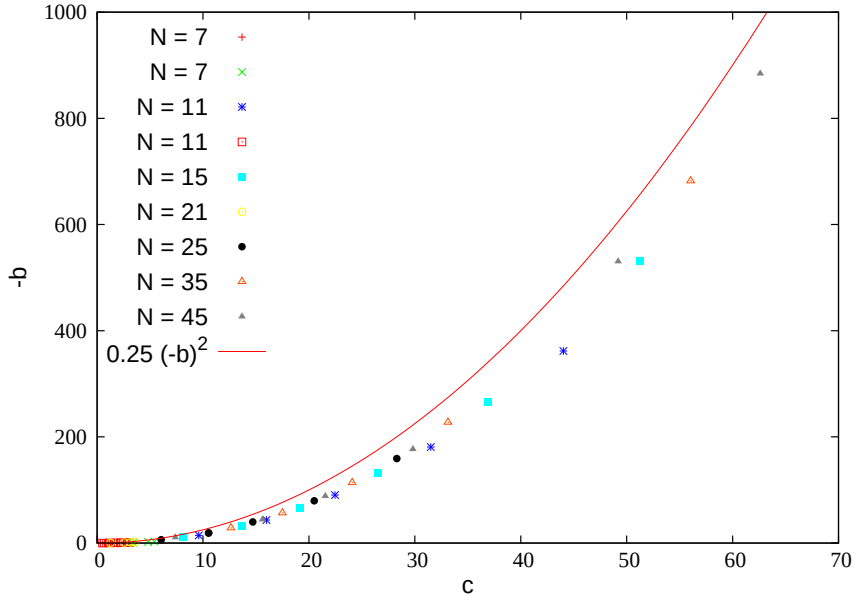

Figure 3.12.: Numerically obtained Disordered/Matrix phase transition curve for different size systems together with theoretical curve for the pure potential model. The uncertainties are small in comparison to the symbol size and therefore omitted.

One way to detect the transition is to compare the relative magnitude of the different modes of Φ having in mind that they might scale differently with the matrix size N. Another way, which is less ambiguous is to search for a peak of the specific heat of the system C_v. The two definitions don't necessarily agree. In Fig. 3.13 and 3.14 we present the specific heat and the order parameters $|Tr\Phi|$ and $Tr\Phi^2$ of $N = 2$, $b = -2.5$ system.

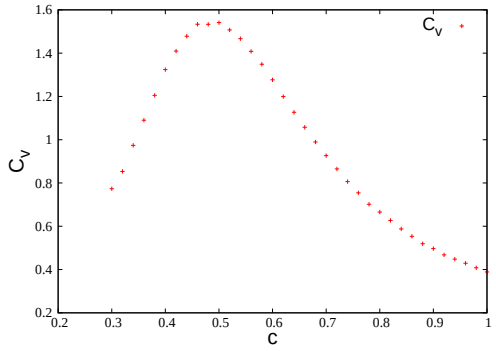

Figure 3.13.: Specific heat near the matrix/uniform phase transition of $N = 2$ system. For $b = -2.5$ as function of c. The uncertainties are small in comparison to the symbol size and therefore omitted.

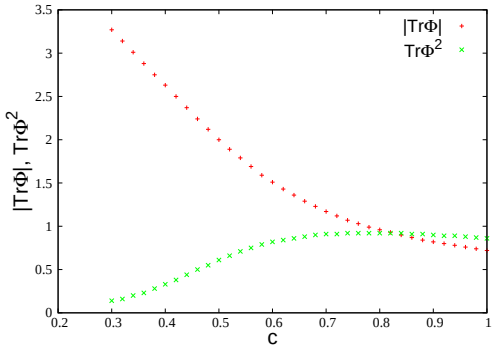

Figure 3.14.: Expectation values of $|Tr\Phi|$ and $Tr\Phi^2$ near the matrix/uniform phase transition of $N = 2$ system. For $b = -2.5$ as function of c. The uncertainties are small in comparison to the symbol size and therefore omitted.

In the (b, c) parameter space the transition is expected to occur on a straight line

$$c_{mu}(N) = K_1(N)(-b) + K_2(N). \tag{3.65}$$

As pointed out in [56, 39] this transition is hard to detect because of the big energy barrier between the local minima which characterize the two regimes. In the vicinity of a first order transition the phenomenon of phase coexistence occurs—the system can exist in each of the phases. An efficient Monte Carlo simulation should be able to drive the system between the two competing regimes. Our HMC algorithm based on (3.30) can explore the phase transition efficiently only for systems with size $N = 2, 3$. As an illustration of the numerical difficulties and

we present the Monte Carlo history of the action of $N = 2$ and $N = 3$ systems near the Matrix/Uniform phase transition in Fig. 3.15 and 3.16. We can see that 10^6 Monte Carlo steps are enough to measure the observables of the $N = 2$ system with good precision, but for the $N = 3$ system we need significantly more steps. For completeness we also include histograms which represent the probability distribution of the action of the system corresponding to these runs in Fig. 3.17 and 3.18.

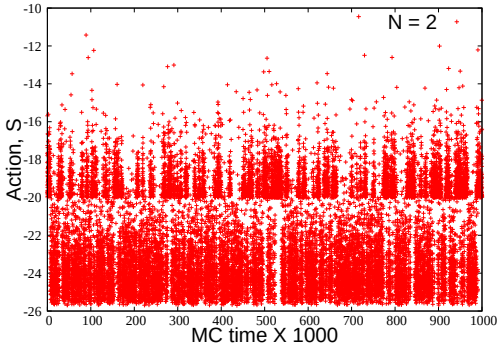

Figure 3.15.: Monte Carlo history of the action of $N = 2$ system near the Uniform/Non-Uniform phase transition.

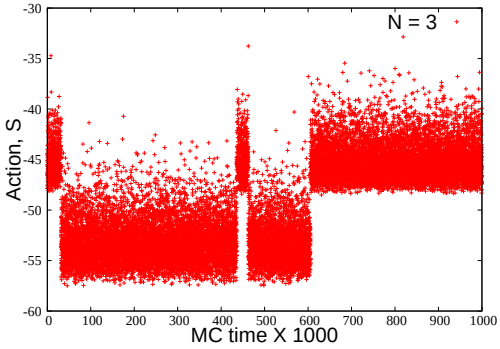

Figure 3.16.: Monte Carlo history of the action of $N = 3$ system near the Uniform/Non-Uniform phase transition.

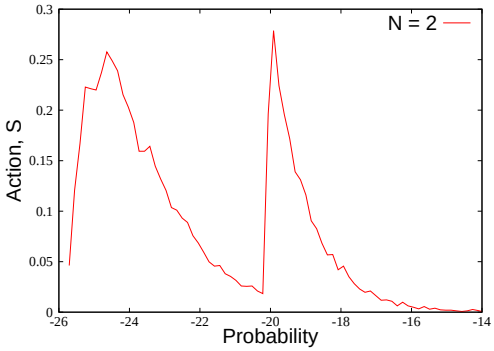

Figure 3.17.: Probability distribution of the action of $N = 2$ system near the Uniform/Non-Uniform phase transition.

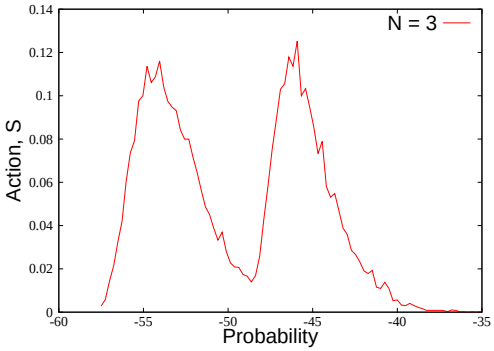

Figure 3.18.: Probability distribution of the action of $N = 3$ system near the Uniform/Non-Uniform phase transition.

Using the above criterion for the phase transition point we are able to detect the phase transition for $N = 2$ and $N = 3$ systems. The data are presented in

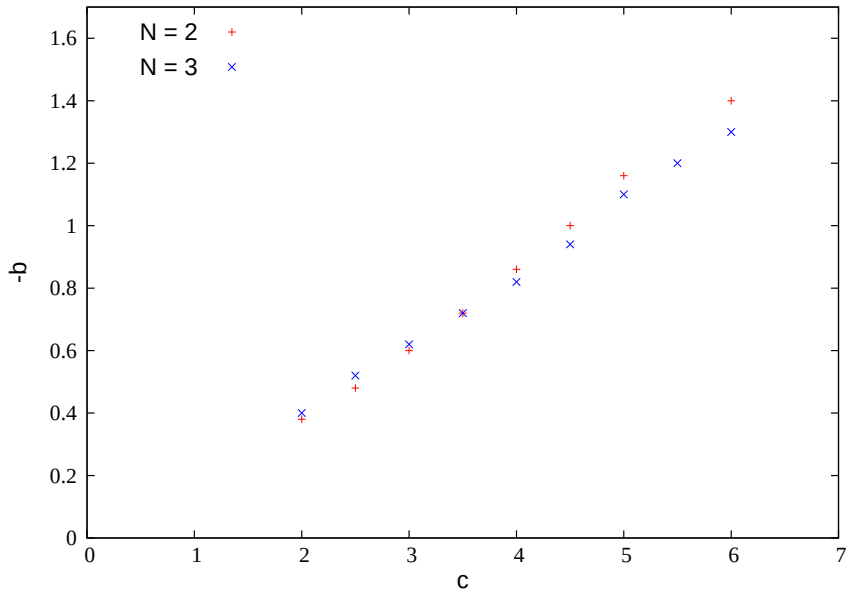

Figure 3.19.: Numerically obtained transition lines between Uniform and Non-uniform phase for $N = 2$ and $N = 3$ systems. The uncertainties are small in comparison to the symbol size and therefore omitted for clarity.

Fig. 3.19. Linear fits of those data produce $c_{mu}(N = 2) = (0.261 \pm 0.006)(-b) + (-0.17 \pm 0.02)$ and $c_{mu}(N = 3) = (0.227 \pm 0.005)(-b) + (-0.06 \pm 0.02)$. Our algorithm does not allow us to efficiently determine the transition line between the matrix phase and the uniform phase for models with $N \geq 4$. We need an algorithm which is specially designed bring the system out of the local minima of the action while preserving the detailed balance condition. Such algorithm has been proposed in [39].

3.10.4. Non-uniform to uniform phase transition for bigger systems

As we showed in the previous section, our algorithm cannot determine the transition between the matrix phase and the uniform phase for matrices with $N > 4$. Since the potential wells of the theory grow with the matrix size N, the system tends to stay trapped when it finds a local minimum of the action. In other words we expect *ergodicity breaking* in the large N limit. This means that the result of our simulations will depend on the initial configurations of Φ. This is illustrated

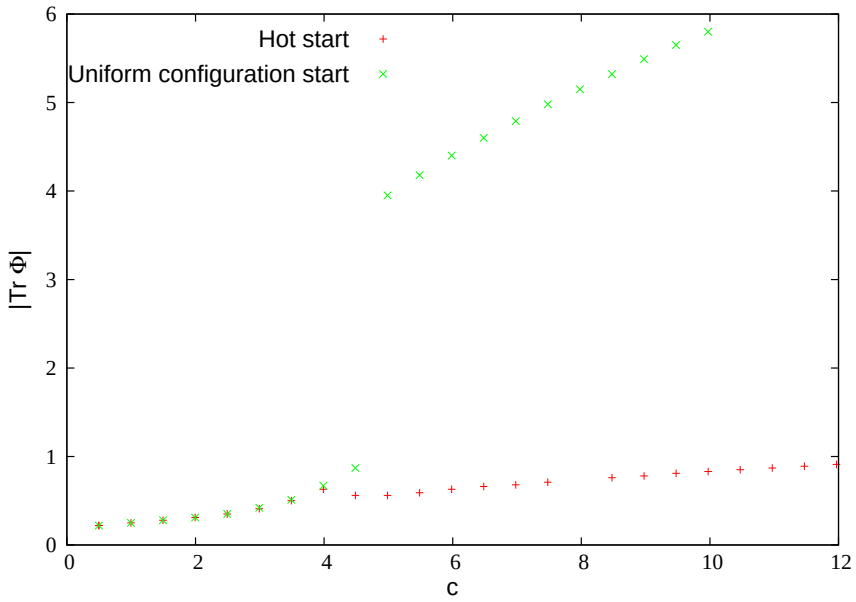

Figure 3.20.: The order parameter $|Tr\Phi|$ for $N = 7$ system, $c = 4.83$ as function of b. The system is simulated from hot start and from uniform initial configuration. The uncertainties are small in comparison to the symbol size and therefore omitted for clarity.

in Fig. 3.20. From this data we see that the outcome of the numerical simulation is dependent on the initial conditions. In order to properly determine the ground state we also compare the energies of the system in the two local minima. In Fig. 3.21 we present the action of the same systems. The plot shows that the action of the uniform phase is lower. Therefore we interpret that phase as the ground state. This scheme does not allow us to properly determine the transition point from (3.65) but rather gives us an upper bound for the value of $c_{mu}(N)$.

Proceeding this way we estimate the transition curve between the Matrix and Uniform phases. The numerical results for a few matrix sizes are shown in Fig. 3.22. Our data confirm that the transition curve is a straight line of the form (3.65). However the transition points for different matrix sizes do not collapse in the (b, c)-phase diagram and the parameters $K_1(N)$ and $K_2(N)$ are indeed functions of the matrix size N. This is in contrast with the transition between disordered and matrix phase. On table 3.1 we present the results from the fits of our data for $K_1(N)$ and $K_2(N)$ for different matrix sizes.

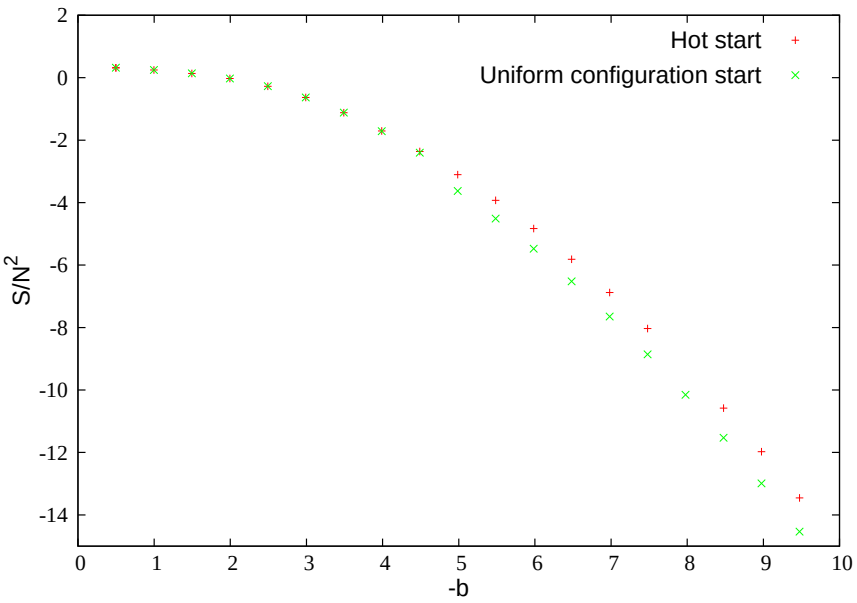

Figure 3.21.: The action per degree of freedom S/N^2 for $N = 7$ system, $c = 4.83$ as function of b. The system is simulated from hot start and from uniform initial configuration. The uncertainties are small in comparison to the symbol size and therefore omitted for clarity.

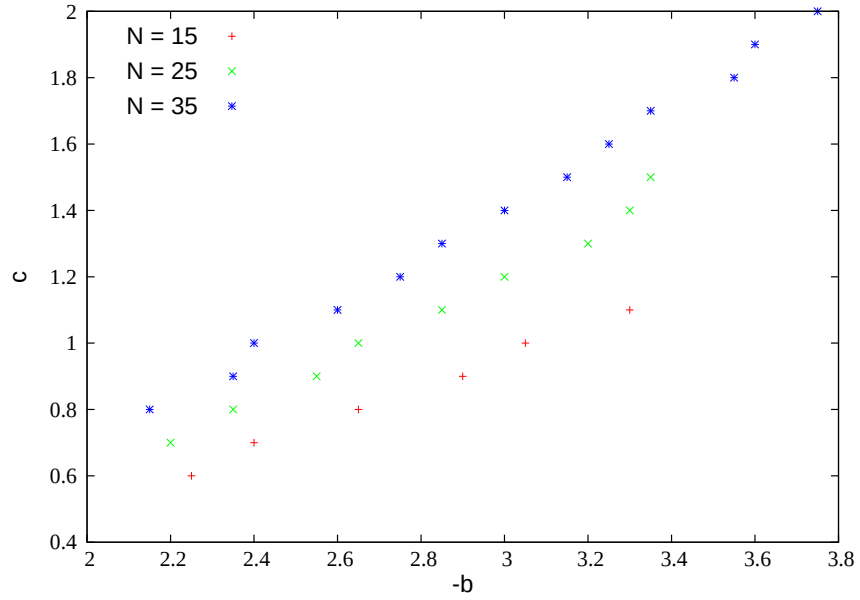

Figure 3.22.: Transition curve between Matrix and Uniform phases of systems with different size. The uncertainties are small in comparison to the symbol size and therefore omitted for clarity.

3.10.5. Numerical obtained phase diagram

As we demonstrated in §3.10.3 our estimate of the transition curve between the non-uniform and uniform phases of the system is dependent on the matrix size N. Here we present the phase diagram of the theory for a $N = 7$ system and give estimation of the coordinates of the triple point. In Fig. 3.23 we present the phase diagram. Our data points are compatible with the form of (3.63) and (3.65). For the transition curve between disordered and matrix phase we have $c_{md} = 0.107 \pm 0.003(-b)^2$. The transition between matrix and uniform phases is given by the line $c_{mu} = (-1.25 \pm 0.22) + (0.61 \pm 0.04)(-b)$. The transition between the disordered and uniform phase is $c_{du} = (-0.04 \pm 0.01) + (0.251 \pm 0.007)(-b)$. We interpret the meeting point of the two curves as the triple point. It has coordinates $(-b_{tr},\, c_{tr}) = (2.07 \pm 0.06,\, 0.47 \pm 0.02)$. This is close to the value reported in [39] which is $(-b_{tr},\, c_{tr}) = (2.3,\, 0.52)$ but does not fully agree. We explain this difference with the problems of our algorithm to properly identify the uniform to non-uniform phase transition.

3.10.6. Stripe phases

As we already saw in the Disordered and Uniform phases the field Φ contains only modes c_{lm} with $m = 0$ which correspond to diagonal matrices. In the matrix phase there might exist sub-regions in which the ground state of Φ contains modes c_{lm} with $|m| > 0$ with non-zero expectation value. We call these regimes of the theory *stripe phases*.

Table 3.1.: Fit of the numerical data for the transition between matrix and uniform phase.

N	K_1	K_2	σ_{est}
7	-1.25 ± 0.22	0.61 ± 0.04	0.18
15	-0.44 ± 0.05	0.47 ± 0.02	0.06
25	-0.74 ± 0.07	0.65 ± 0.03	0.03
35	-0.85 ± 0.05	0.76 ± 0.02	0.03

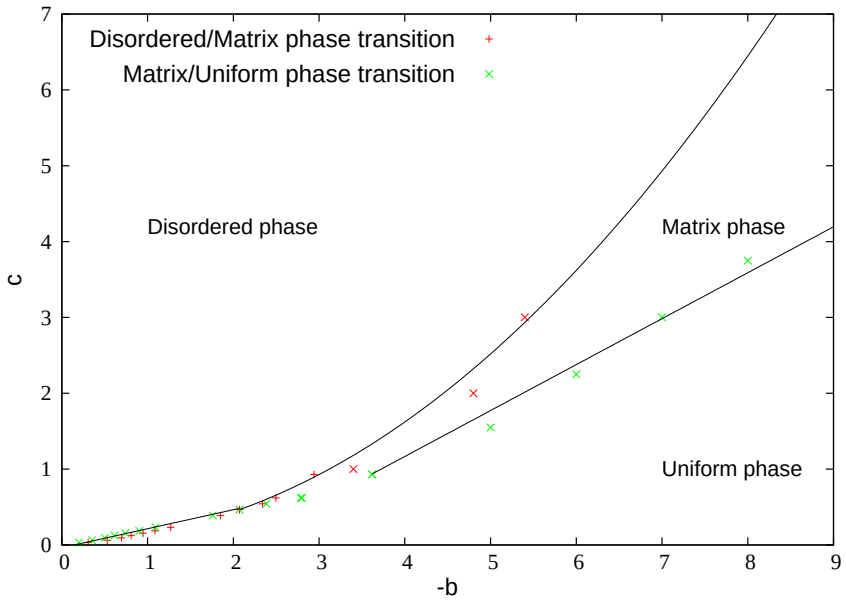

Figure 3.23.: Phase diagram of $N = 7$ system, together with fits of the transition curves between the three phases. The uncertainties are small in comparison to the symbol size and therefore omitted for clarity.

Before we start to search for such configurations we need to understand the roles the different modes of the field play in the different terms of the action. It is convenient to look into the terms in momentum representation. From (3.14) we can see that all modes contribute on equal footing to mass term. From (3.15) we can see that the kinetic term penalizes modes with momentum l by factor of $l(l+1)$. Thus in the regions of the phase diagram where the kinetic term is important we expect only modes with low l and correspondingly low m to be non-zero. For that reason we expect modes with higher l to contribute only when the kinetic term is negligible. The relative contribution from different modes to the self-interaction term (3.18) is not as clear as in the case of the other two terms. For that reason we try to study the relative contribution of the modes deep into the disordered phase as we vary the parameter c. We have performed simulations for an $N = 7$ system with parameters $\kappa = 1$, $b = -1$ and c in the interval [5, 20000]. According to our numerical results in the disordered phase the main contribution always comes from modes $c_{l,\,m=0}$ and $c_{l,\,m=\pm1}$ thus we conclude that the quartic term suppresses modes with $m \geq 2$. This is demonstrated in Fig. 3.24 and 3.25. We see that even when $c \gg \kappa$ and therefore the kinetic term is small, the modes with higher momentum are suppressed.

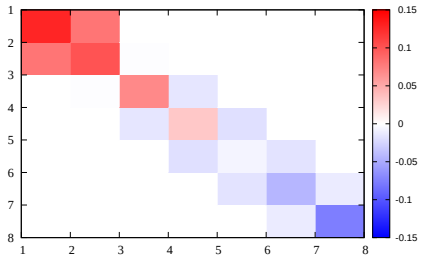

Figure 3.24.: The real part of the gauge-fixed entries of the matrix Φ as averaged over a Monte Carlo simulation in Disordered phase, close to the triple point. $b = -1$, $c = 5$, $N = 7$.

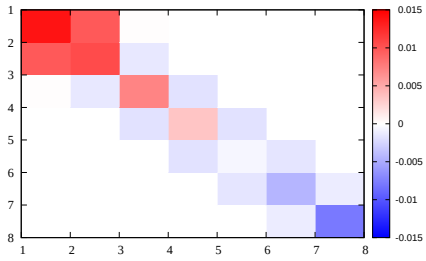

Figure 3.25.: The real part of the gauge-fixed entries of the matrix Φ as averaged over a Monte Carlo simulation deep into the Disordered phase, $b = -1$, $c = 20000$, $N = 7$.

The above results suggest that the higher momentum modes can have non—negligible contribution only deep into the matrix phase. In Fig. 3.26 and 3.27 we present the matrix entries of Φ in the matrix phase in a region close to the triple point and far away from the triple point but deep into matrix phase. From a comparison of the graphs we can see that indeed far away from the disordered phase and uniform phase the modes with higher momentum m have higher relative contribution. In the first case when the system is close to the triple point, the main contribution comes from modes $c_{l,\, m=0,\pm 1}$. On the other hand when the system is deep into the matrix phase there is a contribution of modes with momentum up to $m = 3$.

3.11. Final remarks

In this chapter we presented a matrix regularization of the scalar field theory in terms of matrix model in two different bases. The two approaches are equivalent but give different insight into the dynamics and the structure of the theory. We derived a HMC algorithm based on (3.6). We studied the phase diagram of the theory and showed the existence of regions in the matrix phase where the different

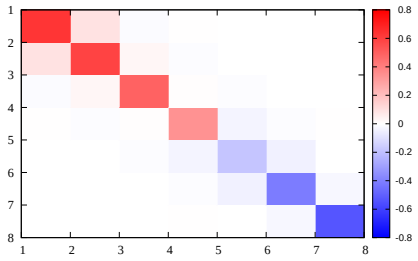

Figure 3.26.: The real part of the gauge-fixed entries of the matrix Φ as averaged over a Monte Carlo simulation in Matrix phase, close to the triple point. $b = -3$, $c = 1$, $N = 7$.

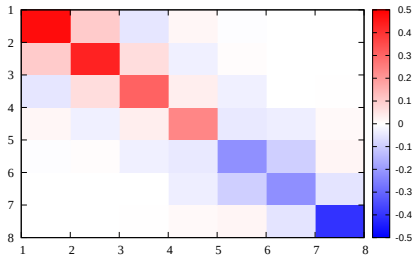

Figure 3.27.: The real part of the gauge-fixed entries of the matrix Φ as averaged over a Monte Carlo simulation deep into the Matrix phase, $b = -400$, $c = 200$, $N = 7$.

normal modes have different contribution to the matrix Φ— the so called stripe phases. Using our algorithms we were able to observe stripe phases for systems with size up to $N = 25$. However the question of their existence in the $N \to \infty$ limit cannot be answered by numerical studies and remains open. There are more open questions as regard to this model. An interesting numerical task would be an identification of the critical curves where higher modes of the field are excited. Yet another direction of research could be a study of the phase diagram of the model with higher order kinetic term as formulated in 3.6. Our preliminary results suggest that the higher order derivative term indeed suppresses the stripe phases and the matrix phase of the model, as we expected. A direct comparison of the matrix regularization to the lattice approach is possible if one studies numerically the model quoted in [31] as it should have continuum ϕ^4 theory in its large N limit.

Chapter 4.

Simulating the Three Matrix Model

When matrix models are considered as statistical mechanical systems, important questions to be addressed are: what phases do they exhibit and are the usual thermodynamic critical exponent relations valid? In this chapter we try to demonstrate the finite-size scaling properties of a matrix model which consists of Yang-Mills and Myer's terms using numerical techniques. The model has been studied extensively in [66, 25, 26] by numerical techniques. In [5, 6] some perturbation calculations have been carried out as well.

The structure of this chapter is as follows. In §4.1 we describe the model along with its main features following [26, 5]. Next in §4.2, §4.3, and §4.4 we discuss the different phases of the theory. In §4.5 and §4.6 we develop two Hybrid Monte Carlo algorithms that can be used for numerical studies of the theory. In §4.7 we discuss the difficulties that arise when one studies critical systems using numerical techniques.

4.1. Overview of the model

The model under consideration provides an example for a system which radically changes its geometric properties across a phase transition in its parameter space. On the low-temperature side the system has the features of the fuzzy sphere S_F^2. This geometry completely disappears across a critical point.

Let X_a, $a = 1, 2, 3$, be three traceless N-dimensional hermitian matrices. We consider the action (really the energy functional divided by temperature, as all our considerations will be in Euclidean signature)

$$\mathcal{S}[X] = N \operatorname{Tr}\Big(-\frac{1}{4}[X_a, X_b]^2 + \frac{2ig}{3}\epsilon_{abc} X_a X_b X_c \Big), \tag{4.1}$$

where ϵ_{abc} is the totally antisymmetric Levi-Civita symbol, $g \in \mathbb{R}$ is a parameter of the model. An important feature of the action (4.1) is that it is real for all hermitian matrices X_a. The change $g \to -g$ is clearly equivalent to $X_a \to -X_a$, therefore it will be sufficient to restrict our study to the case $g \geq 0$, which we shall assume. This model has a first order phase transition [5, 66]. The expectation value of a generic observable A of the theory is defined via the path integral

$$\langle A \rangle = Z^{-1} \int A[X] e^{-\mathcal{S}[X]} dX, \quad \text{where} \quad Z = \int e^{-\mathcal{S}[X]} dX \tag{4.2}$$

and

$$dX = \prod_{a=1}^{3} \prod_{i=1}^{N} \prod_{j=1}^{i} d\mathfrak{Re}((X_a)_{ij}) d\mathfrak{Im}((X_a)_{ij}) \delta(\operatorname{Tr} X_a). \tag{4.3}$$

In the above measure by $\delta(\operatorname{Tr} X_a)$ we denote Dirac δ-function which eliminates the contribution from the matrices with non-zero trace.

We can write the stationary condition equations of the system based on $\mathcal{S}$. There is no time dependence and derivatives with respect to time. The equations are simply $\delta\mathcal{S} = 0$

$$N\Big([X_b, [X_a, X_b]] - \epsilon_{abc} ig [X_b, X_c] \Big) = 0 \tag{4.4}$$

and every configuration of matrices X_a that solves (4.4) is a (local) stationary point of (4.1).

It will sometimes be convenient to scale out a factor of $\sqrt{N}$ and work with the parameter $\widetilde{g} = g\sqrt{N}$, as this gives a phase diagram that does not depend on

N. If we make the substitution $X_a \to \widetilde{g}\frac{D_a}{\sqrt{N}}$ the action reads

$$\mathcal{S}[D] = \frac{\widetilde{g}^4}{N}\,\mathrm{Tr}\Big(-\frac{1}{4}[D_a, D_b]^2 + \frac{2i}{3}\epsilon_{abc}D_aD_bD_c\Big). \tag{4.5}$$

From the above it is clear that the partition function is symmetric under $\widetilde{g} \to -\widetilde{g}$, or equivalently under $g \to -g$. For $\widetilde{g} \neq 0$ we can interpret $T = \widetilde{g}^{-4}$ as a temperature for the system. [1]

The physical properties of the system in its different phases are characterized by the expectation value of the action $\langle\mathcal{S}\rangle$ and the eigenvalue distribution of the matrices X_a. An important characteristic is the specific heat C_v of the system. It is defined as

$$C_v = \frac{\langle(\mathcal{S} - \langle\mathcal{S}\rangle)^2\rangle}{N^2} = \frac{\langle\mathcal{S}\rangle}{N^2} - \widetilde{g}^4\frac{d}{d\widetilde{g}^4}\Big(\frac{\langle\mathcal{S}\rangle}{N^2}\Big). \tag{4.6}$$

The specific heat of the system is nothing else than the dispersion of the energy of the system at a given temperature. As such we can use it to estimate the magnitude of the fluctuations of the system around a stable configuration with $\langle\mathcal{S}\rangle$ and specific heat C_v. If we apply Jensen's inequality[2] to the definition of C_v (4.6) we have

$$\begin{aligned} N^2C_v &= \big\langle(\mathcal{S} - \langle\mathcal{S}\rangle)^2\big\rangle = \big\langle(|\mathcal{S} - \langle\mathcal{S}\rangle|)^2\big\rangle \geq \langle|\mathcal{S} - \langle\mathcal{S}\rangle|\rangle^2 \\ &\Rightarrow \langle|\mathcal{S} - \langle\mathcal{S}\rangle|\rangle \leq N\sqrt{C_v}. \end{aligned} \tag{4.7}$$

For convenience we shall define $S := \langle\mathcal{S}\rangle$. From a thermodynamical point of view this represents the internal energy divided by the temperature.

If we use the fuzzy sphere coordinates constraint (2.8), we can define

$$\mathcal{R}^2 = \frac{\langle\mathrm{Tr}\,D_a^2\rangle}{Nc_2}, \tag{4.8}$$

[1] Generally we prefer to discuss the physical properties of the system in terms of the temperature T, though it may be more convenient in some situations to use $\widetilde{g}$ or g. Note however that, as there are no dimensional quantities in the action, T here is dimensionless.

[2] The inequality states that if $f(x)$ is a convex function and $\langle x\rangle$ and $\langle f(x)\rangle$ are the mean values of x and $f(x)$, then $f(\langle x\rangle) \leq \langle f(x)\rangle$

where c_2 is the second order Casimir of $su(2)$, to be an order parameter of the system. It has a nonzero value only in one of the phases of the system.[3] Another observable of the system that is of interest to us is the dispersion of the $\mathcal{R}^2$. This quantity is the analogue of magnetic susceptibility in a magnetic system

$$\chi = \frac{\langle (\mathrm{Tr}\, D_a^2 - \langle \mathrm{Tr}\, D_a^2 \rangle)^2 \rangle}{N^2 c_2}. \tag{4.9}$$

The model has at least two phases, which we call the commuting matrix phase and the fuzzy sphere phase. All of the above quantities behave quite differently on different sides of the phase boundary. In the next paragraphs we give some details about the two phases and their main properties with regard to the observables of the system.

4.2. The commuting matrix phase

This is the high temperature (disordered) phase of the model with $T > T_c$. It is described by fluctuations around a ground state in which the three matrices are mutually commuting. This ground state can be represented by matrices X_a which are linear combinations of hH_mh^{-1}, $m = 1 \ldots N-1$, where H_m are in the Cartan sub-algebra of $su(N)$ and $h \in SU(N)$. Any such linear combination is a trivial solution to (4.4), so the classical action vanishes on these solutions.

4.2.1. Stability of the matrix phase

The solutions mentioned above can be unstable if any of the eigenvalues get too close to one another, as we now demonstrate. The matrices close the classical solution can be expressed as

$$X_a = X_{0,a} + \delta X_a, \tag{4.10}$$

with $X_{0,a}$ three mutually commuting hermitian matrices. Since they commute, we are free to perform an $N \times N$ unitary transformation on $X_{0,a}$ to simultaneously

[3] In fact $\mathcal{R}$ tends to zero in the matrix phase only in large N limit

diagonalize them. In that basis they have the form

$$\big(X_{0,a}\big)_{ij} = \lambda_i^a \delta_{ij}, \qquad \text{(no sum over } i\text{)}. \tag{4.11}$$

Let us compute the commutator between two matrices[4]

$$\begin{aligned}\big[X^a, X^b\big] &= [X_0^a + \delta X^a, X_0^b + \delta X^b] \\ &= [X_0^a, X_0^b] + [X_0^a, \delta X^b] - [X_0^b, \delta X^a] + [\delta X^a, \delta X^b].\end{aligned}$$

The first term in the above expression vanishes identically because two diagonal matrices always commute. The terms that are linear in the fluctuations can be written as

$$[X_0^a, \delta X^b]_{ij} = \Delta_{ij}^a \delta X_{ij}^b,$$

where $\Delta_{ij}^a = \lambda_i^a - \lambda_j^a$. It is to be noted that the above commutator is expressed in terms of the element-wise multiplication of the two matrices Δ_{ij}^a and δX_{ij}^b rather than the usual matrix multiplication.

For the cubic term we have

$$\begin{aligned}\operatorname{Tr} X^a \big[X^b, X^c\big] &= \big(X_0^a + \delta X^a\big)\big[X_0^b + \delta X^b, X_0^c + \delta X^c\big] \\ &= (X_0^a)_{ij}\, \Delta_{ji}^b\, \delta X_{ji}^c - (X_0^a)_{ij}\, \Delta_{ji}^c\, \delta X_{ji}^b + (X_0^a)_{ij}\, [\delta X^b, \delta X^c]_{ji} \\ &+ \delta X_{ij}^a\, \Delta_{ji}^b\, \delta X_{ji}^c - \delta X_{ij}^a\, \Delta_{ji}^c\, \delta X_{ji}^b + \delta X_{ij}^a\, [\delta X^b, \delta X^c]_{ji}.\end{aligned}$$

In the above expansion we keep only terms up to second order in the fluctuations δX^a. The terms that are linear in the variations δX^a satisfy the equations of the motion of the system, thus they are identically zero. Using the cyclic property of the trace we finally arrive at

$$\frac{2i}{3} \operatorname{Tr} \epsilon_{abc} X_a X_b X_c = i\epsilon_{abc}\, \Delta_{ij}^a \delta X_{ij}^b\, \delta X_{ji}^c. \tag{4.12}$$

[4]For the rest of the section we will adopt notation with upper indeces for the matrices X_a

Next we compute the quartic term

$$\begin{aligned}
&\mathrm{Tr}\left[X^a, X^b\right]^2 = \mathrm{Tr}\left(\Delta^a_{ij}\,\delta X^b_{ij} - \Delta^b_{ij}\,\delta X^a_{ij} + [\delta X^a\,, \delta X^b]\right)^2 \\
&= \Delta^a_{ij}\,\delta X^b_{ij}\Delta^a_{ji}\,\delta X^b_{ji} - \Delta^a_{ij}\,\delta X^b_{ij}\Delta^b_{ji}\,\delta X^a_{ji} + \Delta^a_{ij}\,\delta X^b_{ij}[\delta X^a\,, \delta X^b]_{ji} \\
&- \Delta^a_{ij}\,\delta X^b_{ij}\Delta^b_{ji}\,\delta X^a_{ji} + \Delta^b_{ij}\,\delta X^a_{ij}\Delta^b_{ji}\,\delta X^a_{ji} - \Delta^b_{ij}\,\delta X^a_{ij}[\delta X^a\,, \delta X^b]_{ji} \\
&+ [\delta X^a\,, \delta X^b]_{ij}\Delta^a_{ji}\,\delta X^b_{ji} - [\delta X^a\,, \delta X^b]_{ij}\Delta^b_{ji}\,\delta X^a_{ji} + \mathrm{Tr}[\delta X^a\,, \delta X^b]^2.
\end{aligned}$$

As in the previous case we keep only terms up to quadratic order in the variation δX^a. For the Yang-Mills term we have

$$-\frac{1}{4}\,\mathrm{Tr}\left[X^a, X^b\right]^2 = \frac{1}{2}\left(\left(\Delta_{ij}.\Delta_{ij}\right)\delta^{ab} - \Delta^a_{ij}\Delta^b_{ij}\right)\delta X_{a,ij}\,\delta X_{b,ij}. \tag{4.13}$$

Stability of fluctuations around a classical solution are therefore determined by the eigenvalues of the operator

$$\frac{1}{2}\left(\Delta^2_{ij}\delta^{ab} - \Delta^a_{ij}\Delta^b_{ij}\right) + ig\,\epsilon_{abc}\,\Delta^c_{ij}\,, \tag{4.14}$$

where $\Delta^2_{ij} = \Delta^a_{ij}\Delta^a_{ij}$. The solutions of the characteristic equation are of the form $0,\ \frac{1}{2}\Delta^2_{ij} \pm g\sqrt{\Delta^2_{ij}}$. Thus there is a negative eigenvalue, and hence an instability, if some eigenvalues in the solution are too close together. In particular, if

$$\Delta^2_{ij} < 4g^2, \tag{4.15}$$

for any pair i, j, then there is a direction which is unstable. The solution is stable if all the eigenvalues of $X_{0,a}$ are far enough apart. Note that there are no unstable directions for $g = 0$, the instability is induced by the Myers' term.

4.2.2. Fluctuations of the matrix phase

Fluctuations can of course modify the above analysis. It is possible that they stabilize the unstable solutions. An analytic approach to this question is difficult and will not be attempted here, but it is certainly the case that they modify the expectation value of the action and shift it away from $\mathcal{S} = 0$. To study this effect

consider a Schwinger-Dyson type analysis,

$$\begin{aligned} 0 &= \int [DX] \operatorname{Tr} \frac{\partial}{\partial X_a} \left(X_a e^{-\mathcal{S}} \right) \\ \Rightarrow \qquad 0 &= 3(N^2-1) - \operatorname{Tr} \left\langle X_a \frac{\partial \mathcal{S}}{\partial X_a} \right\rangle \\ \Rightarrow \qquad 3(N^2-1) &= -N \operatorname{Tr} \left\langle [X_a, X_b]^2 \right\rangle + 2igN\epsilon_{abc} \operatorname{Tr} \langle X_a X_b X_c \rangle \\ &= 4 \langle \mathcal{S} \rangle - \frac{i2gN}{3} \epsilon_{abc} \operatorname{Tr} \langle X_a X_b X_c \rangle , \end{aligned} \tag{4.16}$$

where $3(N^2-1)$ is the number of degrees of freedom in the three hermitian matrices X_a. Thus we expect

$$\frac{\langle \mathcal{S} \rangle}{N^2} = \frac{3\big(N^2-1\big)}{4N^2} + \frac{ig}{6N} \epsilon_{abc} \operatorname{Tr} \langle X_a X_b X_c \rangle . \tag{4.17}$$

It is shown numerically in [24] that $\operatorname{Tr} \langle X_a X_b X_c \rangle \approx \frac{1}{N^{1/2}} \Big(\frac{1}{T^{1/4}} + \mathcal{O}\big(\frac{1}{T^{1/2}}\big) \Big)$ at large T and large N also, in this limit,

$$\frac{S_m(T)}{N^2} = \frac{3}{4} > 0. \tag{4.18}$$

The specific heat does not depend on T,

$$C_v = \frac{3}{4}, \tag{4.19}$$

each degree of freedom contributes a value of $\frac{1}{4}$ to the specific heat. The model behaves like pure Yang-Mills model in the large N limit.

For large N, the eigenvalue distribution in this phase is compatible with a parabolic distribution [14, 24, 65]. In a gauge in which X_3 is diagonal (which can always be achieved by a $SU(N)$ transformation) the diagonal entries of $\langle X_3 \rangle$ can be arranged in descending order and give a parabolic distribution with normalized density

$$\rho(\lambda) = \frac{3(Q^2 - \lambda^2)}{4Q^3}, \tag{4.20}$$

with Q determined numerically to be 2.0.

The eigenvalue distribution (4.20) gives us a way to estimate the value of the observable $\mathcal{R}$. Let us consider the eigenvalues of the matrix X_1. We can relate the expectation value of $\operatorname{Tr} X_1^2$ to an integral of the eigenvalue x over the above distribution

$$\frac{1}{N}\left\langle \operatorname{Tr} X_1^2 \right\rangle = \int_{-Q}^{Q} x^2 \rho(x) dx = \frac{Q^2}{5}.$$

Now if we plug-in the numerical value for Q for the radius we get

$$\mathcal{R}^2 = \frac{12}{5\widetilde{g}^2 c_2} = \frac{12T^{1/2}}{5c_2}. \tag{4.21}$$

The above relation confirms that in large N limit for fixed temperature $\mathcal{R}$ vanishes in this phase as stated before.

4.3. The fuzzy sphere phase

The fuzzy sphere phase is a cold (ordered) phase and is radically different to the commuting matrix phase. The background matrices in this phase are represented by a solution to (4.4) in which X_a are proportional the generators of $su(2)$, $X_a = gL_a$ with $[L_a, L_b] = i\epsilon_{abc}L_c$, up to $U(N)$ transformation hL_ah^{-1} with $h \in SU(N)$. For the classical solution we have $\sum_a X_a^2 = g^2 c_2 \mathbf{1}$, with c_2 the second order Casimir for the N-dimensional representation of $su(2)$. This implies $\frac{\left\langle \operatorname{Tr} X_a^2 \right\rangle}{g^2 N c_2} = 1$.

The value of the action at the ground state in this phase is approximated by calculating the value of the action for the classical solution $X_a = gL_a$. This gives

$$S_{\mathrm{f}}(T) = -\frac{c_2 c_2^{adj}}{12T} + \langle \text{fluctuations} \rangle\,, \tag{4.22}$$

where $c_2^{adj} = 2$ is the adjoint Casimir operators of $su(2)$. In [5] one-loop corrections to the classical solution from (4.22) have been computed in large N limit. Since the matrices X_a are proportional to the $su(2)$ generators they have a discrete

eigenvalue spectrum with N distinct eigenvalues of the form

$$\lambda = \Big\{ -g\frac{N-1}{2}, -g\frac{N-3}{2}, \dots g\frac{N-1}{2} \Big\}. \tag{4.23}$$

An approximate analytic expression for the critical behaviour in the $N \to \infty$ limit on the fuzzy sphere side was given in [26]. If we make the ansatz $X_a = \phi\, g\, L_a$ in the fuzzy sphere phase and write an effective potential for the theory in terms of ϕ, then the classical solutions are given by

$$\phi(\widetilde{g}) = \frac{1}{4}\left(1 + \sqrt{1+\delta(\widetilde{g})} + \sqrt{2 - \delta(\widetilde{g}) + \frac{2}{\sqrt{1+\delta(\widetilde{g})}}} \right), \tag{4.24}$$

$$\delta(\widetilde{g}) = \frac{4}{\widetilde{g}^{4/3}} \left(\Big(1 + \sqrt{1 - \frac{\widetilde{g}_e}{\widetilde{g}}}\Big)^{\frac{1}{3}} + \Big(1 - \sqrt{1 - \frac{\widetilde{g}_e}{\widetilde{g}}}\Big)^{\frac{1}{3}} \right). \tag{4.25}$$

The expectation value of the action can be written in terms of ϕ

$$\frac{\langle S \rangle'_{\mathrm{f}}(\widetilde{g})}{N^2} = \frac{3}{4} - \frac{\widetilde{g}^4 \phi^3(\widetilde{g})}{24}. \tag{4.26}$$

In a large N semi-classical approximation, equations (3.25) and (3.26) of reference [26] with $m = 0$, give, in the large $\widetilde{g}$ limit for the specific heat

$$C_v = \frac{3}{4} + \frac{\widetilde{g}^5 \phi^2}{32} \frac{d\phi}{d\widetilde{g}}, \qquad \text{with} \qquad \phi = 1 - \frac{2}{\widetilde{g}^4} - \frac{12}{\widetilde{g}^8} + \mathcal{O}\left(\frac{1}{\widetilde{g}^{12}}\right). \tag{4.27}$$

Thus

$$C_v = 1 + \frac{2}{\widetilde{g}^4} + \mathcal{O}\left(\frac{1}{\widetilde{g}^8}\right) \tag{4.28}$$

and

$$C_v \underset{T\to 0}{\longrightarrow} 1\,. \tag{4.29}$$

The magnetic susceptibility χ is dependent on the temperature, and it diverges at T_c. Here it is worth to comment on the normalization factor in (4.9). As we can see on the side of the fuzzy sphere, the susceptibility is defined as the dispersion

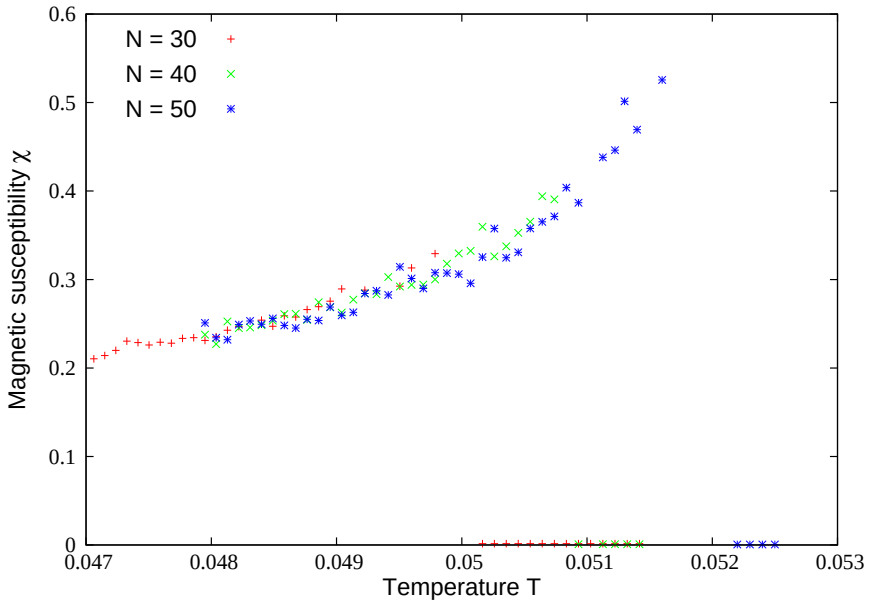

Figure 4.1.: Numerical measurement of the magnetic susceptibility χ for systems with size $N = 30, 40, 50$. The plots for χ of systems with different matrix size N are normalized by factor $\sim N^4$. This produces a single curve, which is independent of N. The uncertainties are small in comparison to the symbol size and therefore omitted for clarity.

of the fluctuations of $\mathcal{R}^2$ from (4.8) around its classical value. Numerically we find that for fixed temperature the quantity $\langle(\mathrm{Tr}\, D_a^2 - \langle \mathrm{Tr}\, D_a^2\rangle)^2\rangle$ behaves like N^4. We use this observation to fix the normalization factor of (4.9). We require that χ agrees for different system sizes at the same temperature. Values for χ which are obtained from simulations are plotted on Fig. 4.1 in these two phases.

As we can see the properties of the matrices are quite different on the two sides of the phase transition. In Fig. 4.2 and 4.3 we present the eigenvalue distributions of X_a for systems deep into the matrix phase and fuzzy sphere phase. They are in a good agreement with (4.20) and (4.23). In Fig. 4.4 we also present the numerical measurement of the action as function of the coupling $\widetilde{g}$ together with plots of (4.18) and the background of (4.22).

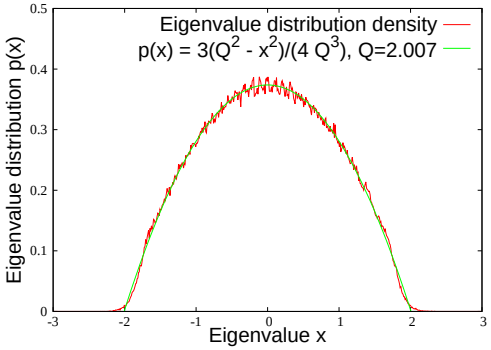

Figure 4.2.: Eigenvalue distribution of $N = 25$ system at $\widetilde{g} = 0$ in the matrix phase. The distribution fits to a curve of the form $\frac{3}{4Q^3}(Q^2 - x^2)$ with $Q = 2.007 \pm 0.002$. The noise is mainly due to finite size effects.

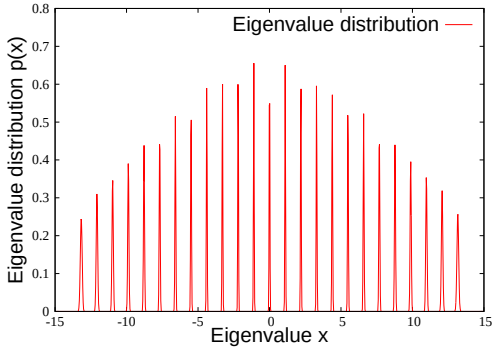

Figure 4.3.: Eigenvalue distribution of $N = 25$ system at $\widetilde{g} = 5.5$ system in the fuzzy sphere phase. The distribution is discrete with eigenvalues of the form $\{-g\frac{N-1}{2}, -g\frac{N-3}{2}, \ldots, g\frac{N-1}{2}\}$. In large $\widetilde{g}$ limit the peaks tend to δ-functions.

4.4. Excited fuzzy sphere states

A closer examination of the equations of motion (4.4) shows that they have more solutions. They come in the form of reducible fuzzy sphere solutions, with X_a proportional to $su(2)$ generators in a reducible representation of the form

$$R_1(M_1) \oplus R_2(M_2) \ldots \oplus R_K(M_k), \tag{4.30}$$

where $R_i(M_i)$ is an $su(2)$ irreducible representation of dimension M_i and $\sum_{i=1}^{K} M_i = N$. The matrices X_a for this solution can always be chosen to have block-diagonal form and we will assume is for the rest of our discussion. All of the metastable configurations are represented by the n-tuple $(M_1, M_2, \ldots, M_K)$. They can be listed and indeed all the solutions described so far — even the commuting matrix phase and the irreducible fuzzy sphere phase — can be classified this way. The special case $M_1 = M_2 = \ldots = M_N = 1$ corresponds to the commuting matrices phase and the ground state in this case can be viewed as arising from N one-dimensional (or trivial) representations of $su(2)$. The other extreme, when $K = 1$ and the representation is irreducible, we shall refer to as "the" fuzzy sphere

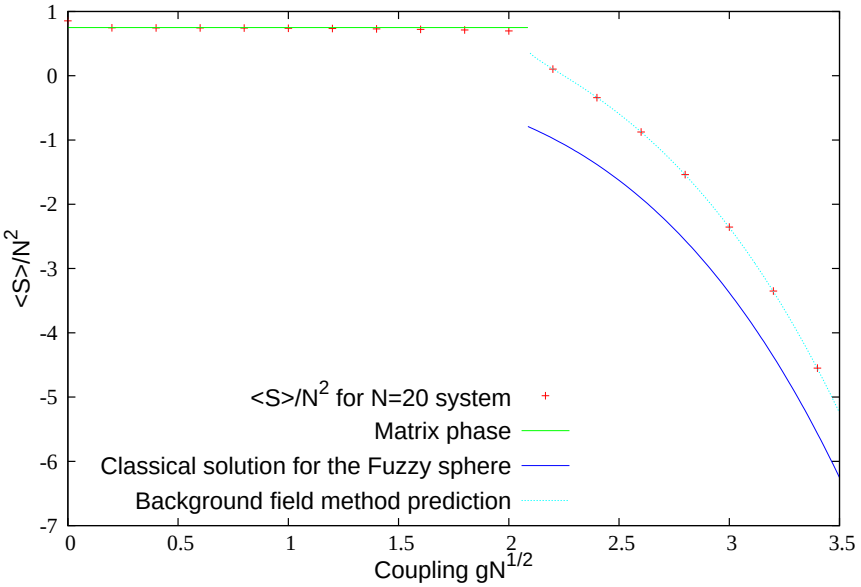

Figure 4.4.: Simulation of $N = 20$ system as function of the coupling $\widetilde{g}$. On the matrix phase the numerically obtained values are in good agreement with (4.18). We also plot the classical value of the ground state (4.22) and the semi-classical approximation (4.26). As we can see the semi-classical approximation is indeed in a very good agreement with the numerical results. The uncertainties are small in comparison to the symbol size and therefore omitted for clarity.

state. Nevertheless the commuting matrix solution is genuinely different to all the others, the configuration represented by diagonal matrices is a state built from the one-dimensional representations so the ϵ term in (4.4) plays no rôle and the system has no memory of $su(2)$. There are one dimensional representations of an arbitrary algebra.

For a fixed N, the degeneracy of excited states with $1 \leq K \leq N$ grows like the number of partitions $p(N)$ of N. The asymptotic behaviour for large N is given by [45]

$$p(N) \sim \frac{e^{\pi\sqrt{2N/3}}}{4\sqrt{3}N}, \tag{4.31}$$

which grows very rapidly with N. We can use some of the observables defined in §4.1 to distinguish between the fuzzy sphere from the section §4.3 and these excited configurations with $K > 1$. First we can use the eigenvalues of the matrices: since any irreducible representation $R(M)$ of $su(2)$ has M distinct eigenvalues, configurations of the form (4.30) have $max\{M_i\} < N$ distinct eigenvalues in their spectra. Another observable that is sensitive to the excited states is the expectation value of the action. We have

$$S_{\text{ef}}(T, (M_1, M_2, \ldots, M_K)) = -\sum_{i=1}^{K} \frac{M_i c_2(M_i) c_2^{adj}}{12T} + \langle \text{fluctuations} \rangle \,. \tag{4.32}$$

In the above equation by $c_2(M_i)$ we denote the second order Casimir of $su(2)$ of the reducible representation of dimension M_i. Thus $S_{\text{f}}(T) < S_{\text{ef}}(T, K) < S_{\text{m}}(T)$ for $\forall K : 1 < K < N$. The radius of the sphere (4.8) changes as well

$$\mathcal{R}_{\text{ef}}(T, (M_1, M_2, \ldots, M_K)) = \sum_{i=1}^{k} \frac{M_i c_2(M_i)}{N c_2(N)} < 1. \tag{4.33}$$

However neither of these observables can be used to distinguish between excited states composed by the same number of smaller representations but permuted. For example the states $R_1(M_1) \oplus R_2(M_2)$ and $R_2(M_2) \oplus R_1(M_1)$ are indistinguishable because according to (4.32) $S_{\text{ef}}(T, (M_1, M_2)) = S_{\text{ef}}(T, (M_2, M_1))$ and $\mathcal{R}_{\text{ef}}(T, (M_1, M_2)) = \mathcal{R}_{\text{ef}}(T, (M_2, M_1))$. Also these configurations have the

same number of distinct eigenvalues. The Monte Carlo histories of the action and the radius of $N = 20$ system which visits excited states are plotted on Fig. 4.5 and 4.6.

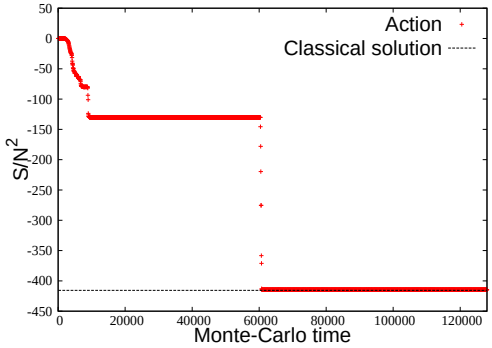

Figure 4.5.: Monte Carlo history of the action of $N = 20$ system at coupling $\widetilde{g} = 10$.

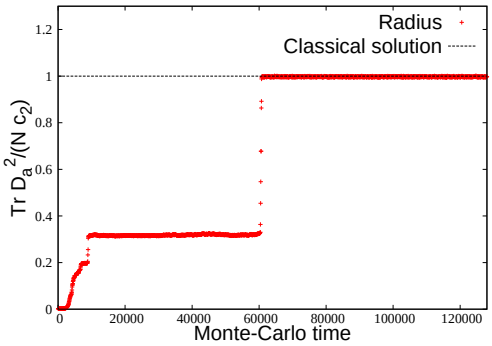

Figure 4.6.: Monte Carlo history of the radius of $N = 20$ system at coupling $\widetilde{g} = 10$.

Far from the phase transition these states do not play an important role in the thermodynamics of the system. Our numerical results in Fig. 4.7 indicate that they behave very much like true fuzzy sphere states. Near the phase transition however they get closer energetically. In the following, if the system is found in a state with $1 < K < N$ we can for all practical purposes regard it as if it is in the fuzzy sphere phase.

4.5. Hybrid Monte Carlo approach

In this section we apply the Hybrid Monte Carlo algorithm described in A.2. The matrices of the theory X_a are $N \times N$ hermitian traceless matrices. They represent $3(N^2 - 1)$ degrees of freedom. We extend the system by introducing conjugate momenta P_a. In order to preserve ergodicity and phase volume element conservation the momenta are defined to be again $N \times N$ hermitian traceless matrices. This way we can define a Hamiltonian for the extended system

$$\mathbf{H}(X, P) = \frac{1}{2} \operatorname{Tr} P_a^2 + \mathcal{S}(X). \tag{4.34}$$

The system defined above has $6(N^2-1)$ degrees of freedom. We generate configurations for the matrices X_a based on its Hamiltonian dynamics. Similarly to §3.4 for the derivatives with respect to the matrix elements we have

$$\frac{\partial (X_a)_{i_2 j_2}}{\partial (X_b)_{i_1 j_1}} = \delta_{i_1 i_2}\delta_{j_1 j_2}\delta_{ab} \quad \frac{\partial (P_a)_{i_2 j_2}}{\partial (P_b)_{i_1 j_1}} = \delta_{i_1 i_2}\delta_{j_1 j_2}\delta_{ab}. \tag{4.35}$$

Now we derive the equations of the motion for the system based on (A.6).

For the derivative of (4.34) with respect to the momenta we have

$$\frac{\partial}{\partial (P_a)_{ij}} \sum_b \frac{1}{2} \operatorname{Tr} P_b^2 = (P_a)_{ji}. \tag{4.36}$$

After we carry out the summation and using the cyclic properties of the trace for the derivative of the Myer's term we get

$$\frac{\partial}{\partial (X_a)_{ij}} \Big(\frac{1}{3} \sum_{bcd} \operatorname{Tr} \epsilon_{bcd} X_b [X_c \, , X_d] \Big) = \epsilon_{abc} ([X_b \, , X_c])_{ji} \tag{4.37}$$

Next we compute the derivative of the Yang-Mills term

$$\begin{aligned}
&\frac{\partial}{\partial (X_a)_{ij}} \sum_{b,\,c} \operatorname{Tr} [X_b \, , X_c]^2 \\
&= \frac{\partial}{\partial (X_a)_{ij}} \sum_{b,\,c} \operatorname{Tr} \left((X_b)_{kl} \, (X_c)_{lm} \, (X_b)_{mn} \, (X_c)_{nk} - (X_b)_{kl} \, (X_c)_{lm} \, (X_c)_{mn} \, (X_b)_{nk} \right) \\
&= \sum_{b,\,c} \big(\delta_{ab}\delta_{ik}\delta_{jl} \, (X_b)_{lm} \, (X_a)_{mn} \, (X_b)_{nk} + (X_b)_{kl}\delta_{ac}\delta_{il}\delta_{jm} \, (X_c)_{mn} \, (X_b)_{nk} \\
&+ (X_a)_{kl} \, (X_b)_{lm} \, \delta_{ab}\delta_{im}\delta_{jn} \, (X_b)_{nk} + (X_a)_{kl} \, (X_b)_{lm} \, (X_c)_{mn} \, \delta_{ac}\delta_{in}\delta_{jk} \\
&- \delta_{ab}\delta_{ik}\delta_{jl} \, (X_c)_{lm} \, (X_c)_{mn} \, (X_b)_{nk} - (X_b)_{kl} \, \delta_{ac}\delta_{il}\delta_{jm} \, (X_c)_{mn} \, (X_b)_{nk} \\
&- (X_b)_{kl} \, (X_c)_{lm} \, \delta_{ac}\delta_{im}\delta_{jn} \, (X_b)_{no} - (X_b)_{kl} \, (X_c)_{lm} \, (X_c)_{mn} \, \delta_{ab}\delta_{in}\delta_{jk} \big).
\end{aligned}$$

After some reordering of the terms and replacement of the dummy indices we get

$$\frac{\partial}{\partial (X_a)_{ij}} \sum_{b,\,c} \operatorname{Tr} [X_b \, , X_c]^2 = 2 \sum_b [X_b, [X_a, X_b]]_{ji}. \tag{4.38}$$

Now using (4.37) and (4.38) we can write down the equations of motion of our extended system. They have the form

$$\begin{aligned}(\dot{X}_a)_{ij} &= (P_a)_{ji} \\ (\dot{P}_a)_{ij} &= N \sum_{b \neq a} \left([X_b, [X_a, X_b]] - \epsilon_{abc} ig [X_b, X_c] \right)_{ji}.\end{aligned} \tag{4.39}$$

The above equations are numerically integrated using the scheme described in §A.2.2 with Omelyan integrator with variable time step ϵ.

As consistency checks we have observed the phase volume conservation (A.14) and also the identity

$$4 \left\langle -N \frac{1}{4} \operatorname{Tr}[X_a, X_b]^2 \right\rangle + 3 \left\langle N \frac{2ig}{3} \epsilon_{abc} \operatorname{Tr} X_a X_b X_c \right\rangle = 3(N^2 - 1), \tag{4.40}$$

which follows from (4.17). They hold within good precision in our simulations.

The algorithm fulfills all the requirements from A.1. It has complexity $\sim \mathcal{O}(N^3)$ because of the matrix multiplication.

4.6. Hybrid Monte Carlo approach II

The system under study has a gauge symmetry: the action is invariant under the transformation $X_a \to U^\dagger X_a U$. The algorithm we presented in the previous section does not fix that symmetry. By gauge-fixing this symmetry of the matrices we can gain some insight into the dynamics of the system and it also provides some speed up. In what follows we will provide an alternative Hybrid Monte Carlo algorithm for simulation of the system (4.1) in which the gauge is fixed in such a way that the matrix X_3 is always diagonal. We do so by applying an $SU(N)$ transformation to the three matrices X_a. In general we can diagonalize only one of them. As we noted earlier the action of the system is invariant under

$SU(N)$ transformations. After the transformation we have

$$\begin{aligned} X_1 &\to U^{-1} X_1 U, \\ X_2 &\to U^{-1} X_2 U, \\ X_3 &\to U^{-1} \Lambda_3 U, \end{aligned} \tag{4.41}$$

where $\Lambda_3 = \mathrm{diag}\{\lambda_1, \lambda_2, \ldots, \lambda_N\}$, $\sum_{i=1}^{N} \lambda_i = 0$ is a real diagonal N-dimensional matrix. Unlike the gauge-fixing procedure described in 3.7 the transformations (4.41) are applied not only for the measurement. Therefore they affect the form of the action of the system. Now we write down the action in the terms of the new matrices.

4.6.1. Gauge-fixed action and path integral redefinition

First we re-arrange the Myers term

$$\epsilon_{abc} \,\mathrm{Tr}\, X_a X_b X_c = 3 \,\mathrm{Tr}\, X_3 [X_1, X_2].$$

Then we expand the trace in terms of the transformed matrices

$$\begin{aligned} \mathrm{Tr}\, \Lambda_3 [X_1, X_2] &= \sum_i \lambda_i \sum_j (X_1)_{ij} \, (X_2)_{ji} - \sum_i \lambda_i \sum_j (X_2)_{ij} \, (X_1)_{ji} \\ &= \sum_{i,j} \lambda_i (X_1)_{ij} \, (X_2)_{ji} - \sum_{i,j} \lambda_j \sum_j (X_1)_{ij} \, (X_2)_{ji} \\ &= \sum_{i,j} \Delta_{ij} (X_1)_{ij} \, (X_2)_{ji}. \end{aligned} \tag{4.42}$$

The Yang-Mills term between X_1 and X_2 remains unchanged. For the cross terms between Λ_3 and a fixed matrix X_a we have

$$\begin{aligned} \mathrm{Tr}[\Lambda_3, \, X_a]^2 &= \sum_{i,j} (X_a)_{ij} \lambda_j \lambda_i (X_a)_{ji} - \sum_{i,j} \lambda_i^2 (X_a)_{ij} (X_a)_{ji} \\ &= \sum_{i,j} (X_a)_{ij} \lambda_i (X_a)_{ji} \Delta_{ji}. \end{aligned} \tag{4.43}$$

The action now has the form

$$\mathcal{S}_{\text{gf}}[X_1, X_2, \Lambda_3] = N\Big(-\frac{1}{2}\,\text{Tr}[X_1, X_2]^2 - \sum_{a=1}^{2}\sum_{i,j}(X_a)_{ij}\lambda_i(X_a)_{ji}\Delta_{ji} + 2ig\sum_{i,j}\Delta_{ij}(X_1)_{ij}\,(X_2)_{ji}\Big). \tag{4.44}$$

The action (4.44) is equivalent to (4.1). They have the same value when X_3 is diagonal. However we can not use the above action with the path integral from (4.2). The reason is that now the system has fewer degrees of freedom. In the new action there are $2(N^2-1)+(N-1)$ instead of $3(N^2-1)$. Thus the measure (4.3) needs to be modified accordingly. The measure of the configuration spaces of X_1 and X_2 stays the same. For the the measure dX_3 we have

$$dX_3 \to d\Lambda_3 = \prod_{i=2}^{N}\prod_{j=1}^{i-1}(\lambda_i - \lambda_j)^2 d\lambda_i. \tag{4.45}$$

The factor which involves the differences between eigenvalues in the measure is the Vandermonde determinant. It arises because of the variable substitution (4.41). More details about its derivation can be found in [27]. We see that configurations with two or more eigenvalues close to each other are suppressed as they have measure tending to zero. This gives rise to the so called *eigenvalue repulsion*. This repulsion force makes the excited states from §4.4 unstable because two copies of lower dimensional representations of the $su(2)$ would have the same eigenvalues. In order to take this force into account in our evaluation of the path integral of the system we can define effective action that corresponds to it

$$\mathcal{S}_{\text{rep}}[\Lambda_3] = -\sum_{i=2}^{N}\sum_{j=1}^{i-1}\log(\lambda_i - \lambda_j)^2. \tag{4.46}$$

Thus in order to evaluate (4.2) we need to use the effective action constructed by the sum of (4.45) and (4.46).

$$\mathcal{S}_{\text{eff}}[X_1, X_2, \Lambda_3] = \mathcal{S}_{gf} + \mathcal{S}_{rep}. \tag{4.47}$$

It is important to stress that while the action (4.47) gives us the right partition of the system, it is not the physical action of the system. It is rather a mixture of action of the system together with part which takes into account the entropy of the configuration presented in the form of an entropic force. Therefore the measurements of observables of the system which depend on the action such as S and C_v should be defined as functions of (4.45). That way we get results which are consistent with the formulation in §4.5.

4.6.2. Extended system. Hamiltonian equations of motion

First we need to define the conjugate momenta. To X_1 and X_2 we assign conjugate momenta P_1 and P_2 as in §4.5. The matrix Λ_3 has $N-1$ degrees of freedom. We define its conjugate momenta to be $P_3 = \mathrm{diag}\{\pi_1, \pi_2, \ldots, \pi_N\}$, with the constraint for the elements of Λ_3, $\sum_{i=1}^{N} \pi_i = 0$. Now our extended system has $4(N^2-1) + 2(N-1)$ degrees of freedom. The Hamiltonian of the system reads

$$\mathbf{H}(X,P) = \frac{1}{2}\sum_{a=1}^{2} \mathrm{Tr}\, P_a^2 + \frac{1}{2}\sum_i \pi_i^2 + \mathcal{S}_{\text{eff}}(X). \tag{4.48}$$

In addition to the derivatives from (4.35) we have

$$\begin{aligned} &\frac{\partial \lambda_i}{\partial \lambda_j} = \delta_{ij} \qquad \frac{\partial \pi_i}{\partial \pi_j} = \delta_{ij} \\ &\frac{\partial \Delta_{ij}}{\partial \lambda_k} = \delta_{ik} - \delta_{jk}. \end{aligned} \tag{4.49}$$

All other derivatives are zero. The derivative with respect to the momentum π is $\partial_{\pi_k}\big(\frac{1}{2}\sum_i \pi_i^2\big) = \pi_k$.

Now we compute the derivatives of the Myers term

$$\begin{aligned} \frac{\partial}{\partial \lambda_k}\Big(\sum_{ij} \Delta_{ij} (X_1)_{ij}\,(X_2)_{ji}\Big) &= \sum_{ij} \big(\delta_{ik} - \delta_{jk}\big)(X_1)_{ij}\,(X_2)_{ji} \\ &= [X_1,\, X_2]_{kk} \end{aligned} \tag{4.50}$$

and

$$\begin{aligned}&\frac{\partial}{\partial (X_a)_{kl}}\Big(\sum_{ij}\Delta_{ij}(X_b)_{ij}\,(X_c)_{ji}\Big)\\&=\sum_{ij}\Delta_{ij}\big(\delta_{ab}\delta_{ik}\delta_{jl}\,(X_c)_{ji}+\delta_{ac}\delta_{il}\delta_{jk}\,(X_b)_{ij}\big)=\epsilon_{3ab}\Delta_{lk}(X_b)_{lk}.\end{aligned}\tag{4.51}$$

For the Yang-Mills derivatives we have

$$\begin{aligned}&\frac{\partial}{\partial\lambda_k}\big(\sum_{i,j}(X_a)_{ij}\lambda_i(X_a)_{ji}\Delta_{ji}\big)\\&=\sum_{i,j}(X_a)_{ij}\delta_{ik}(X_a)_{ji}\Delta_{ji}+\sum_{i,j}(X_a)_{ij}\lambda_i(X_a)_{ji}(\delta_{jk}-\delta_{ik})\\&=2\sum_i(X_a)_{ki}\Delta_{ik}(X_a)_{ik}\end{aligned}\tag{4.52}$$

and

$$\begin{aligned}&\frac{\partial}{\partial(X_a)_{kl}}\big(\sum_{i,j}(X_b)_{ij}\lambda_i(X_b)_{ji}\Delta_{ji}\big)\\&=\sum_{i,j}\delta_{ik}\delta_{lj}\lambda_i(X_a)_{ji}\Delta_{ji}+\sum_{i,j}(X_a)_{ij}\lambda_i\delta_{jk}\delta_{il}\Delta_{ji}\\&=-(X_a)_{lk}(\Delta_{lk})^2.\end{aligned}\tag{4.53}$$

For the derivative of the term involving X_1 and X_2 we use the expression (4.38). Next we compute the entropic force which comes from the eigenvalue repulsion (4.46)

$$\frac{\partial}{\partial\lambda_k}\Big(\sum_{i=1}^{N}\sum_{j=1}^{i-1}\log(\lambda_i-\lambda_j)^2\Big)=\sum_{i=1}^{N}\sum_{j=1}^{i-1}\frac{\delta_{ik}-\delta_{jk}}{\Delta_{ij}}=\sum_{i=1\,i\neq k}^{N}\frac{2}{\Delta_{ki}}.\tag{4.54}$$

Finally we write down the equations of motion

$$\begin{aligned}
(\dot{X}_a)_{ij} &= (P_a)_{ji} \\
\dot{\lambda}_i &= \pi_i \\
(\dot{P}_a)_{ij} &= N\big([X_b,[X_a,X_b]]_{ji} - ig\epsilon_{3ab}\Delta_{ji}(X_b)_{ji}\big) \\
\dot{\pi}_i &= N\Big(\sum_j (X_a)_{ij}\Delta_{ji}(X_a)_{ji} - ig[X_1,X_2]_{ii}\Big) + \sum_{j=1\, j\neq i}^{N} \frac{2}{\Delta_{ij}}.
\end{aligned} \tag{4.55}$$

The dynamics of (4.55) keep both λ_i and π_i diagonal during the simulation by construction. They can be used as an alternative to (4.39) to generate configurations for the matrices. We use again the Omelyan type integration scheme to solve them. There are a few differences. First as we stated before, the basis of the system has been chosen in such a way that X_3 is always diagonal, hence we replace the whole matrix by its eigenvalues. This allows us to extract certain observables such as the polarization tensor coefficients c_{lm} which would otherwise be averaged to zero because of the random unitary rotations during a simulation. From a computational point of view, the equations (4.55) are more efficient than the first version. This is because they involve a smaller number of full matrix multiplications. However the complexity of the algorithm is still $\sim \mathcal{O}(N^3)$ because of the remaining commutator between X_1 and X_2. The algorithm is ergodic with the exception of the states which involve two or more very close eigenvalues of Λ_3. Those configurations become inaccessible because of the eigenvalues repulsion term (4.46). However the integrals over those configurations have zero measure and therefore those configurations are not important. The eigenvalues repulsion term has also an impact on the algorithm's stability. Because of that term one should be careful not to start the algorithm in a state in which Λ_3 contains two or more eigenvalues that are very close to each other, as the logarithm and its derivative are divergent at zero. This leads to problems with generating of new configurations. As for the dynamics of the matrix evolution, the eigenvalue repulsion term forces the system to avoid excited fuzzy sphere solutions.

From practical point of view, the two algorithms have their relative advantages and disadvantages. If there is no coexistence the two algorithms produce the same results. In that regime the algorithm of choice is the one with the gauge-fixing as it is more efficient in terms of computer resources and it allows us to generate

more data points. However the gauge-fixed algorithm seems to perform worse in the situations where we expect coexistence of the phases- in those cases we use the first algorithm.

4.7. Near-critical simulation difficulties

The emphasis of our studies of the model will be on the properties of the system near the phase transition between the two phases. A numerical analysis of the properties of a generic system very close to a phase transition is usually complicated due to some phenomena which occurs in critical systems. In this section we discuss the features of the system that hinder our numerical methods and their impact on our work. We also describe how we handle them.

4.7.1. Critical slowdown

As we pointed out, in every near-critical physical system there are fluctuations which extend over regions of size comparable to the size of the whole system. This purely physical phenomenon has its manifestation in the simulations of near critical systems. It is described by the theory of dynamical critical phenomena. Detailed treatment of the subject can be found in *e.g.* [41, 61]. When $T \to T_c$ the time τ needed for a non-equilibrium system to reach equilibrium grows.[5] More details on the impact of critical slowdown on our numerics is discussed in the Appendix and here we merely observe that, for the systems studied in this work, the critical slowdown has significant impact on the accuracy only for systems with $N \geq 100$.[6]

[5] We consider a system sufficiently close to equilibrium that it does not need to cross over any energy barriers in order to reach equilibrium.

[6] It is evident from Fig. 5.23 that the relative error in the measurement of the near-critical specific heat grows with the system size as consequence of the autocorrelation time.

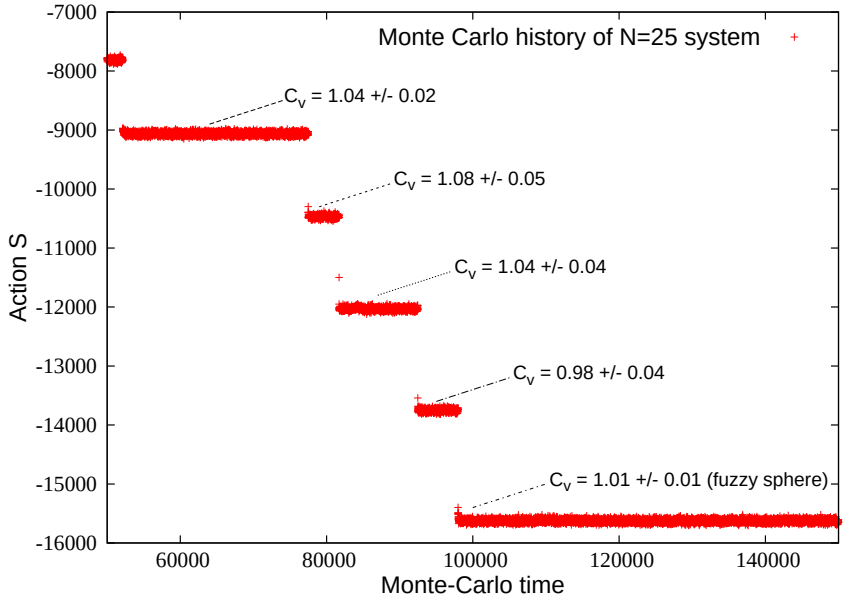

Figure 4.7.: Monte Carlo history of a $N = 25$ system visiting different excited states, together with the corresponding values of C_v in their specific domains (for $\widetilde{g} = 5$, $T = 0.0016$ and $\frac{T}{T_c} = 0.03$).

4.7.2. Excited states

Another property to be taken into consideration is the presence of the excited fuzzy sphere configurations given by (4.30). As mentioned earlier, those configurations possess energies which are intermediate between the commuting matrix phase and the fuzzy sphere phase. This means that, in the region where the two phases coexist, we would expect to see jumps between excited states and the commuting matrix phase rather than the transition between the commuting matrix phase and the fuzzy sphere. As the Monte Carlo evolution of the system is based on stochastic dynamics we do not have control over which configurations are sampled, nevertheless we do not consider this to be a problem for extracting critical exponents since we expect all these excited states to to be in the same universality class and therefore to have the same critical exponents. This expectation is supported by our simulations. We are able to measure the values of C_v for different excited states and the fuzzy sphere and they agree up to the numerical uncertainties, as illustrated in Fig. 4.7.

4.7.3. Energy separation between different phases

Ideally in the vicinity of the phase transition the system will jump between the two phases and if we can get enough Monte Carlo steps, we will have enough statistics to properly determine the ground state, or the relative weight of the local minima of the action, and extract the relevant quantities. A Monte Carlo history of a system in that regime is depicted in Fig. 5.5. We can see that the system spends roughly the same amount of MC time in both phases, an indication that the system is close to the transition point. However for large N the jump between the two phases becomes a rare event, and indeed our numerical studies indicate that this is already the case for $N \simeq 14$. This, in combination with the asymmetry of the phase transition, makes it very hard to simulate the system efficiently in the regime where the two phases coexist. For systems with size $N \geq 15$ we cannot achieve a regime of coexistence using our methods in order to explore the full configuration space of the systems.

On the other hand if we restrict ourselves to the fuzzy sphere side we can perform a *cold start* on the Monte Carlo runs, so that the phase transition is always approached from the low temperature side. This biases the system toward the fuzzy sphere phase, but has the advantage of giving reproducible results. An example is shown in Fig. 4.8, with $N = 50$ at $T = 0.0514 < T_c$. The system is below the critical temperature but, while the value of the action is compatible with a fuzzy sphere configuration for quite some Monte Carlo time, it suddenly jumps to a commuting matrix configuration. We can obtain information about the fuzzy sphere phase by restricting our measurements to this domain.

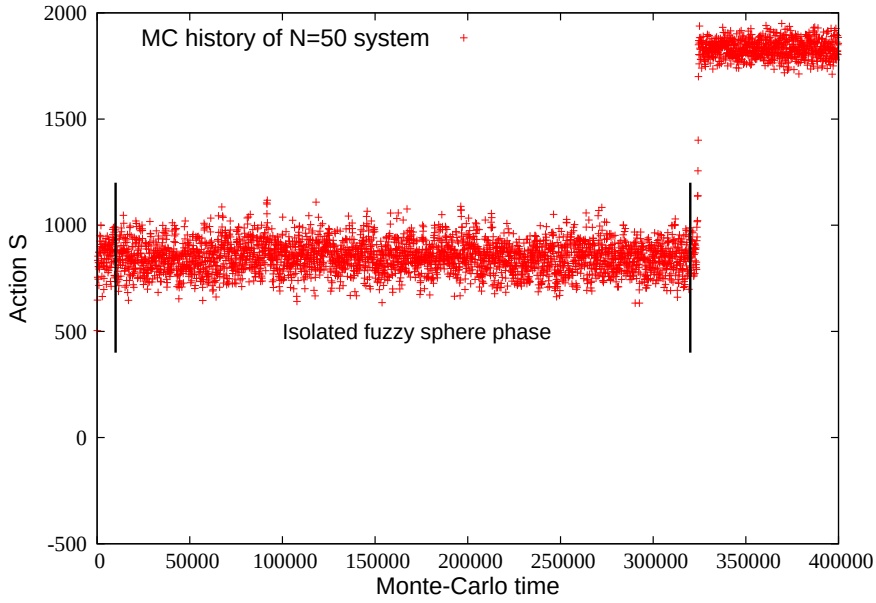

Figure 4.8.: Monte Carlo history of a $N = 50$ system which spends some time in fuzzy sphere phase and crosses to matrix phase.

Chapter 5.

Numerical results for the critical Three matrix model

In the previous chapter we discussed the main properties of the Matrix model which consists of Yang-Mills and Myer's interaction terms and developed Monte Carlo algorithms which allow us to simulate it. In this chapter we apply our numerical methods and report the results.

The structure of the chapter is as follows. In §5.1 and §5.2 we present background field method based analysis of the fluctuations of on the fuzzy sphere phase side. In §5.3 following C. Domb and J.L. Lebowitz [33] we describe finite-size scaling in terms of system characteristic size such as length L and then we give a formulation in terms of the matrix size N which is more natural in the context of matrix models. In §5.4 we present the main features of the phase transition of the full system and in §5.5 we present our numerical results for small matrix size. In §5.6 we present our numerical results for the critical behaviour of the fluctuations in the fuzzy sphere phase regime. We measure the critical exponents of the specific heat and the magnetic susceptibility and establish finite size scaling. We have published part of the results related to scaling from this chapter in [64]. At the end in §5.7 we make some final comments.

5.1. Critical behaviour of the fuzzy sphere

As we will see in later sections, the studying of the phase transition of matrices with $N \geq 15$ is problematic with our algorithms. However if we restrict ourselves to the fuzzy sphere side of the transition, we can study the fluctuations of the fuzzy sphere for bigger systems.

In [26] based on the background field method an estimation of the coupling $\widetilde{g}_{\rm c}$ (or equivalently of $T_{\rm c}$) where the fuzzy sphere is not stable has been given. In a semi-classical approximation the fuzzy sphere phase does not exist for temperature T bigger than $T_{\rm c}$. Here we would like to make a remark that the transition temperature $T'_{\rm c}$ that we study in §5.5.1 is not to be confused with the critical temperature $T_{\rm c}$. The transition temperature $T'_{\rm c}$ is the temperature at which occurs coexistence of the two phases of the system. The critical temperature $T_{\rm c}$ presents the temperature at which the fuzzy sphere becomes unstable when the transition is studied in the framework of the background field method on the fuzzy sphere phase side. There is no reason to assume that $T_{\rm c}$ and $T'_{\rm c}$ are equal a priori. In [26] $\widetilde{g}_{\rm c}$ (or $T_{\rm c}$) has been estimated:

$$\widetilde{g}_{\rm c} = \left(\frac{8}{3}\right)^{\frac{3}{4}} \quad \Leftrightarrow \quad T_{\rm c} \ = \left(\frac{3}{8}\right)^{3} \approx 0.05273. \tag{5.1}$$

Expansion of the specific heat around $\widetilde{g}_{\rm c}$ gives

$$C_{\rm v}(\widetilde{g}) = \begin{cases} \frac{29}{36} + \frac{1}{4\sqrt{6}}\sqrt{\frac{\widetilde{g}_{\rm c}}{\widetilde{g}-\widetilde{g}_{\rm c}}} + \mathcal{O}((\widetilde{g}-\widetilde{g}_{\rm c})^{\frac{1}{2}})\,, & \text{for } \widetilde{g} > \widetilde{g}_{\rm c}\,; \\ \frac{3}{4}\,, & \text{for } \widetilde{g} < \widetilde{g}_{\rm c}\,. \end{cases} \tag{5.2}$$

Thus the specific heat diverges on the low temperature side of the transition, which is the characteristic behaviour of second order phase transition critical point. This suggests that the critical behaviour of the fuzzy sphere shows features of a second order transition.

The general theory of continuous phase transitions and critical phenomena suggests that, near the phase transition, the specific heat $C_{\rm v}$ and the magnetic

susceptibility on either side should behave as

$$C_{\rm v}(T) \sim A_{0\pm} + A_{\pm} \times |T - T_{\rm c}\ |^{-\alpha}, \tag{5.3}$$

$$\chi(T) \sim C_{0\pm} + C_{\pm} \times |T - T_{\rm c}\ |^{-\gamma}. \tag{5.4}$$

In the semi-classical approximation the three matrix model under consideration here seems to have a rather unusual phase transition in that the exponent α has a different value depending on which direction the phase transition is approached from

$$\alpha = \frac{1}{2} \qquad \text{for} \qquad T - T_{\rm c}\ \to 0_{-}\,.$$

Of course this is not the full picture of the transition as we have ignored the large fluctuations that bring the system between different phases.

5.2. Internal and free energy

The internal energy per degree of freedom, $U = T\frac{<\mathcal{S}>}{N^2}$, arising from the semi-classical approximation of [26], is plotted in Fig. 5.1 and the slope of this curve near $T_{\rm c}$, when expressed in terms of $\widetilde{g}$, results in the form (5.2) for the specific heat. The semi-classical approximation on the low-temperature side is given by

$$\frac{S}{N^2} = \frac{3}{4} - \frac{\phi^3(T)}{24T}. \tag{5.5}$$

On the high temperature side the internal energy is

$$U = \frac{3}{4}T \tag{5.6}$$

from (4.18), and so approaches the phase transition with a finite slope, giving constant specific heat (4.19).

On the low temperature side the internal energy has a jump proportional to the black vertical dotted line, which is the typical behaviour of a first order phase transition. This jump corresponds to the latent heat of the transition. This

implies that a small correction to T near T_e can give a very large correction to the latent heat, $\Delta U(T_e)$. Thus the transition has properties which are characteristic of both first and second order phase transitions.

The free energy per degree of freedom was also derived, in the same approximation as the internal energy above, in [26]. On the low temperature side it is[1]

$$\frac{F}{N^2} = T\left[\ln\left(\frac{\phi}{T}\right) - \frac{1}{3}\right] - \frac{\phi^4}{24}. \tag{5.7}$$

Conversely, on the high temperature side, integrating

$$U(T) = -T^2 \frac{d}{dT}\left(\frac{F}{T}\right) = \frac{3}{4}T, \tag{5.8}$$

leads to

$$\frac{F}{N^2} = C_1 T - \frac{3}{4} T \ln T, \tag{5.9}$$

with C_1 an integration constant. Adjusting C_1 so that $F(T_e)$ matches on the high and low side gives $C_1 = \frac{\ln 6}{4} - \frac{7}{12} \approx -0.1354$ and results in the free energy per degree of freedom shown in Fig. 5.2. There is a jump in the specific entropy, $s = -\frac{1}{N^2}\frac{dF}{dT}$ as we go through the phase transition, $\Delta s = \frac{1}{3}$.

Of course this classical and semi-classical analysis is not the whole story and indeed the purpose of the present work is to study the characteristics of this phase transition numerically.

5.3. Finite size critical systems

Phase transitions with divergent observables are possible only in the thermodynamic limit, which in our case would correspond to taking $N \to \infty$. We can of course only perform numerical studies of systems consisting of finite size ma-

[1] One must be careful in specifying the measure when determining the free energy, and the measure for the matrices X_a differs from that for the D_a by a temperature dependent factor [26]. The from of the free energy quoted here is that associated with the D_a.

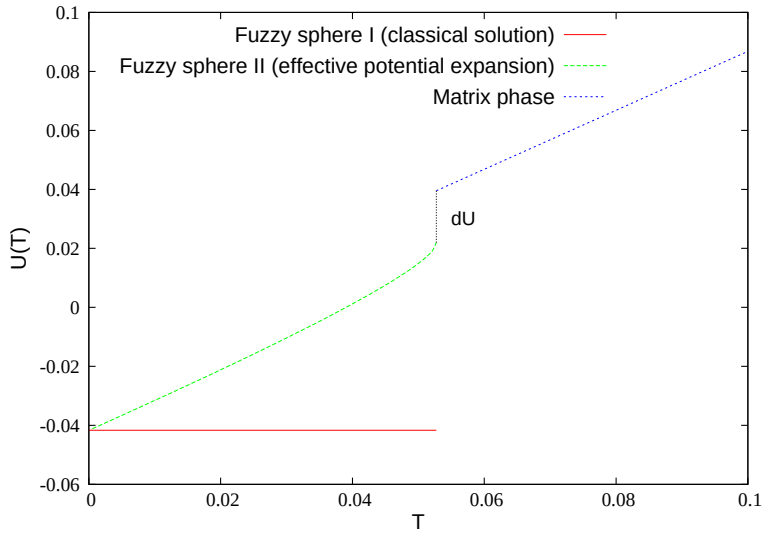

Figure 5.1.: A semi-classical approximation for the internal energy per degree of freedom of the three matrix model, as a function of temperature, showing critical behaviour on the low temperature side (equations (5.5), (4.24) and (4.25)) and non-critical behaviour on the high temperature side. The slope of this curve near T_c, when expressed in terms of $\widetilde{g}$, results in the form (5.2) for the specific heat.

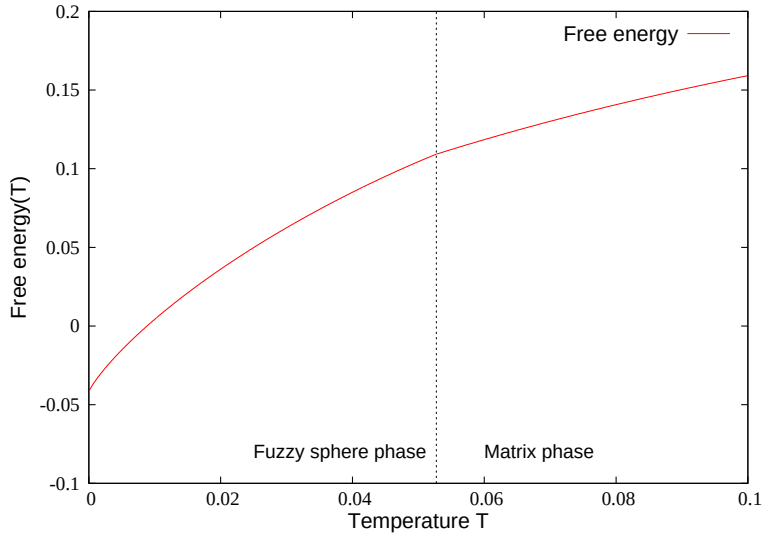

Figure 5.2.: A semi-classical approximation for the free energy per degree of freedom of the three matrix model, as a function of temperature, from equations (5.7) and (5.9). By construction the free energy is continuous at the critical point, but it is not differentiable, the left derivative is slightly greater than the right derivative, leading to the jump in entropy described in the text.

trices. Thus the systems we simulate will only undergo *pseudo* phase transition with peaks of the observables near the critical point instead of singularities as we can see from Fig. 5.10 and 5.11. Increasing N brings the system closer to the thermodynamic limit but also increases the computer resources required for the numerical study. Truly $N \to \infty$ systems can only be approximated by finite N systems and the results must be extrapolated. The finite-size effects are described in the framework of the so called *finite size scaling*. The reviews in [33, 68, 81, 76, 41] provide very detailed treatment of the subject. The important point is that the finite size effects tend to scale with the number of degrees of freedom. Using this scaling we can make predictions for large size systems. In Fig. 5.3 we plot the specific heat C_v as a function of the temperature for systems with $N = 40$ and 100 in an interval of temperatures around the transition. The deviation of some of the largest values of C_v in the numerical data from the theoretical curve shows the finite size shift that we wish to analyze. We can see that the bigger system with $N = 100$ provides a better approximation to the theoretical curve. This can be seen more clearly in Fig. 5.4 which is focused on the area around the critical point for different values of N.

In the next section we present the main ideas of finite size scaling by following [33] and adopting the notations for our needs. We also comment on the specifics of scaling related to the matrix nature of our systems.

5.3.1. Thermodynamic limit away from the critical point

Let $F(T, V, N_d)$ be the free energy for a system with N_d degrees of freedom confined in a domain with volume V at temperature T. In the thermodynamic limit the free energy per degree of freedom is usually taken to be

$$f_\infty(T, \rho_0) = \lim_{N_d \to \infty V \to \infty} \Big(\frac{1}{N_d} F(T, V, N_d) \Big), \tag{5.10}$$

with $\rho_0 = V/N_d$ finite. In our case we effectively have only one parameter which describes the size of the system, $N_d = 3(N^2 - 1) \sim N^2$. The thermodynamic

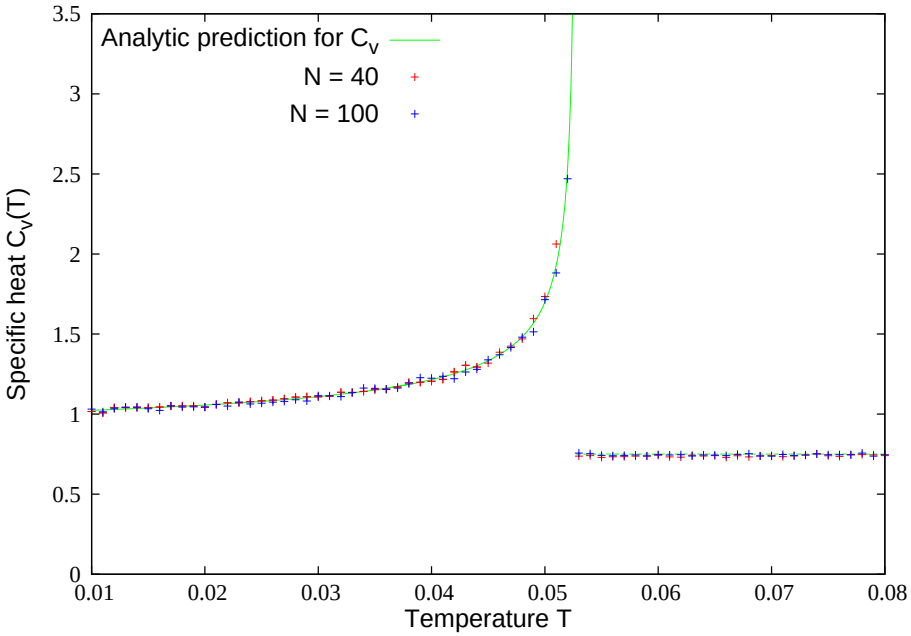

Figure 5.3.: Specific heat for $N = 40$ and $N = 100$ as a function of temperature (or equivalently, $\frac{1}{g^4}$), compared to the theoretical prediction (4.27). The deviation of the numerical data from the theoretical curve on the fuzzy sphere phase side, for the largest values of C_v plotted very close to the critical point, is a finite size effect. The uncertainties significant, but omitted for clarity. The reader can consult Fig. 5.24 and 5.25 to see the magnitude of the errors.

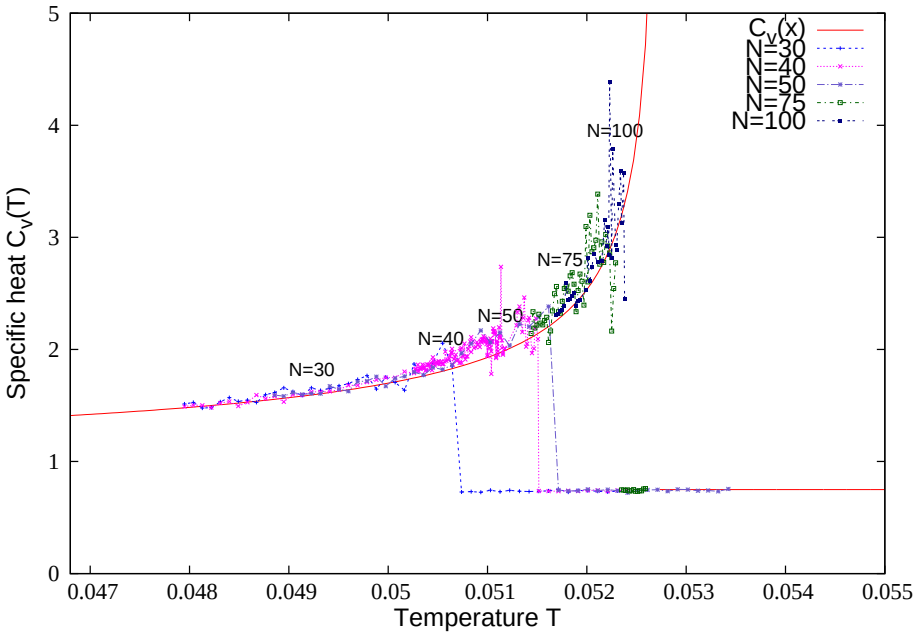

Figure 5.4.: Specific heat for different system sizes, compared to the theoretical prediction (4.27). The plot is focused on the area around the critical point.The uncertainties significant, but omitted for clarity. The reader can consult Fig. 5.24 and 5.25 to see the magnitude of the errors.

limit then reads

$$f_\infty(T) = \lim_{N\to\infty} \left(\frac{1}{N^d} F(T,N) \right). \tag{5.11}$$

Far away from a critical point we expect this limit to exist and to be independent of the geometry. For finite systems, with free surface boundary conditions, the free energy is usually split into *bulk* and *surface* free energy $f_s(T)$, which in our case would be expressed as

$$F(T,N) = N^2 f_\infty(T) + N f_s(T) + \mathcal{O}(N). \tag{5.12}$$

When the volume is finite there is a characteristic system size $L \sim V^{\frac{1}{d}}$, where d is the dimension, and

$$V \sim L^d \sim N^{d\vartheta}, \tag{5.13}$$

where the linear size of the system to grows like[2]

$$L \sim N^{\vartheta}. \tag{5.14}$$

If we assume that our system has physical volume, for the thermodynamic limit to be well defined we would need N_d/V to be a finite constant in the limit $N \to \infty$. This implies

$$d\vartheta = 2. \tag{5.15}$$

Finally relation (5.14) then gives

$$L \sim N^{2/d}. \tag{5.16}$$

5.3.2. Finite size effects and correlation length

Let us consider a finite-size system of characteristic size L as an approximation to a system in the thermodynamic limit which has a critical temperature $T_{\rm c}$. When the finite-size system approaches the critical temperature $T_{\rm c}$ there are a number of important effects that must be taken into account. First there is a temperature, called the *rounding temperature* $T^*(L)$, at which $N^2 f_\infty(T) \gg N f_{\rm s}(T)$ is not fulfilled and the finite system starts to behave differently to the infinite system. One expects that $\lim_{L\to\infty} T^*(L) \to T_{\rm c}$, as bigger systems should provide a better approximation to the thermodynamic limit. We assign an exponent θ to the rounding temperature in terms of the system size

$$|T^*(L) - T_{\rm c}|/T_{\rm c} \sim A_\theta \times L^{-\theta} \tag{5.17}$$

(note the distinction between ϑ in (5.14)and θ in (5.17)). We also note that in general the rounding temperatures as extracted from measurements of two different observables— in our case these are the specific heat and the magnetic susceptibility- need not agree a priori. Thus they might have two different exponents θ_{C_v} and θ_χ. Our numerical results indicate that the two rounding temper-

[2]The case $\vartheta = 1$ corresponds to the case of a lattice theory where the linear size of the system is proportional to the number of lattice sites.

atures are very close to each other and should produce the same exponent. This can be seen from the comparison of the critical behaviour of C_v and χ for the $N = 12$ system which is plotted on Fig. 5.10 and 5.11. Indeed the two observables have peak at approximately the same temperature. This is the reason we work with $\theta := \theta_{C_v}$.

Another finite size effect, which is directly visible in Fig. 5.4, is that the thermodynamic quantities which are expected to diverge at the critical point merely have extremal values in finite systems, at some temperature $T_{\rm m}(N) \neq T_{\rm c}$. Such temperatures are called *pseudo-critical*. Again we expect that $\lim_{N\to\infty} T_{\rm m}(N) \to T_{\rm c}$, so we define the *shift exponent* λ, again in terms of L, by

$$|T_{\rm m}(L) - T_{\rm c}|/T_{\rm c} \sim A_\lambda \times L^{-\lambda}. \tag{5.18}$$

Again as in the case of the rounding temperatures the pseudo-critical temperatures as obtained from C_v and χ are in good agreement. That is why we define only one shift exponent.

Thus at finite size, the divergent quantities have maxima $C_{\rm vm}(L) = C_v\big(T_{\rm m}(L)\big)$ and $\chi_{\rm m}(L) = \chi\big(T_{\rm m}(L)\big)$. We expect $C_{\rm vm}(L) \to \infty$ as $L \to \infty$ and $\chi_m(L) \to \infty$ as $L \to \infty$. A system with size L should diverge to infinity by some power law

$$C_{\rm vm}(L) \equiv C_{\rm v}(T_{\rm m}(L)) \sim A_{\omega_{C_{\rm v}}} \times L^{\omega_{C_{\rm v}}}, \tag{5.19}$$

$$\chi_{\rm m}(L) \equiv \chi_{\rm v}(T_{\rm m}(L)) \sim C_{\omega_\chi} \times L^{\omega_\chi}. \tag{5.20}$$

The exponents θ, λ, $\omega_{C_{\rm v}}$ and ω_χ describe the critical behaviour of our finite system. $\omega_{C_{\rm v}}$ and ω_χ are in general different as they are related to the critical exponents α and γ. If we assume that the only relevant quantity in an expansion around $T_{\rm c}$ is the correlation length, then the exponents λ and θ should be the same, though the amplitudes A_θ and A_λ may differ.

Usually the correlation length $\xi(T)$ of a system plays a crucial role in the explanation of finite size critical systems such as the Ising model or gas systems.[3] It can be defined as the rate of the asymptotically exponential decay of the two-

[3]In the case of matrix models, due to the non-local type of interaction between the entries and the absence of notion of distance between elements, we can only speculate on the existence of correlation length.

point function of the non-critical system

$$\Gamma(r,T) \sim \exp(-r/\xi(T)) \quad r \to \infty\,, \tag{5.21}$$

from which the $\xi(T)$ can be computed as

$$\xi^{-1}(T) = -\lim_{r\to\infty}(\ln(\Gamma(r,T)/r)). \tag{5.22}$$

The expression (5.22) is hard to apply on numerical data because one needs to take the $r \to \infty$ limit in finite size system. Ways around this problem are proposed in [33]. In particular one might consider higher moments of the correlation length.

At a critical point the correlation length diverges and, in many systems, the critical behaviour of $\xi(T)$ can be expressed as[4]

$$\xi(T) \sim \xi_0 t^{-\nu}, \tag{5.23}$$

where $t \equiv \frac{|T-T_c|}{T_c}$ is the reduced temperature, the exponent ν therefore dictates how fast the correlation length diverges when $t \to 0$ in an infinite system.

In a finite size system ξ is constrained by the size of the system and

$$\xi(T^*(L)) \sim L\,. \tag{5.24}$$

We can classify the regimes in the system in terms of the scaled variable $y = L/\xi(T)$. If $y \gg 1$, the system is below the rounding temperature and the the system behaves like a system in the bulk. As we approach get closer to the critical point eventually $\xi \to L$, $y \to 1$ and the finite size effects become important. The system no longer resembles the behaviour of the infinite system in thermodynamic limit that we try to approximate. For $y \ll 1$ the critical behaviour of the system is determined entirely from its finite size.

[4] In fact there are systems where the correlation length diverges faster then any polynomial. Famous example is *Kosterlitz-Thouless Phase Transition* where $\xi(T)$ diverges exponentially [51].

5.3.3. Scaling in terms of N

In our matrix model we do not have the concept of a volume, or an associated finite size, so we cannot use (5.17), (5.18), (5.20) or (5.24) directly. Instead we define

$$|T^*(N) - T_\mathrm{c}|/T_\mathrm{c} \sim A_{\overline{\theta}} \times N^{-\overline{\theta}}\,, \tag{5.25}$$

$$|T_\mathrm{m}(N) - T_\mathrm{c}|/T_\mathrm{c} \sim A_{\overline{\lambda}} \times N^{-\overline{\lambda}}\,, \tag{5.26}$$

and

$$C_\mathrm{vm}(N) := C_\mathrm{v}(T_\mathrm{m}(N)) \sim A_{\overline{\omega}} \times N^{\overline{\omega}_{C_\mathrm{v}}}, \tag{5.27}$$

$$\chi_\mathrm{m}(N) := \chi(T_\mathrm{m}(N)) \sim C_{\overline{\omega}} \times N^{\overline{\omega}_\chi}. \tag{5.28}$$

Combining (5.26) and (5.28) the divergence in any thermodynamic quantity P_m can be expressed in terms of the reduced pseudo-critical temperature $t_\mathrm{m}(N) \equiv \frac{|T_\mathrm{m}(N)-T_\mathrm{c}|}{T_\mathrm{c}}$ as

$$C_\mathrm{vm}(N) \sim N^{\overline{\omega}_{C_\mathrm{v}}} \sim t_\mathrm{m}(N)^{-\overline{\omega}_{C_\mathrm{v}}/\overline{\lambda}},$$
$$\chi_\mathrm{m}(N) \sim N^{\overline{\omega}_\chi} \sim t_\mathrm{m}(N)^{-\overline{\omega}_\chi/\overline{\lambda}}.$$

We define another exponent $C_\mathrm{vm} \sim t^{-\overline{\rho}}$, and finite-size scaling implies

$$\overline{\omega}_{C_\mathrm{v}} = \overline{\rho}\,\overline{\lambda}. \tag{5.29}$$

In the large N limit we expect $t_m \to t$ and so

$$\alpha = \overline{\rho} = \frac{\overline{\omega}_{C_\mathrm{v}}}{\overline{\lambda}}. \tag{5.30}$$

Thus, at finite N, the specific heat has a maximum $C_\mathrm{vm}(N) = C_\mathrm{v}\big(T_\mathrm{m}(N)\big)$, with $C_\mathrm{vm}(N) \to \infty$ as $N \to \infty$.

The relation (5.29) is derived without any reference to the correlation length of the system or any other notion of distance. Thus it cannot be used to measure

the dimensionality or any characteristic size of the system. It is important to us because it contains only exponents that are directly accessible to our numeric measurements and can be used to test the finite-size scaling hypothesis in the context of matrix models.

If we assume the existence of a correlation length $\xi(T)$, and a characteristic size for the system L, we can make a connection between the scaling exponents $\overline{\theta}$, $\overline{\lambda}$ and $\overline{\omega}_{C_\mathrm{v}}$, which describe the scaling behaviour of the system in terms in N, and their counterparts θ, λ and ω_{C_v} which have the analogous meaning but described in terms of L. By definition $T^*(N)$ is the temperature where (5.12) ceases to be valid and there is no obvious connection between $T^*(N)$ and N.

By combining (5.17), (5.23) and (5.24), and assuming $t_m \to t$ for large N, we obtain

$$\theta = 1/\nu. \tag{5.31}$$

This relation was obtained in [17] for the special case of an anisotropic slab of material, but it is probably more generally true.

Then using (5.15) we can express $\overline{\theta}$ as

$$\overline{\theta} = \frac{2}{d\nu}. \tag{5.32}$$

We have not accessed a physical correlation length in our matrix model therefore we do not have any obvious definition of ν. We can use (5.32) to define ν, at least on the fuzzy sphere side of the transition where it is reasonable to define the dimension of the system to be $d = 2$.

If we assume scaling and assert that the only characteristic of the system that determines the finite size scaling is the correlation length, then there is no other choice but to assume the same of the shift exponent

$$\overline{\lambda} = \overline{\theta} = \frac{2}{d\nu}. \tag{5.33}$$

Again this relation is supported by renormalization group calculations ([33], p.168).

Although for many systems $\overline{\lambda} = \overline{\theta}$, in general for critical exponent $\alpha > 0$ we expect $|T^*(N) - T_c| \geq |T_m(N) - T_c|$ because it is not possible to achieve $T_m(N)$ before $T^*(N)$. In order to see a maximum in some observable it must have already started to deviate from the theoretical prediction since the latter, being divergent, does not have a maximum. Thus in general $T^*(N) \neq T_m(N)$ and the amplitudes in (5.25) and (5.26) may be different. Nevertheless the exponents $\overline{\lambda}$ and $\overline{\theta}$ have a similar physical interpretation — they both characterize the ability of finite system to approximate the critical behavior of an infinite one. In this work we will measure only $\overline{\lambda}$, for purely technical reasons.

If the concept of a dimension d exists we can, using (5.16), derive similar relation between $\overline{\omega}$ and ω;

$$\overline{\theta} = \theta\frac{2}{d}\,, \quad \overline{\lambda} = \lambda\frac{2}{d}\,, \quad \overline{\omega} = \omega\frac{2}{d}\,, \tag{5.34}$$

and of course equation (5.29) can also be written in terms of the system size L,

$$\omega = \rho\lambda\,, \tag{5.35}$$

which follows from (5.29) and the relations (5.34).

However we stress that we cannot draw any immediate conclusions about the correlation length or dimensionality in the matrix model discussed here, because we have not measured d or ν directly but only the product $d\nu$ via measurement of $\overline{\lambda}$ and $\overline{\omega}$ and equation (5.33).

Finally we write some of the most important relations which arise from the scaling hypothesis as taken from [41]. In the thermodynamic limit there are many relations between the critical exponents α, β, γ, δ, ν, and η. The exponents α, β, and γ describe the behaviour of the specific heat C_v, the magnetization M, and of the magnetic susceptibility ξ of a system as a function of the temperature. The exponent δ defines the form of the critical isotherm in the $M - H$ plane of a magnetic system. The exponent η describes the power-law behaviour of the two-point correlation function close to the critical temperature.

$$\alpha + 2\beta + \gamma = 2, \tag{5.36}$$

$$\beta\delta = \beta + \gamma, \tag{5.37}$$

$$\gamma = \nu(2 - \eta), \tag{5.38}$$

$$2 - \alpha = d\nu. \tag{5.39}$$

From the above relations we can see that the critical exponents of a system are not independent and from two of them we can recover the rest. The scaling relations are supported by the experiment for various systems. The relation (5.39) (known as *Josephson scaling law*) is special in a sense as it explicitly includes the dimensionality d of the system. It is an example of a *hyperscaling* relation.

For convenience we present a table with all exponents we use through this chapter in table 5.1.

5.4. Phase transition

It is clear from the previous sections that the commuting matrix and the fuzzy sphere phases are quite different. The background values of the solutions of equations (4.18) and (4.22) give $S_{\mathrm{m}}(T) \neq S_{\mathrm{f}}(T)$ for $\forall T > 0$. Thus this might naively be classified as a first order phase transition — with latent heat. An important characteristic of critical systems near first order transition is the *coexistence* of the phases— the system can exist in both phases at a given temperature. Such behaviour is reported by Murty et al in [21]. They encounter coexistence of the phases at the transition temperature in the 10-state Potts Model.

The Monte Carlo history of the action and the radius of a system which undergoes coexistence is shown on Fig. 5.5 and 5.6. Both graphs can be used to distinguish the time spent of in the matrix phase and in the fuzzy sphere phase by the system. We can see that when the system has energy which corresponds to the matrix phase, the radius of the system fluctuates close to zero. The energy of the system in the fuzzy sphere phase agrees with (4.26) and the radius $\mathcal{R} < 1$.

exponent	description
α	Critical exponent of C_v
α_f	α on the fuzzy sphere phase side
β	Critical exponent of M
γ	Critical exponent of χ
γ_f	γ on the fuzzy sphere phase side
δ	Defines the isotherm $M - H$
η	Critical behaviour of the 2-point correlation function
θ	Rounding temp. exponent w.r.t. the number of lattice sites
θ_{C_v}	θ as defined for the case of C_v
θ_χ	θ as defined for the case of χ
$\bar{\theta}$	Rounding temperature exponent w.r.t. the matrix size
$\bar{\theta}_{C_\mathrm{v}}$	$\bar{\theta}$ as defined for the case of C_v
$\bar{\theta}_\chi$	$\bar{\theta}$ as defined for the case of χ
λ	Shift exponent w.r.t. the number of lattice sites
$\bar{\lambda}$	Shift exponent w.r.t. the matrix size
$\bar{\lambda}_\mathrm{f}$	$\bar{\lambda}$ on fuzzy sphere phase side
ν	Correlation length exponent w.r.t. the number of lattice sites
ρ	Critical exponent of a generic observable
ω	Rate of diverge in the limit $a \to 0$
ω_{C_v}	ω as defined for the case of C_v
ω_χ	ω as defined for the case of χ
$\bar{\omega}$	Rate of diverge in the limit $N \to \infty$
$\bar{\omega}_{C_\mathrm{v}}$	$\bar{\omega}$ as defined for the case of C_v
$\bar{\omega}_\chi$	$\bar{\omega}$ as defined for the case of χ
$\bar{\omega}_{C_\mathrm{v},\mathrm{f}}$	$\bar{\omega}_{C_\mathrm{v}}$ on the fuzzy sphere phase side
$\bar{\omega}_{\chi,\mathrm{f}}$	$\bar{\omega}_\chi$ on the fuzzy sphere phase side

Table 5.1.: Table with all occurring exponents.

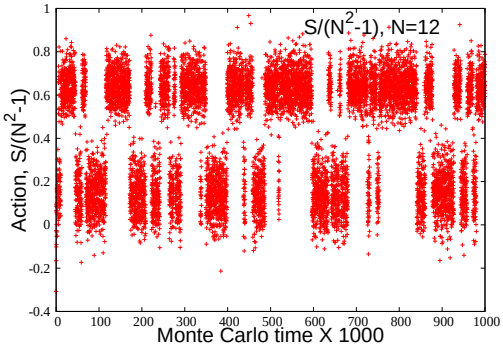

Figure 5.5.: Monte Carlo history of the action of $N = 12$ system.

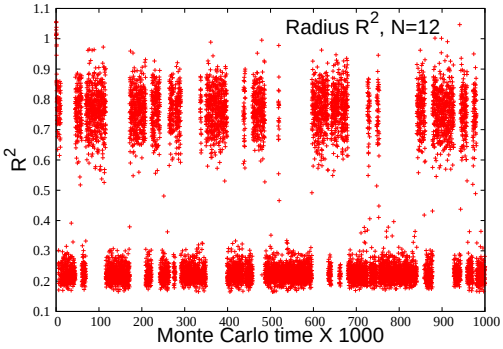

Figure 5.6.: Monte Carlo history of the observable $\mathcal{R}^2$ of $N = 12$ system.

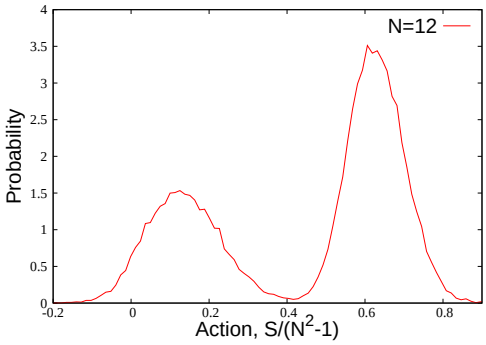

Figure 5.7.: Probability distribution of the action of $N = 12$ system in a coexistence regime.

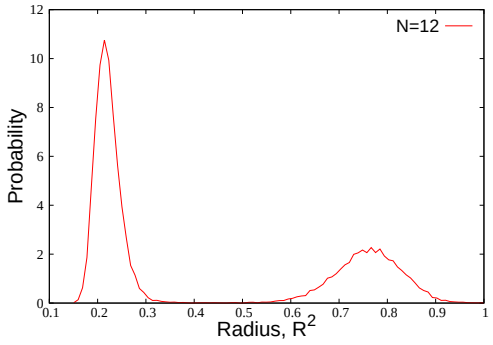

Figure 5.8.: Probability distribution of the observable $\mathcal{R}^2$ of $N = 12$ system in a coexistence regime.

We will give more details on this in the next section. We also plot the probability distributions of those observables in Fig. 5.7 and 5.8.

The theory of first order phase transitions suggests that at the transition point the free energy of the system is continuous but non-differentiable. This leads to a finite jump in its first derivative— the internal energy (or equivalently in our case the action) and δ-function divergences in secondary quantities like the specific heat C_c and the susceptibility χ. Having in mind that a system near a first order phase transition spends roughly equal Monte Carlo time in both phases

we can formally rewrite (4.2) in the form

$$\begin{aligned}\langle A\rangle \approx & Z^{-1}\int A[h^{-1}(L_a+\delta X_a)h]e^{-\mathcal{S}[h^{-1}(L_a+\delta X_a)h]}dhd(\delta X_a)+\\ & Z^{-1}\int A[h^{-1}(H_a+\delta X_a)h]e^{-\mathcal{S}[h^{-1}(H_a+\delta X_a)h]}dhd(\delta X_a).\end{aligned} \tag{5.40}$$

In the above the measure dh corresponds to the Haar measure of the $U(N)$ symmetry and $d(\delta X_a)$ is integration over the fluctuations around the corresponding background configuration H_a in the case of the matrix stationary point and L_a in the case of the fuzzy sphere stationary point. Analytical evaluation of the above integrals is difficult and we will resort to numerical techniques in order to determine the properties of the system in the vicinity of the transition. We can also write the probability distribution of the action S of the system in terms of double Gaussian distributions centered around $S_{\rm f}(T)$ and $S_{\rm m}(T)$. In other words all the properties of the system which can be expressed as first moments of such distributions will behave like a mixture of the two phases. These include the order parameter $\mathcal{R}$, the expectation value of S, and the eigenvalues of the matrices. In Fig. 5.9 we present the eigenvalue spectrum of $N = 12$ system in the fuzzy sphere phase, in the matrix phase, and near the transition. We can see that the critical spectrum exhibits properties from both fuzzy sphere and matrix phases.

In Fig. 5.10 and 5.11 we plot $C_{\rm v}$ and χ of the $N = 12$ system in the vicinity of the transition temperature. As the plots indicate, the critical behaviour of the two observables of the system is identical. Both observables have their maximum at transition temperature $T \approx 0.044$.

5.5. Numerical studies of the critical behaviour of the full system

Now we proceed with numerical studies of the phase transition between the two phases. The critical properties of the system are extracted in the regime of coexistence in the system. As noted earlier that makes the probing of big systems challenging. The problem is analogous to the one we encountered in the detection of the uniform/non-uniform phase transition of the scalar field theory in §3.10.3.

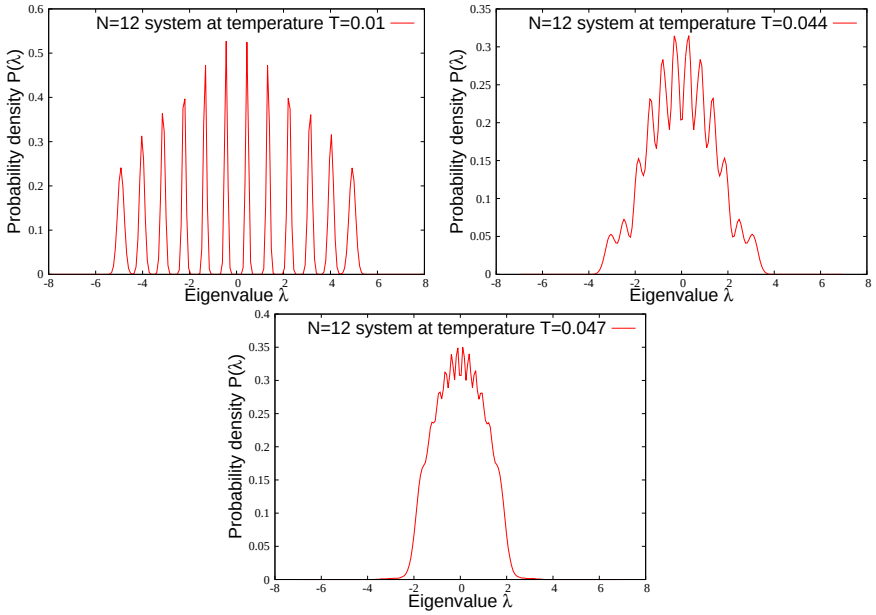

Figure 5.9.: Eigenvalue spectrum of the $N = 12$ system in fuzzy sphere phase, matrix phase, and near the transition point.

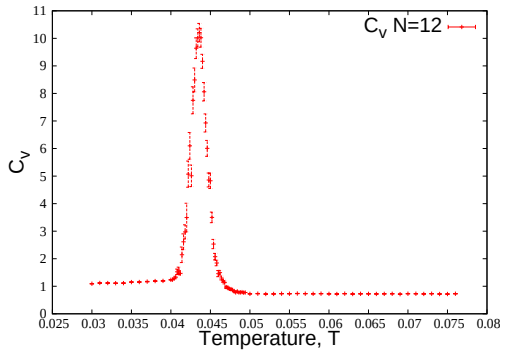

Figure 5.10.: Specific heat of the $N = 12$ system as a function of the temperature.

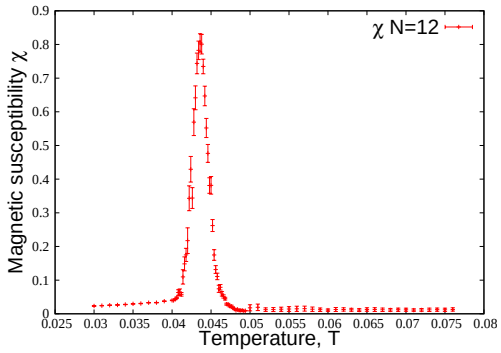

Figure 5.11.: Susceptibility of the $N = 12$ system as a function of the temperature.

This is the reason why we have simulated systems in a relatively small size range. We have data for systems of size $N = 6, 7, \ldots, 14$. In this regime we don't have any theoretical estimation for the transition temperature T_c' in the large N limit and we can only rely on our numerical data.

5.5.1. Critical temperature and shift exponent

The observables which can be used to determine the point of the phase transition include the expectation value of the action S, (or equivalently the internal energy U), the specific heat C_{v}, the order parameter $\mathcal{R}$, the magnetic susceptibility χ and others. All of the observables produce results which agree within the numerical uncertainties for the value of the pseudo-critical temperature with the exception of the smallest systems that we simulated $N = 6, 7$. In Fig. 5.10 and 5.11 we can see that the peak in the specific heat and the susceptibility of an $N = 12$ system is located at the at the same temperature T'_{m} , and they show consistency with the critical behaviour of U and $\mathcal{R}^2$ presented in Fig. 5.12 and 5.13.

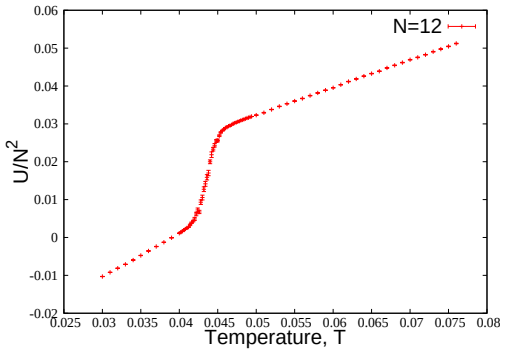

Figure 5.12.: The internal energy U per degree of freedom as a function of the temperature for $N = 12$ system.

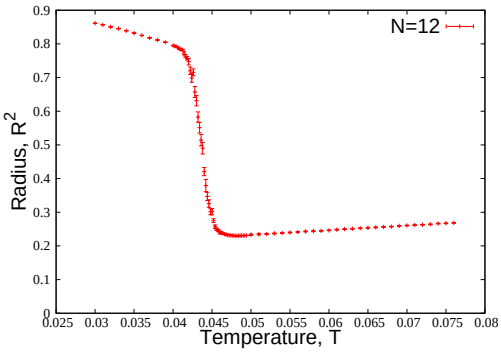

Figure 5.13.: The order parameter $\mathcal{R}^2$ as a function of the temperature for $N = 12$ system.

The graph of the internal energy looks qualitatively consistent with Fig. 5.1. Of course our system is of finite size and we don't see a jump in U. Strictly speaking we cannot rely on numerical data to determine if the transition is a first order (with finite jump in U) or the energy is continuous. Both U and $\mathcal{R}$ vary significantly in a small temperature interval around the critical temperature. We can read off the pseudo-critical temperature T'_{m} (12) as the middle point in that steep region. For that particular system we have T'_{m} $(N = 12) = 0.0436 \pm 0.0006$.

In order to get some estimation of the transition temperature T'_{c} we try to detect T'_{m} (N) for each simulated matrix size and then we extrapolate to $N \to \infty$. In Fig. 5.14 we present the specific heat of systems of different sizes. From this

N	$T'_{\mathrm{m}\,C_\mathrm{v}}(N)$	$\Delta T'_{\mathrm{m}\,C_\mathrm{v}}(N)$	$T'_{\mathrm{m}\,\chi}(N)$	$\Delta T'_{\mathrm{m}\,\chi}(N)$
6	0.048	0.004	0.052	0.004
7	0.048	0.002	0.051	0.002
8	0.050	0.002	0.051	0.002
9	0.049	0.002	0.049	0.002
10	0.047	0.002	0.047	0.002
11	0.045	0.002	0.045	0.002
12	0.0436	0.0006	0.0436	0.0006
13	0.0422	0.0006	0.0422	0.0006
14	0.0408	0.0006	0.0408	0.0006

Table 5.2.: Pseudo-critical temperatures as extracted from C_v and χ for different matrix sizes. The uncertainties denoted by $\Delta T'_{\mathrm{m}\,C_\mathrm{v}}(N)$ and $\Delta T'_{\mathrm{m}\,\chi}(N)$ decrease for bigger matrices because the peaks in the critical quantities get higher and narrower.

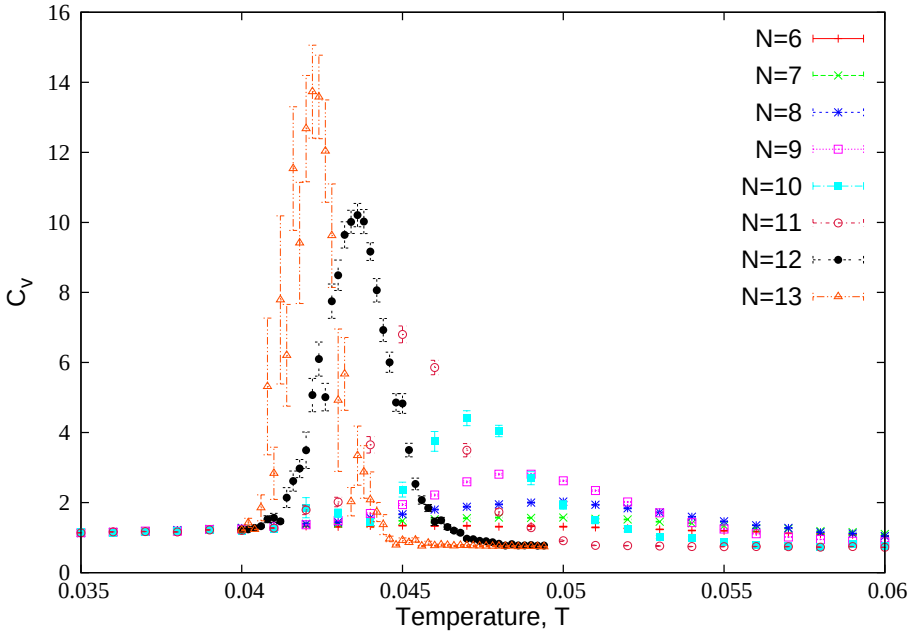

Figure 5.14.: Specific heat in the critical region of systems with size $N = 6, 7, \ldots, 13$.

data we extract the pseudo-critical temperatures. They are presented in Table 5.2. We can see that the values of the pseudo-critical temperature agree within the numerical uncertainties if extracted from different observables— in that case C_{v} and χ. Another thing to note is that the systems with $N = 6$, 7, 8 behave qualitatively differently from the rest of the set. For these systems the temperature T'_{m} (N) increases with the system size which is opposite to the behaviour of the rest of the matrices. The reason for that discrepancy is that for the small matrix sizes effectively there is no energy barrier between the two phases. The thermal fluctuations are bigger than the energy barrier between the two regimes. For those system sizes the transition is essentially continuous and we omit them. We have demonstrated the difference of the energetic profiles of $N = 6$ and $N = 10$ system at transition temperature on Fig. 5.15 and 5.16. We see that in the case of the smaller systems the energy values of the two phases overlap. A clearer view of the situation is provided by the probability distribution of the action of the two systems in Fig. 5.17 and 5.18. We can see that the distribution changes from one modal in the $N = 6$ case to two modal for $N = 10$.

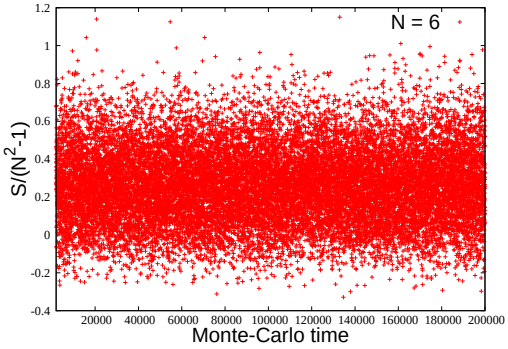

Figure 5.15.: Monte Carlo history of the action per degree of freedom of critical $N = 6$ system.

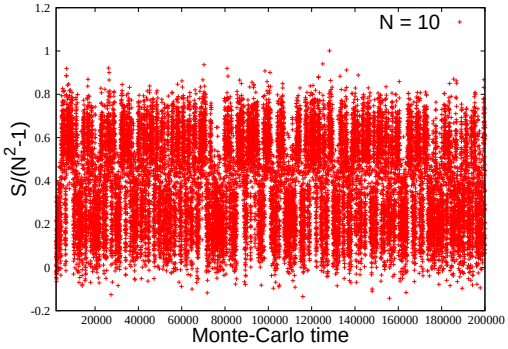

Figure 5.16.: Monte Carlo history of the action per degree of freedom of critical $N = 10$ system.

An alternative but consistent view is provided by the order parameter $\mathcal{R}$. We present the critical behaviour of $\mathcal{R}$ for different matrix sizes on Fig. 5.19.

Now that we have the pseudo-critical temperatures for different matrix sizes the question that rises is how do we extrapolate the results to the large N limit? Unfortunately we cannot give definitive answer to that question relying only on numerical results. If we assume scaling and that the simulated systems are big

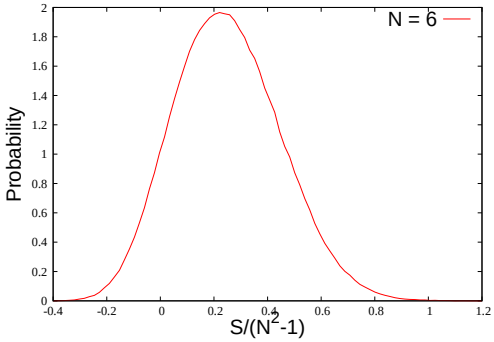

Figure 5.17.: Probability for the values of the action per degree of freedom of critical $N = 6$ system.

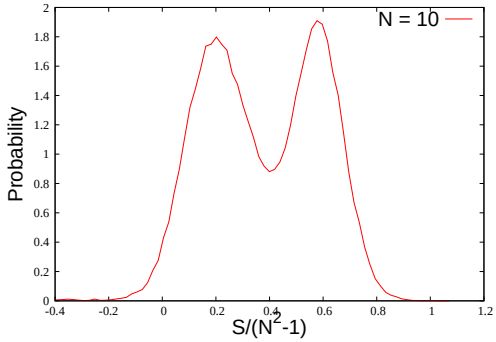

Figure 5.18.: Probability for the values of the action per degree of freedom of critical $N = 10$ system.

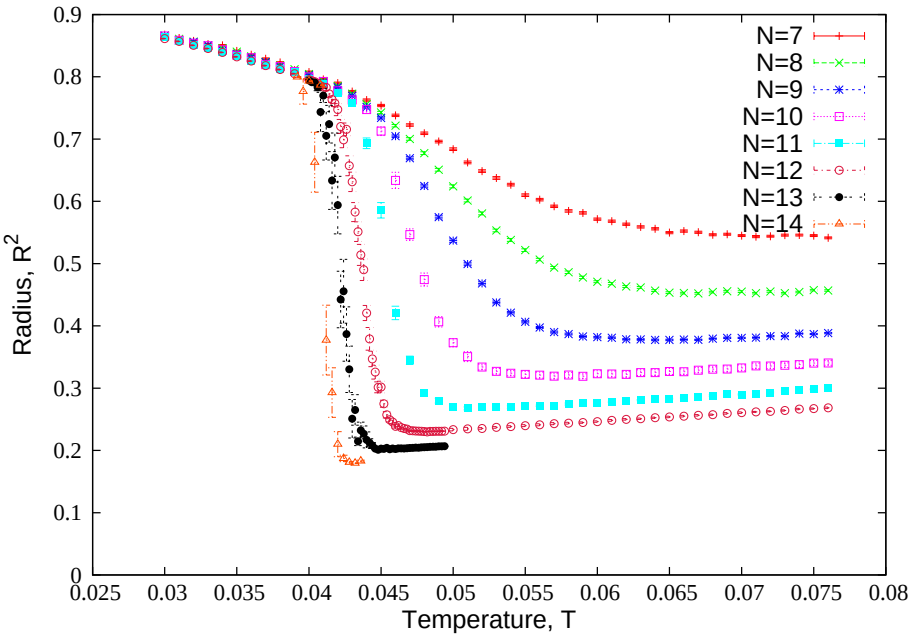

Figure 5.19.: Plot of the order parameter $\mathcal{R}^2$ as function of the temperature for different system sizes. We can see from the graphs that the critical point can be resolved better for systems with bigger size.

enough to undergo the true $N \to \infty$ scaling, the behaviour of the critical point is described by $T'_{\mathrm{m}}(N) = T'_{\mathrm{c}} + CN^{-\bar{\lambda}}$. The data we have does not allow us to fit such a curve. The reason is that we have only a few points and there is a big range of the three parameters that produce a curve relatively close to them. In other words we encounter the problem of over-fitting. What we can do is to set

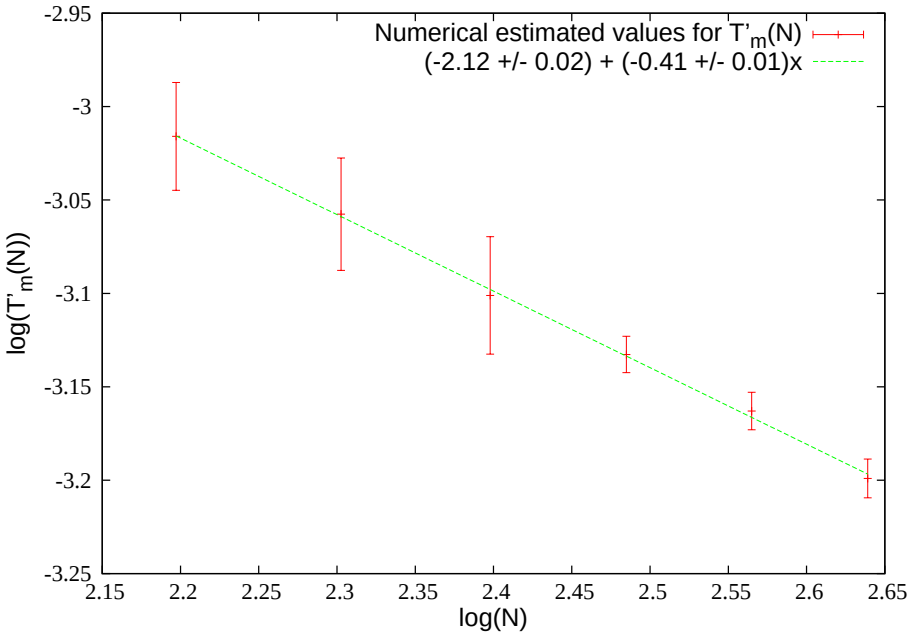

Figure 5.20.: Plot of the pseudo-cricital temperature $T'_{\rm m}\ (N)$ versus the system size in double-logarithmic scale.

upper limit for the critical temperature at the large N limit. It is $T'_{\rm c}\ \leq 0.0408$. Now if we further assume $T'_{\rm c}\ \geq 0$ we can set lower limit for the shift exponent. If we set $T'_{\rm c}\ = 0$, we are left with two parameters and we can extract an exponent from a double logarithmic plot. This fit is presented in Fig. 5.20.

The estimate that we get for the shift exponent assuming $T'_{\rm c}\ = 0$ is $\overline{\lambda}\ \geq 0.41 \pm 0.02$. The above estimate gives only a lower bound for the value $\overline{\lambda}$. In order to improve it we need additional knowledge of the transition temperature $T'_{\rm c}$ either from theoretical considerations or from independent measurements.

5.5.2. Critical exponent and scaling

Also directly accessible from our simulations are the scaling exponents $\overline{\omega}_{C_{\rm v}}$ and $\overline{\omega}_{\chi}$. We use the dataset that we used in the previous paragraph. The fits to data are shown in Fig. 5.21 and 5.22.

The obtained values are $\overline{\omega}_{C_{\rm v}} = 4.33 \pm 0.02$ and $\overline{\omega}_{\chi} = 4.24 \pm 0.16$. There are no theoretical considerations which suggest that the two exponents should agree.

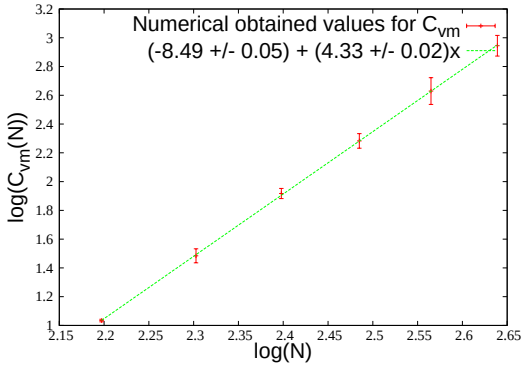

Figure 5.21.: The pseudo-critical values $C_{\mathrm{vm}}(N)$ as function of N in double-logarithmic plot. The linear coefficient in the fit corresponds to the scaling exponent $\overline{\omega}_{C_{\mathrm{v}}}$.

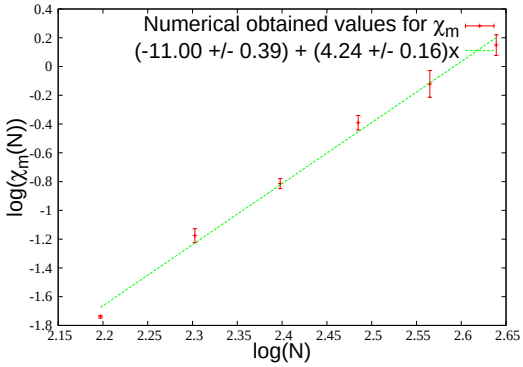

Figure 5.22.: The pseudo-critical values $\chi_{\mathrm{m}}(N)$ as function of N in double-logarithmic plot. The linear coefficient in the fit corresponds to the scaling exponent $\overline{\omega}_{\chi}$.

Thus we assume it is a coincidence. As we have estimates for $\overline{\lambda}$, $\overline{\omega}_{C_{\mathrm{v}}}$ and $\overline{\omega}_{\chi}$ we can use relation (5.29) to give some estimation of the critical exponents α and γ. We get $\alpha \leq 120.27$ and $\gamma \leq 117.8$. The reason for those poor estimates is that we use a very low estimate for $\overline{\lambda}$ from the previous paragraph. However this analysis is relevant only if the transition is continuous (second order). In case that the transition is first order the peaks from 5.14 are expected to converge to a Dirac delta- function in large N limit and the exponents α and γ are not well defined.

5.6. Numerical studies of the critical behaviour of the fuzzy sphere

Now we study the critical behaviour of the system on the side of the fuzzy sphere. As we noted earlier, the phase transition on the fuzzy sphere side has some of the characteristics of a second order phase transition. That means that we can define finite size scaling exponents similar to the ones considered in 5.3. We denote with $\bar{\omega}_{C_{\mathrm{v}},\mathrm{f}}$, $\bar{\omega}_{\chi,\mathrm{f}}$ and $\bar{\lambda}_{\mathrm{f}}$ the finite size scaling exponents and α_{f} and γ_{f} for the critical exponents for C_{v} and χ.

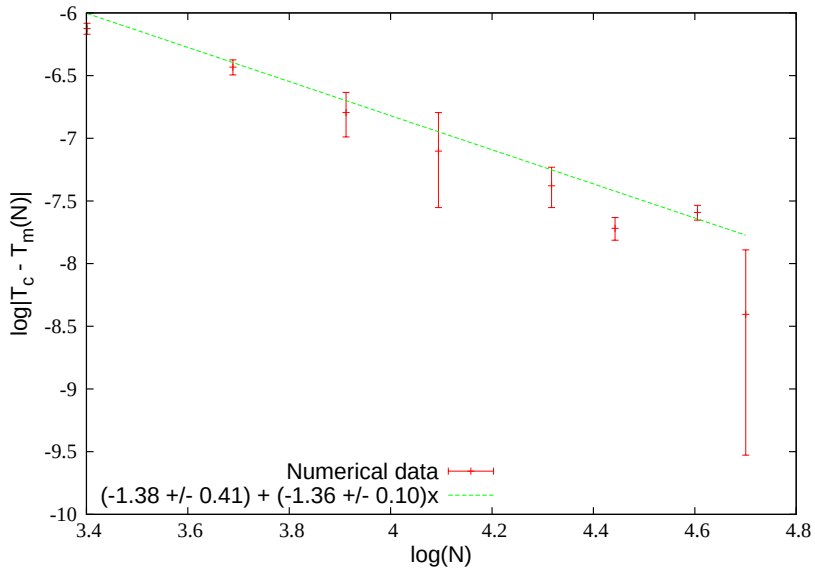

Figure 5.23.: Numerical measurement of $|T_{\mathrm{m}}\ (N) - T_{\mathrm{c}}\ |$ presented in double logarithmic scale. The data are compatible with a straight line which is an indication that the predicted value of T_{c} is in agreement with the numerical data. The error bars ΔT are obtained as the neighborhood of the peak where the values of the respective C_{v} agrees with the peak value within the numerical uncertainty.

5.6.1. Critical temperature and shift exponent

Before we can measure the critical exponents of the fuzzy sphere we need to check if our numerical results are compatible with the predicted value for critical temperature T_{c} . We have done simulations for system sizes $N = 30,\ 40,\ 50,\ 60,\ 75,\ 85,\ 100,\ 110$. In Fig. 5.23 we have plotted our numerical results for $|T_{\mathrm{m}}\ (N) - T_{\mathrm{c}}\ |$ as a function of N in double-logarithmic scale. The data is compatible with straight line which is an indication that (5.1) gives a good estimation for the critical temperature at the $N \to \infty$ limit. This fit directly produces the value of the shift exponent as well. We get $\bar{\lambda}_{\mathrm{f}} = 1.36 \pm 0.10$.

There is one important difference between the shift of the critical point studied here and the shift in the pseudo-critical temperature of the whole system from §5.5.1 . While the temperatures $T_{\mathrm{m}}\ (N)$ grow with the system size, the temperatures $T'_{\mathrm{m}}\ (N)$ decrease. This is a clear indication that critical behaviour of the fuzzy sphere alone is not enough to explain the criticality of the whole system.

One needs to know also the critical behaviour of the matrix phase together with the physics of the jumps between the two phases.

5.6.2. Measurement of the critical exponents

Scaling suggests that, for a fixed value of the temperature lower than $T^*(N)$, the values of the specific heat should be consistent for different N, provided N is large enough, and our measurements verify this expectation. We treat such values as independent measurements of $C_{\rm v}(T)$ and then take the weighted average over such values. If we have a number of independent measurements of $C_{\rm v}$, labeled by a discrete index i for different values of matrix size N_i, then the weighted average, $C_{\rm v}(T)$, is defined to be

$$C_{\rm v}(T) = \frac{\sum_i \frac{1}{\sigma^2_{N_i}} C_{\rm v}(T, N_i)}{\sum_i \frac{1}{\sigma^2_{N_i}}}, \tag{5.41}$$

where σ_i is the uncertainty in measurement i. Fig. 5.24 plots a weighted average $C_{\rm v}$ using data corresponding to values of N ranging from 30 to 110.

We can now approximate the near-critical behavior of the specific heat as $C_{\rm v} \sim A_{\rm f0\text{-}} + A_{\rm f\text{-}}|T_{\rm c} - T|^{-\alpha_{\rm f}}$ and a least squares fit produces the results in table 5.3. These values are in a good agreement with the approximate theoretical curve (5.2) and now we also have a numerical estimate the amplitude $A_{\rm f\text{-}} = 0.15 \pm 0.03$ for the ordered phase.

On the high temperature side of the transition our numerical measurements also show good agreement with the value $C_{\rm v} = \frac{3}{4} = const$ and there are two alternatives: either $A_+ = 0$ or $\alpha = 0$ for $T > T_{\rm c}$. If we assume the critical exponent is equal on the two sides of the transition we are led to the conclusion that $A_+ = 0$. Then we have the universal ratio $U_0 = A_+/A_- = 0$, the amplitudes A_+ and A_- are system and/or interaction dependent, but U_0 is universal.

We have measured the values of $C_{\rm v}$ at the points $T_{\rm m}\ (N)$ which gives us $C_{\rm vm}(T_{\rm m}\ (N))$. The results are plotted in Fig. 5.25. The slope of the linear fit produces the scaling exponent $\bar{\omega}_f$. We expect the specific heat to scale like

Table 5.3.: Critical behaviour parameters.

quantity	numerical	uncertainty	prediction
$A_{\text{f0-}}$	0.81	0.09	0.806
$A_{\text{f-}}$	0.15	0.03	0.147
α_{f}	0.51	0.04	0.5

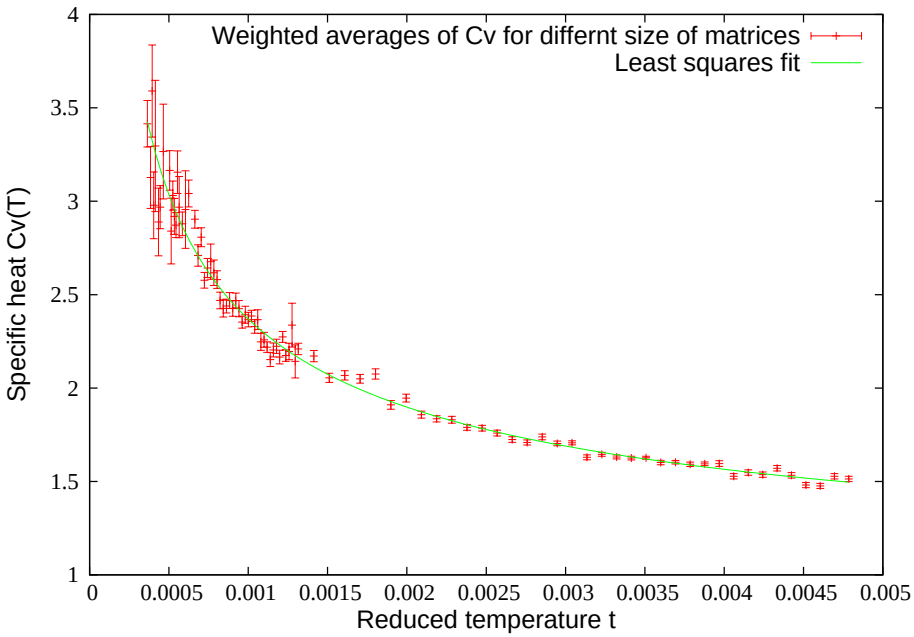

Figure 5.24.: Weight averaged C_{v} obtained from different values of N ranging from 30 to 110.

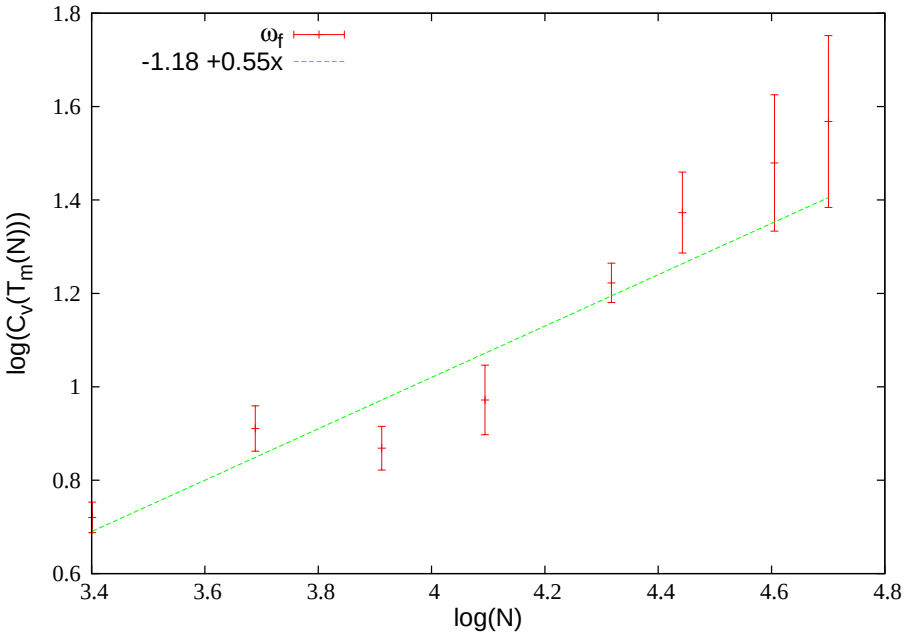

Figure 5.25.: Plot of the values of C_v at temperatures $T_\mathrm{m}\ (N)$ in double-logarithmic scale and a linear fit to it. The error bars represent the jackknife errors on our measurements.

$C_\mathrm{v}(T_\mathrm{m}\ (N)) = C_{\bar{\omega}_\mathrm{f}} N^{\bar{\omega}_\mathrm{f}}$. Our data produces values $C_{\bar{\omega}_\mathrm{f}} = 0.31^{+0.09}_{-0.07}$ and $\bar{\omega}_\mathrm{f} = 0.55 \pm 0.07$. As we have the critical exponent α_f together with $\bar{\lambda}_\mathrm{f}$ and $\bar{\omega}_\mathrm{f}$ we can verify the scaling relation (5.30). For the right-hand side of the relation we get $\alpha_\mathrm{f}\,\bar{\lambda}_\mathrm{f} = 0.69 \pm 0.11$ which agrees with the reported value for $\bar{\omega}_\mathrm{f}$ within 21% accuracy.

5.6.3. Scaled critical temperature and specific heat

The idea of scaling is based on certain assumptions about the thermodynamical properties of the systems. From a practical point of view it is helpful to us because we can use scaling to predict the properties of large N systems from the properties of smaller systems. Let's say we know the scaling exponents $\bar{\lambda}_\mathrm{f}$ and $\bar{\omega}_\mathrm{f}$ of our system together with $T_\mathrm{m}\ (N_1)$ and $C_\mathrm{v}(T_\mathrm{m}\ (N_1))$ for some fixed system size N_1. We can apply the scaling ansatz to obtain the critical temperature and the corresponding value of the specific heat for a system of arbitrary size N using the

critical values for some fixed size system. Define

$$\widetilde{C}_{\rm v}(T_{\rm m}\ (N)) := (C_{\rm v}(T_{\rm m}\ (N_1)) - A_{0\rm f})\Big(\frac{N}{N_1}\Big)^{\overline{\omega}_{\rm f}} + A_{0\rm f}, \tag{5.42}$$

and

$$\widetilde{T}_{\rm m}(N) := (T_{\rm m}\ (N_1) - T_{\rm c}\ )\big(\frac{N}{N_1}\big)^{-\overline{\lambda}_{\rm f}} + T_{\rm c}\ \ . \tag{5.43}$$

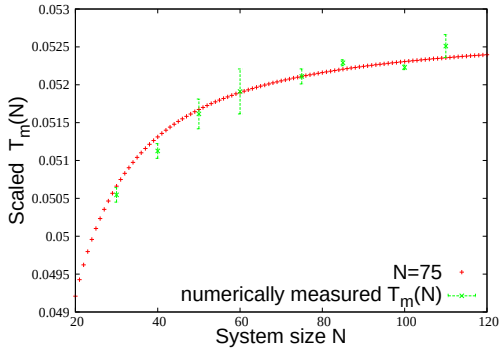

Figure 5.26.: The critical temperature obtained from scaling of system with $N_1 = 75$ compared to the numerical values, using (5.43) with $\overline{\lambda}_{\rm f} = 1.31$ and $T_{\rm c} = 0.0527$.

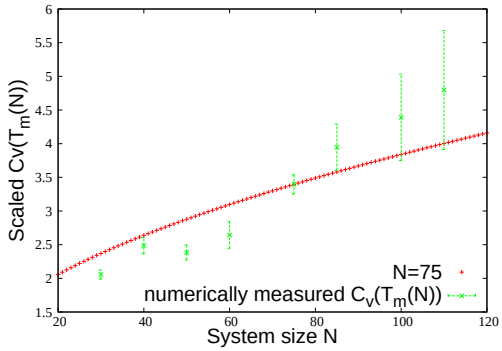

Figure 5.27.: The critical value of $C_{\rm v}$ obtained from scaling of systems with $N_1 = 75$ compared to the numerical values, using (5.42) with $\overline{\omega}_{\rm f} = 0.55$ and $A_{0\rm f} = 0.086$.

Figures 5.26 and 5.27 show $\widetilde{C}_{\rm v}(T_{\rm m}(N))$ and $\widetilde{T}_{\rm m}(N)$, obtained from (5.42) and (5.43), for a system with size $N_1 = 75$, together with the numerical values of $C_{\rm v}(T_{\rm m}\ (N))$ and $T_{\rm m}\ (N)$ respectively. Those graphs can be used as a guideline if one wants to perform simulations for larger size systems.

5.7. Final remarks

In the last two chapters we studied the critical behaviour of the Three Matrix Model using two different Hybrid Monte Carlo algorithms. Both algorithms have their advantages in certain situations. The first algorithm from §4.5 shows more jumps between the phases in the coexistence temperature regions. The algorithm

with gauge-fixed diagonal matrix X_3 from §4.6 is more efficient in terms of computer resources, but has problems in the regions with expected coexistence of the phases.

The behaviour of the theory in the vicinity of the phase transition is due to three main types of fluctuations: (critical) matrix phase fluctuations, critical fuzzy sphere fluctuations, and strong fluctuations which drive the system between the two different phases. Our data suggests that the fluctuations of the matrix phase are independent of the temperature even close to the phase transition. The critical behaviour of the fuzzy sphere shows the features of a second-order transition. It has well-defined critical exponents α_{f} and γ_{f} together with finite size exponents λ_{f}, $\omega_{C_{\mathrm{v}}\,\mathrm{f}}$ etc. The nature of the criticality is also supported by analytical arguments. This suggests also that it is driven by quantity which is analogous to correlation length. On the other hand the fluctuations which bring the system between the different phases show characteristics of a first order phase transition. Our numerics show clearly a jump in the internal energy. However the numerical results can not give reliable answer to the question of the nature of the transition due to rounding effects. Better analytical control over the theory is needed to answer the question of the nature of the phase transition and the critical temperature T_{c} . For further numerical studies of the model we need an algorithm which is able to effectively access the coexistence regime for systems with $N \geq 15$.

Chapter 6.

Final remarks and outlook

As we stated earlier, matrix models can be used both as a regulator of a QFT and as a useful formulation of problems related to non-commutative geometry, string theory, and quantum gravity. In both cases relying purely on analytic methods is not enough and the only way to study the theory in a non-perturbative way is by using (Hybrid) Monte Carlo methods. This brings the question can we expect the properties of the usual Monte Carlo simulations to be valid in the domain of matrix models? At first glance matrix theories in general are very different from the usual lattice field theories as the matrix interaction terms are non-local by construction. This is a strong argument against the assumption that the Monte Carlo of matrix models hold properties that are similar to the ones which characterize the usual lattice theories. In this work we try to make connection between Monte Carlo simulations of ordinary lattice theories and Monte Carlo simulations of matrix models. Although the algorithm of choice is Hybrid Monte Carlo, we expect our reults to be valid for a broad class of Monte Carlo integration schemes. In §3 we propose a way to define local coordinates for the matrix Φ^4 field theory defined in the fuzzy sphere with the help of the $SU(2)$ coherent states. The construction can be extended to many matrix theories which are defined on a compact manifold. In §4 and §5 we have presented numerical results which support the validity of the finite size scaling for the case of the matrix theory which contains competing Yang-Mills and Myers terms. Our results are obtained for a particular model, but give hints that scaling could be valid for matrix models in general. In the Appendix §A we go into more technical details and present some

comments on the reasons for the *critical slowdown* in a generic HMC simulation which can be made using our data.

6.1. Scalar field. Conclusions and outlook

In §3 we studied the matrix realization of ϕ^4 theory defined on the fuzzy sphere. The geometry of the model is determined by its kinetic term which is implemented via the adjoint action of the $su(2)$ generators. We also implement a method for gauge-fixing of this $SU(2)$ symmetry. The phase diagram of the model has three main regions where the scalar field exhibits different properties: disordered, matrix and uniform. Our algorithms are able to properly track the one cut/two cut phase transition between the disordered and matrix phases of the model even for relatively big systems $N \sim 50$. The phase transition between the uniform and matrix phases is more difficult to detect and our methods are efficient only for systems with $N = 2, 3$. For bigger systems we have provided only a crude estimation of the transition coordinates in the (c, b) plane. Based on our data for the transition curves, we have provided the full phase diagram of the model for $N = 7$ system. We have also studied the relative contribution of the different normal modes of the gauge-fixed field in the different phases. Our results indicate that in the disordered and uniform regimes, the main contribution to the field comes from the modes $c_{l,\, m=0,\pm1}$. By probing different points of the phase diagram deep into the matrix phase, we were able to find parameters of the theory for which higher momentum modes are also relevant. The excitation of these modes if it persists in the large N limit would imply that there are striped phases in these regions of the parameter space. As a direction of future research it would be interesting to carefully map these regions of the parameters space to get a complete phase diagram of the model.

6.2. Three matrix model. Conclusions and outlook

In §4 and §5 we studied a matrix model which consists of Yang-Mills and Myers term between three hermitian matrices $X_a \in Mat_N(\mathbb{C})$. The system can be

found in two regimes: disordered phase, and fuzzy sphere phase. In the disordered phase, the ground state is represented by mutually commuting matrices. In the fuzzy sphere phase the ground state is represented by the N-dimensional representations of $su(2)$ on $Mat_N(\mathbb{C})$. Therefore in that second phase the system has a notion of $su(2)$ geometry. There are indications that the phase transition between the two phases is first order, but when we approach the transition from the low temperature side, the fluctuations of the fuzzy sphere phase show the properties of second order phase transition.

We have developed two Hybrid Monte Carlo algorithms in order to study the fluctuations of the system near the transition: the first algorithm treats the three matrices in a uniform manner, and the second algorithm works in a specific basis in which the matrix X_3 is always diagonal. Both algorithms have their advantages. The first algorithm performs better in the temperature regions where we expect coexistence of the phases of the system. The algorithm with the diagonalized matrix X_3 is more efficient in terms of computer resources, this is why it is preferred when we study the fluctuations of the fuzzy sphere phase.

We have successfully performed simulations near the first order transition for systems with size $N \leq 14$— we have identified the transition temperature T'_{c} and the behaviour of the observables S, $\mathcal{R}$, C_{v}, χ, etc in a region around T'_{c} . Our numerical data don't allow us to make the extrapolation to $N \to \infty$ of T'_{c} . In order to answer that question about the large N asymptotics we need more analytical control over the theory in the coexistence regime. Also if we want to efficiently access the coexistence regime for bigger systems, we need an algorithm which can drive the system out of the local minima of the action without violating the detailed balance requirement from §A.1.

On the fuzzy sphere phase, we have identified the critical exponents of the observables that we expect to diverge. We have also demonstrated that their finite N behaviour can be described by finite-size scaling— we also measure shift and scaling exponents associated with those observables. Our results are consistent with the one-loop calculations of [25] and the predictions for the critical temperature T_{c} . The systems that we have simulated in that regime have size N in the range between 30 and 110. For the biggest systems we encounter severe

autocorrelation times. If we want to simulate bigger systems we would need an algorithm which minimizes the autocorrelation of the data.

6.3. First order phase transition

As final remarks we would like to note that our Hybrid Monte Carlo methods fail to simulate a system in the coexistence regime for the two models we have studied. This becomes a major problem even for relatively small system sizes: we can access coexistence for $N = 14$ in the three matrix model, but $N = 5$ is already impossible in the case of the scalar field model. The problems near a first order phase transition seem to be common for all Monte Carlo simulations based on importance sampling. If we have knowledge in advance of the local minima of the energy, a possible solution of the problem might be an algorithm which introduces *global* changes into the system that bring the system between the different potential wells. Such changes should not necessarily be based on the Hamiltonian dynamics from A.2. The requirement on such an update scheme is to preserve the condition of detailed balance.

Appendix A.

Monte Carlo: main idea

Monte Carlo is a main tool for nonperturbative studies of strongly-coupled field theories. Here we briefly mention the main idea and properties of the Monte Carlo techniques. A rigorous and consistent description of the method can be found in [61]. The goal of numerical simulations of field theories is to estimate the expectation values of observables of the system, which are functions of field configurations. By definition the expectation value of an operator A in statistical mechanics is given by an integral of the form

$$\langle A \rangle = Z^{-1} \int dX e^{-S(X)} A(X), \qquad Z = \int dX e^{-S(X)}. \tag{A.1}$$

In the above Z is the partition function of the theory and the fields are denoted as X. They may posses an arbitrary number of degrees of freedom d and the measure of the of integral is

$$dX = \prod_{\mu=1}^{d} dX_\mu.$$

In general one needs to evaluate the integral over $\mathbb{R}^d$, so the space to be integrated over becomes very large as d increases.[1] This makes the straightforward evaluation of the integrals impossible.

[1] The measure in a generic quantum field theory is infinite dimensional. In order to study such a system by numerical means one needs to make the number of degrees of freedom finite-usually by introducing a lattice.

A.1. Importance Sampling and Metropolis updating

One way to overcome the problem with the size of the configuration space is the so called *importance sampling*. The contribution to the integrals of the form (A.1) drops exponentially when the value of the action S increases. Therefore a good approximation can be obtained if we evaluate the integrand only in the domains where it has maximum contribution. In order to probe the configuration space only in the parts which contribute most, we can generate random field configurations X_i, $n \in \{1, \ldots, N_s\}$. For a system in equilibrium the density of the states $W_c(X_i)$ is given by the Boltzmann factors

$$W_c(X_i) \propto \exp(-S(X_i)). \tag{A.2}$$

An infinite set of configurations with the above density is called equilibrium (or canonical) ensemble. We can only estimate the canonical ensemble by a set with finite number of configurations. After a significant number of configurations N_s has been generated, we can compute the estimate the observable A by

$$\langle A \rangle_{\mathrm{M}} \equiv \frac{1}{N} \sum_{i=1}^{N_s} A(X_i). \tag{A.3}$$

The *ergodic hypothesis* implies that

$$\lim_{N_s \to \infty} \langle A \rangle_{\mathrm{M}} = \langle A \rangle . \tag{A.4}$$

A discussion on the ergodic hypothesis can be found in [41], page 56.

Now we turn to the generation of the previously mentioned approximation of the canonical ensemble $\{X_i\}$. We start with a random field configuration X and evaluate the action $S(X)$. Then we introduce a random change to the field arriving at X'. We compute the difference $\Delta S = S(X') - S(X)$. The new configuration is accepted with probability

$$P = \min\{1, e^{-\Delta S}\}. \tag{A.5}$$

The set of configurations generated this way is called *Markov chain*. The efficiency of the algorithm depends strongly on the way we introduce the random changes to the system. Usually a global change to the system would lead to a very large difference in the action and it will be accepted with very low probability according to (A.5). This is the reason why usually one resorts to changes which involve only a few degrees of freedom between the accept/reject decision. This recipe for generation of the Markov chain can be classified as a case of *Metropolis* algorithm. It should have the following properties

1. Ergodicity. From every configuration X, there is nonzero probability during the update process of arriving at any other configuration X'.

2. In the case with multiple local minima of the action, the algorithm should be able to drive the system between those configurations. This guarantees that the calculated observables during the simulations don't depend on the initial conditions. This property is related to the ergodicity.

3. Detailed balance. Detailed balance is a sufficient but not necessary condition which if fulfilled guaranties that the density of the configurations tends to W_c when the number of generated configurations is large.

A.2. Hybrid Monte Carlo (HMC)

Hybrid Monte Carlo is the most popular algorithm for QCD simulations. It originates in the work of S. Duane et al [35]. A very descriptive and easy to follow presentation of it is given in the tutorial of Stefan Schaefer [73]. And an overview of the recent developments with regard to simulations of dynamical fermions can be found in [74].

A.2.1. Basic idea

As we pointed out in the previous section during a Metropolis update scheme we usually introduce only local changes of the system. This means that the system is led to the minimum of the free energy for each degree of freedom and not as a

whole. The HMC algorithm is a modification of the Metropolis which allows for global changes to the system to be accepted. The main idea of the method is to introduce the conjugate momenta P_μ to our fields X_μ and treat the system as a Hamiltonian one. In this way we can let the system of interest evolve according to the Hamiltonian equations[2]

$$\begin{aligned} \dot{X}_\mu &= \frac{\partial \mathbf{H}(X,P)}{\partial P_\mu} \\ \dot{P}_\mu &= -\frac{\partial \mathbf{H}(X,P)}{\partial X_\mu}. \end{aligned} \tag{A.6}$$

The Hamiltonian is defined as

$$\mathbf{H}(X,P) = \frac{1}{2}P^2 + \mathbf{S}(X). \tag{A.7}$$

The expectation values of the system are extracted in the same way as in the case of Metropolis

$$\langle A \rangle_{\mathrm{HMC}} \equiv \frac{1}{N}\sum_{n=1}^{N_s} A(X_n). \tag{A.8}$$

A.2.2. Algorithm

The simulation works as follows. We start with a random configuration (X,P). We are free to choose any configuration for X as it is only an initial value and the outcome of the simulation should not depend on it, but we should be more careful with P, it will be discussed shortly. We compute the value of $\mathbf{H}(X,P)$. Now we approximate the system (A.6) by

$$\begin{aligned} (X((n+1)\epsilon))_\mu &\approx \frac{\partial}{\partial P_\mu}\mathbf{H}(X(n\epsilon),P(n\epsilon))\epsilon + (X(n\epsilon))_\mu, \\ (P((n+1)\epsilon))_\mu &\approx -\frac{\partial}{\partial X_\mu}\mathbf{H}(X(n\epsilon),P(n\epsilon))\epsilon + (P(n\epsilon))_\mu. \end{aligned} \tag{A.9}$$

The derivative with respect to P in (A.9) is independent of the model and always evaluates to $\partial_{P_\mu}\frac{1}{2}P_\mu^2 = P_\mu$. What depends on the model is the other part

[2]These equations don't represent the real dynamics of the system.

$\partial_{X_\mu} H(X,P) = \partial_{X_\mu} S(X)$. Following the notation in [73] we denote the steps we use in the integration of the system by

$$\begin{aligned} \mathcal{I}_1(\epsilon) &: (X_\mu, P_\mu) \to (X_\mu + \frac{\partial}{\partial P_\mu}\mathbf{H}\epsilon, P_\mu), \\ \mathcal{I}_2(\epsilon) &: (X_\mu, P_\mu) \to (X_\mu, P_\mu - \frac{\partial}{\partial X_\mu}\mathbf{H}\epsilon). \end{aligned} \tag{A.10}$$

Usually the integration during one Hybrid Monte Carlo step is done by consecutively applying the transformations (A.10). Two schemes are widely used:

1. Leapfrog integration

$$[\mathcal{I}_1(\frac{\epsilon}{2})\mathcal{I}_2(\epsilon)\mathcal{I}_1(\frac{\epsilon}{2})]^{N_I}. \tag{A.11}$$

2. Omelyan

$$[\mathcal{I}_1(\xi\epsilon)\mathcal{I}_2(\frac{\epsilon}{2})\mathcal{I}_1((1-2\xi)\epsilon).\mathcal{I}_2(\frac{\epsilon}{2})\mathcal{I}_1(\xi\epsilon)]^{N_I}. \tag{A.12}$$

   The parameter ξ is tunable and its optimal value depends on the system under study. In this work we have used the value $\xi \approx 0.1931833$ as recommended in [73].

The Omelyan integrator is about twice as expensive in terms of computer time compared to Leapfrog, but also reduces the violation of energy conservation roughly by the factor of 2. The parameter N_I specifies how many times we apply the sequence of the transformations between two accept/reject decisions in either integration scheme. Thus $l = N_I\epsilon$ could be interpreted as the "trajectory length" in the phase space. Bigger values of l lead to uncorrelated data, but decreases the acceptance rate. In order to keep the acceptance rate higher with a big value for l, we need to decrease ϵ and increase N_I. However, increasing N_I means more time spent on integration. The best values of the parameters depend on the particular simulation. Usually for a Hybrid Monte Carlo simulation, the

target acceptance rates are in the range $60\% - 80\%$ and ϵ is changed dynamically during the simulation.[3]

After applying the transformations (A.11) or (A.12) to the system it has evolved from configuration (X, P) to a new configuration (X', P'). The new configuration is accepted with probability

$$P = \min\{1, e^{-\Delta \mathbf{H}}\}, \tag{A.13}$$

where $\Delta \mathbf{H} = \mathbf{H}(X', P') - \mathbf{H}(X, P)$.

A.2.3. Properties of the algorithm

As the above equations are approximation of the system of first order, in the case of the Leapfrog and Omelyan integrators, the Hamiltonian of the system is conserved along a phase space trajectory $(X, P) \to (X', P')$ up to $\mathcal{O}(\epsilon^2)$. Similar to Metropolis we accept the new proposed state of the system with probability $\min\{1, e^{-\Delta \mathbf{H}}\}$. This means that we can control the acceptance rate during the simulation by tuning the parameter ϵ. Also the relation $\Delta \mathbf{H} \propto \epsilon^2$ can be used while testing the code. In case the new state is not accepted, we need to restore X to its old state. At the beginning of each step, we generate values for the momentum according to the normal distribution $e^{-\frac{P_\mu^2}{2}}$. In general we are free to choose any distribution for generation of P as long as all the degrees of freedom have the same relative weight. However a normal distribution is preferred over a uniform one in order to avoid problems related to the sharp cut-off to the random momenta. We use the standard Box-Muller method to generate normally distributed numbers. More details on it can be found in [72].

Although we have a discrete version of the Hamiltonian equations, some of the properties of the system (A.6) are preserved. As is obvious from (A.10), the transformations are time-reversal invariant. This means that if we evolve the state (X, P) by applying $\mathcal{I}_1(\epsilon)$ and $\mathcal{I}_2(\epsilon)$ and this leads us to (X', P'), then flip

[3] Once the system has reached equilibrium, it is not recommended for the parameter ϵ to be changed. In the present work we change the parameter during the simulation but those changes are rare and don't affect the results of the computed observables.

the momentum $P' \to -P'$ and again apply $\mathcal{I}_1(\epsilon)$ and $\mathcal{I}_2(\epsilon)$, we should end up in $(X, -P)$.[4] Again this can be used as a consistency check for a simulation.

Another feature of the Hamiltonian equations which is preserved is the phase element conservation. From this follows

$$\left\langle e^{-\Delta H} \right\rangle = 1, \tag{A.14}$$

which provides yet another consistency check.

The expectation values of the observables are computed as in the case of Metropolis (A.3).

A.3. Algorithm complexity

There is a difference in the efficiency between the Metropolis and Hybrid Monte Carlo algorithms which is possibly specific to the context of the matrix models. For a broad class of matrix models the action of the theory is given as a trace over some matrix polynomial of the form

$$P(X) = a_n X^n + a_{n-1} X^{n-1} \ldots + a_1 X^1 + C. \tag{A.15}$$

The most expensive operation in (A.15) in terms of computational resources is the matrix multiplication. In general the complexity of matrix multiplication is $\sim \mathcal{O}(N^3)$. The equations of motion (A.6) contain the derivative of the action functional and can also be expressed in terms of matrix polynomials. Thus if the observables that are measured during the simulation do not require higher than $\sim \mathcal{O}(N^3)$ complexity we can keep the whole HMC algorithm complexity $\sim \mathcal{O}(N^3)$. Important example of algorithms that do not fall into this class are models which include dynamical fermionic terms.

In the case of Metropolis, in order to change every degree of freedom independently, one already has an algorithm whose time grows like $\sim \mathcal{O}(N^2)$. Then in order to keep the algorithm's complexity to be $\lesssim N^3$, one needs to perform only

[4] Of course this is true up to rounding errors in the floating point arithmetic on the computer.

operations which require time $\sim \mathcal{O}(N)$ while computing ΔS. That doesn't seem to be always possible.

A.4. HMC vs. Metropolis sampling

In A.2 and A.1 we presented two algorithms which rely on *importance sampling* in order to generate approximations to the equilibrium ensemble. As the two schemes obey the requirements from A.1 the expectation values $\langle A \rangle_{\mathrm{HMC}}$ and $\langle A \rangle_{\mathrm{M}}$ should converge to the same value. However this is the case only when the simulated system has reached the equilibrium. The energy(or in the case of field theory the action) profile of a system may in principle have lots of local minima. In such situation the system can get trapped near a local minimum and as a result the configurational space that is sampled is far away from the true ground state of the system and the observables are miscalculated. On Fig. A.1 we present the Monte Carlo history of the Three Matrix Model realized with $N = 20$ matrices in the fuzzy sphere phase together with classical ground state of the system as computed from (4.22). As we can see the system visits several excited states but fails to reach the ground state. Thus measurement of $\langle S \rangle$ using the presented data would yield wrong value. This illustrates the problem with thermalization of systems with complex energy profile and makes relevant the question how fast the algorithms find the true ground state of a system. To that end here we briefly compare Metropolis and Hybrid Monte Carlo updating schemes.

In order avoid dependence of the initial condition of the system we perform all the simulations starting from the trivial configurations in which all the elements of the matrices X_a are zeroes. Our goal is to compare the computational time required from systems being simulated with one method or the other to reach the true ground state. Let us denote by τ_{M} the time required by a Metropolis simulation to generate a configuration of the fields X_a and make the accept/reject decision based on (A.5). Also τ'_{HMC} is the computer time required for generating a new configuration for X_a using the Hamiltonian dynamics (A.10) with $N_{\mathrm{I}} = 1$. For simplicity we assume $\tau'_{\mathrm{HMC}} \simeq \tau_{\mathrm{M}}$. The time required for generating of an HMC configuration is proportional to $N_{\mathrm{I}}\tau'_{\mathrm{HMC}}$, thus we compare the performance of the algorithms based on τ_{M} and $\tau_{\mathrm{HMC}} \equiv N_{\mathrm{I}}\tau'_{\mathrm{HMC}}$. We perform simulations

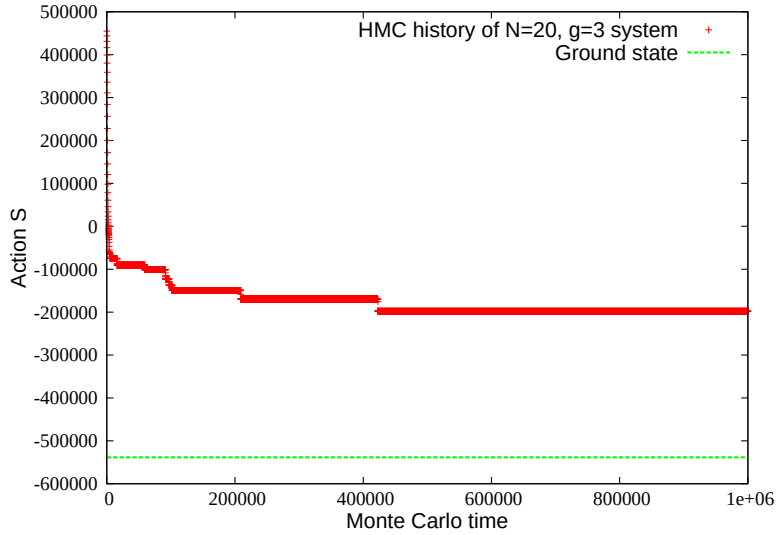

Figure A.1.: Monte Carlo history of $N = 20$ system deep into fuzzy sphere phase. Even for significant number of steps, the system cannot thermalize to its real ground state indicated by the green line.

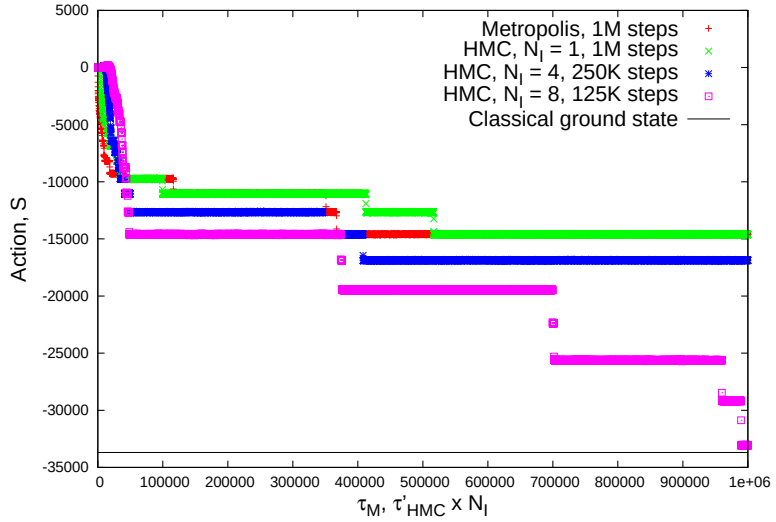

Figure A.2.: Monte Carlo histories of $N = 25$ system deep into fuzzy sphere phase simulated with Metropolis algorithm, and an HMC algorithm with different values of N_{I}.

of the Three Matrix Model with $N = 25$ and $g = 1.2$ using Metropolis and Hybrid Monte Carlo methods. The Monte Carlo histories of a system with that parameters are plotted in Fig. A.2. From the graph we can see that both the Metropolis algorithm and HMC with $N_{\mathrm{I}} = 1$ can't reach the ground state of the

system in 10^6 Monte Carlo steps. There is a slight improvement for HMC with $N_{\mathrm{I}} = 4$— it gets closer to the ground state for 25×10^4 steps. And the HMC simulation with $N_{\mathrm{I}} = 8$ is able to reach the ground state of the systems without problems within 125×10^3 steps. The integration step ϵ is changed dynamically during the simulations in order to achieve a target acceptance rate of about 70%. For the simulations with different N_{I} ϵ stabilizes at different values. In the above simulations with $N_{\mathrm{I}} = 1$, 2, 4, 8 the integration parameter ϵ settles around values 0.018, 0.018, 0.017, 0.015. This analysis tells us that we can improve the ability of an HMC algorithm to escape local minima of the action by increasing the parameter N_{I}. This helps when we simulate systems close to a first order phase transition.

A.5. Critical slowdown

In numerical calculations critical slowdown manifests itself as a correlation between consecutive measurements of given observable P, with an auto-correlation time τ_P. Consider a simulation consisting of N_{MC} Monte Carlo steps producing a set of measurements $\{P_1, \dots P_{N_{\mathrm{MC}}}\}$. If $\tau_P \leq 1$ an expectation value $\langle P \rangle$ can be computed and assigned an uncertainty $\sigma \sim 1/\sqrt{N_{\mathrm{MC}}}$. When $\tau_P > 1$ this error estimation is too optimistic, because the measurements are not fully independent, and a better estimation is given by $\sigma_{\tau_P} \sim 1/\sqrt{N_{\mathrm{MC}}/(2\tau_P)}$. The correlated dataset is effectively equivalent to an uncorrelated dataset consisting of $N_{\mathrm{MC}}/(2\tau_P)$ measurements.

The critical slowdown becomes a major problem with the size of a simulated system. There are different algorithms which are designed in a way that reduces the autocorrelation time. Interesting alternatives that we have come across and which seem to be applicable to matrix models are the *Generalized Hybrid Monte Carlo* from [79] and *Targeted Shadowing Hybrid Monte Carlo* from [48]. The first one utilizes different Hamiltonian dynamics and the second one introduces changes to the extended Hamiltonian of the system.

The autocorrelation time associated with an observable P is expected to be governed by the correlation length and near a critical point should behave as

$$\tau_P \sim \xi(T)^{d+z(P)}, \tag{A.16}$$

with dynamical scaling exponent $z(P)$, which is algorithm and observable dependent. One aim in designing an efficient algorithm is to reduce $z(P)$.

For a critical matrix model with size N we would expect, assuming (5.23), (5.25), (5.26) and (5.33),

$$\tau_P \gtrsim N^{2+z(P)\frac{2}{d}}\,. \tag{A.17}$$

In principle the autocorrelation time for an infinite dataset is computed using the series

$$\tau_P = \frac{1}{2}\sum_{n=-\infty}^{\infty}\sum_{\tau=-\infty}^{\infty}\frac{\langle (P_n - \langle P\rangle)(P_{n+\tau} - \langle P\rangle)\rangle}{\langle (P_n - \langle P\rangle)^2\rangle}\,, \tag{A.18}$$

but in practice the sum $\sum_{\tau=-\infty}^{\infty}$ must obviously be truncated to $\sum_{\tau=-\tau_0}^{\tau_0}$ with τ_0 finite. Clearly the truncated version of (A.18) can only be sensitive to autocorrelation times $\lesssim \tau_0$ so, if $\tau_0 \ll N_{\mathrm{MC}}$, τ_p might be underestimated for systems with severe autocorrelation. On the other hand, if $\tau_0 \sim N_{\mathrm{MC}}$, the convergence of (A.18) becomes very poor.

In our analysis we allow for autocorrelations using the *jackknife* procedure, see *e.g.* [61], which computes the uncertainty taking into account the autocorrelation of the data. As a consistency check we compute the autocorrelation by hand, by adjusting τ_0 manually to determine τ_P and comparing the result with τ_P as determined by the jackknife procedure.

A.5.1. Autocorrelation time of the specific heat

In this subsection we make some comments about the behaviour of the autocorrelation time of C_{v} of the theory defined by (4.1). We try to identify the contributions to the exponent $z(C_{\mathrm{v}})$ of the autocorrelation time (A.16). Although

we work with the specific heat of concrete system, our argument holds for any system near a second order phase transitions which is simulated with Metropolis or Hybrid Monte Carlo techniques. We repeat the inequality 4.7

$$\langle |\mathcal{S} - \langle \mathcal{S} \rangle | \rangle \leq N \sqrt{C_{\mathrm{v}}} \tag{A.19}$$

The expression $\langle |\mathcal{S} - \langle \mathcal{S} \rangle | \rangle$ can be interpreted as the average of the absolute deviation of the action of the system from the expectation value $\langle \mathcal{S} \rangle$. In other words this is a measure of the volume of the configurational space that the system visits during the evaluation of the path integral (A.1) in units of the action S. The system visits mainly states with action in the interval $S \in [\langle \mathcal{S} \rangle - \langle |\mathcal{S} - \langle \mathcal{S} \rangle | \rangle , \langle \mathcal{S} \rangle + \langle |\mathcal{S} - \langle \mathcal{S} \rangle | \rangle]$. We can see that a system with bigger size has to explore configurational space with bigger volume because the right side of (A.19) grows like $\sim N$. Now we look at the Monte Carlo accept/reject probability defined by (A.5). We see that the probability of acceptance of new configuration with higher action is proportional to $e^{-\Delta S}$ and we can relate $|\Delta S| \sim 2 \langle |\mathcal{S} - \langle \mathcal{S} \rangle | \rangle$. So the average ΔS grows with N. This means that if we keep increasing N we will reach some system size N_1 for which the probability $e^{-2\langle |\mathcal{S} - \langle \mathcal{S} \rangle | \rangle}$ is arbitrary small. In this case the event that the system jumps from a configuration with action $S = \langle \mathcal{S} \rangle - \langle |\mathcal{S} - \langle \mathcal{S} \rangle | \rangle$ to a configuration with $S = \langle \mathcal{S} \rangle + \langle |\mathcal{S} - \langle \mathcal{S} \rangle | \rangle$ is very rare. In order to evolve between those two configurations, the system will need to so in a couple of smaller steps— this is precisely the reason for autocorrelation in the data.

On Fig. A.3 and A.4 we demonstrate this with an example. If we consider two systems with $N_1 < N_2$ at near critical temperature $T < T^*(N_1) < T^*(N_2) < T_{\mathrm{c}}$. Finite size scaling predicts $C_{\mathrm{v}}(T, N_1) = C_{\mathrm{v}}(T, N_2)$. From (A.19) we get

$$\langle |\mathcal{S}_{N_1} - \langle \mathcal{S}_{N_1} \rangle | \rangle < \langle |\mathcal{S}_{N_2} - \langle \mathcal{S}_{N_2} \rangle | \rangle \tag{A.20}$$

In the above inequality we have defined S_{N_1} to be the action of the system with size N_1 and S_{N_2} to be the action of the system with size N_2 and their expectation values accordingly.

We present the simulation of two systems with $N_1 = 40$ and $N_2 = 100$ at temperature $T = 0.047$. The graphs show that the system with $N_1 = 40$ explores

interval of energies $S \in (250, 450)$ and the system with $N_2 = 100$ explores interval of energies $S \in (1900, 2600)$. As a result the bigger system needs more Monte Carlo time to explore the whole energy interval and this produces bigger autocorrelation in the data. As a consequence the cost of obtaining N_s uncorrelated data points for two systems with different sizes grows more rapidly than the algorithm complexity. This gives us hint that if we want to take a precise measure of C_v of a system at a given temperature T, we should choose the smallest possible system size N such that $T^*(N) > T$.

Now let us consider the system with $N = 100$ in two different temperatures $T_1 < T_2 < T^*$. From the critical behaviour of C_v we have $C_\mathrm{v} \sim |T - T_\mathrm{c}|^{-\alpha}$ near the critical point. Thus the right side of (A.19) grows like $|T - T_\mathrm{c}|^{-\alpha/2}$ when the system approaches criticality. Thus for a fixed system size the autocorrelation time near a phase transition depends on the critical exponent of the observable— in this case α. In Fig. A.5 we present also the Monte Carlo history of the action of $N = 100$ system at temperature even closer to the transition. The data clearly shows an increase in the autocorrelation time as we approach the critical temperature.

A.5.2. Autocorrelation across different observables

In the previous section we argued that the autocorrelation time of a generic observable of the system C_v near a second order phase transition depends on the system size N and on the critical exponent of the observable. The autocorrelation time of the data of some observable has another dependency on the type of the observable which is not due to the critical exponent. In Fig. A.6 and A.7 we present Monte Carlo history of the action S and the square of the radius $\mathcal{R}^2$ of $N = 50$ matrix model at temperature $T = 0.0505$ produced from the same run.

As we can see from the plots the action dataset has significantly lower autocorrelation than the radius dataset— our autocorrelation time routine reports respectively $\tau_S = 275$ and $\tau_{R^2} = 452$. The bigger autocorrelation of $\mathcal{R}^2$ leads to bigger relative error in the evaluation of the secondary quantity χ in comparison with C_v— 3.7% vs. 2%. This difference into the autocorrelation times can be explained with the different role that the two quantities S and R^2 play during our

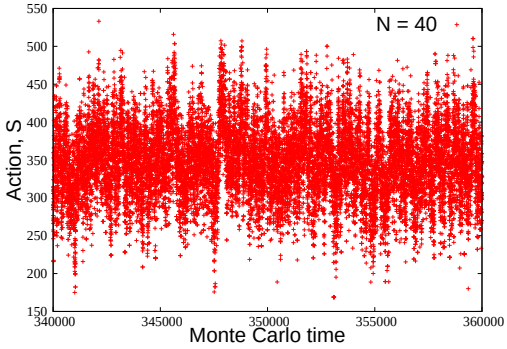

Figure A.3.: Monte Carlo history of the action of $N = 40$ system at temperature $T = 0.0470$ in the fuzzy sphere phase. From 5×10^5 data points we get $C_\mathrm{v} = 1.42 \pm 0.01$ and $\tau_S = 20$.

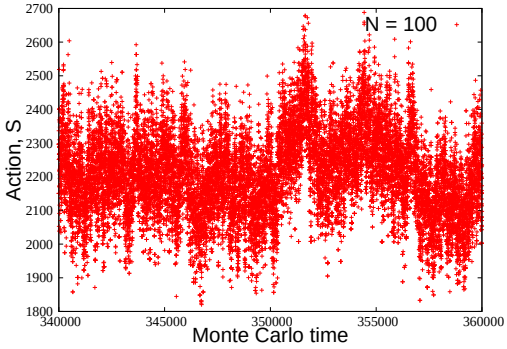

Figure A.4.: Monte Carlo history of the action of $N = 100$ system at temperature $T = 0.0470$ in the fuzzy sphere phase. From 5×10^5 data points we get $C_\mathrm{v} = 1.42 \pm 0.02$ and $\tau_S = 90$.

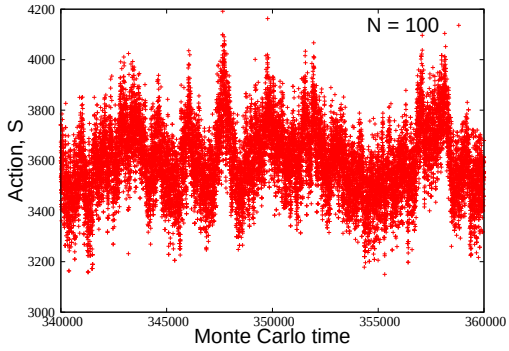

Figure A.5.: Monte Carlo history of the action of $N = 100$ system at temperature $T = 0.0520$ in the fuzzy sphere phase. From 5×10^5 data points we get $C_\mathrm{v} = 2.45 \pm 0.1$ and $\tau_S = 800$.

simulation. If we look into the Monte Carlo algorithm we can see that the evolution of the system is driven by the action S, and the changes in the system are proposed in such way as to maximize the acceptance rate during the simulation while keeping the autocorrelation to minimum. In other words the Hybrid Monte Carlo and Metropolis algorithms are optimized for minimum autocorrelation time

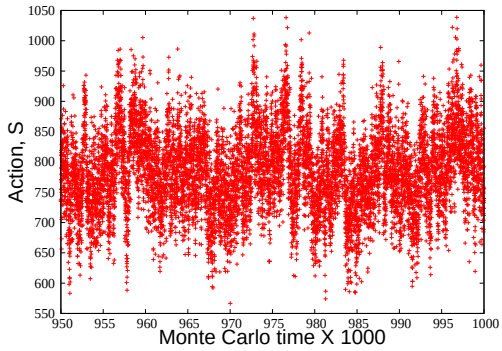

Figure A.6.: Monte Carlo history of the action of $N = 50$ system at temperature $T = 0.0505$ in the fuzzy sphere phase. From 3×10^5 data points we get $C_{\rm v} = 1.94 \pm 0.05(2.7\%)$ and $\tau_S = 275$.

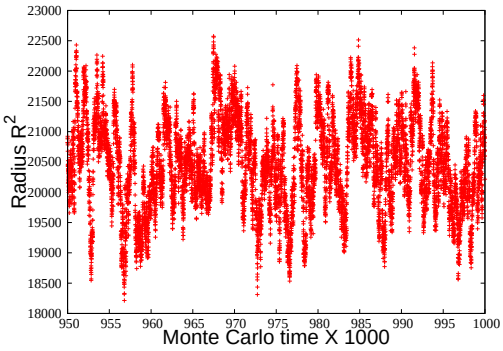

Figure A.7.: Monte Carlo history of the squared radius $\mathcal{R}^2$ of $N = 50$ system at temperature $T = 0.0505$ in the fuzzy sphere phase. From 3×10^5 data points we get $\chi = 0.095 \pm 0.004(4.5\%)$ and $\tau_{R^2} = 452$.

of the observable S. It is natural to assume that the action (and the observables which can be expressed as linear function of it) should have the smallest autocorrelation time. Any observable that can be expressed as a non-linear function of S is to be expected to have higher autocorrelation time than S. Let us consider the two observables S and $\mathcal{R}^2$ on the fuzzy sphere phase side. From (4.8) and (5.5) we have can write $\mathcal{R}^2 \sim S^{2/3}$. This can be seen as the reason for the higher autocorrelation times of $\mathcal{R}^2$.

Appendix B.

GPU implementation

During our studies we ported some of the algorithms for graphical processing unit (GPU) computation. In particular the algorithm from §4.5 was rewritten using the *OpenCL* language. In this chapter we briefly describe the main steps of the implementation of OpenCL simulation in *C++* environment. A detailed description of the language together with its host-side API can be found at [63]. A good reference with wide range purpose algorithms adapted for GPU computation can be found in [60]. An example of Lattice QCD algorithm implementation for GPU can be found in [9].

B.1. OpenCL basics

OpenCL (Open computing language) is a standard which provides access to parallel computing devices in an uniform manner. There are two types of processing units in an OpenCL program. There is a *host* which executes the main program and one or more *computing devices* which carry out the parallel operations as requested by the host. The host device usually is the CPU of the system. The computing devices can be of type CPU, GPU, or dedicated accelerators. Consequently the architecture consists of two major components

1. Host-side application programming interface (API)
2. Device-side language, the OpenCL language

In this section we briefly describe the two parts of OpenCL and mention some important aspects from the user's point of view. At the time of the writing of this thesis, the current OpenCL version is 1.2.

B.1.1. OpenCL host- side API

From the user's point of view the host–side API of OpenCL is the connecting point between the host and the computing devices. Currently there are OpenCL API bindings for *C*, *C++*, *Python*, *FORTRAN*, *Java*, *C#* etc. We use the C++ bindings for the OpenCL API provided by the standard cl.hpp header file. The host–side API fulfills the following tasks

1. Detect and enumerate all OpenCL platforms
2. Detect and enumerate all OpenCL capable devices associated with each platform. Retrieve computing capabilities.
3. Select devices belonging to one or more platforms. The host process obtains context objects for each device.
4. Create one or more *command queue(s)* associated to each context of device
5. Invoke the OpenCL compiler for each device.
6. Memory management on the computing devices. Allocate and release memory blocks used for data storage.
7. Request computational operations. Synchronize the execution and data access between different command queues.

The initialization is done in steps 1—5. A code snippet that performs these tasks is present below.

```
1 // initialize OpenCL
2
3 //  types platformVector and deviceVector are previously
      defined to be
4 //       typedef std::vector<cl::Platform> platformVector;
5 //       typedef std::vector<cl::Device> deviceVector;
6
```

```
7  //       the m_platformsVect object is defined as
8  //       platformVector m_platformsVect;
9
10 // generate a vector that contains all available OpenCL
       platforms
11 cl::Platform::get(&m_platformsVect);
12
13 // use platform 0
14 m_platform = m_platformsVect[0];
15
16 try{
17         deviceVector deviceVect;
18         // enumerate all devices associated to the selected
               platform
19         m_platform.getDevices(m_nDeviceType, &deviceVect);
20         // select device with ID m_nDeviceId (m_nDeviceId has
               been assigned earlier to be 0)
21         m_deviceVect.push_back(deviceVect[m_nDeviceId]);
22
23         // obtain context which contains the selected devics
24         m_context = cl::Context(m_deviceVect);
25
26         // create command queue associated with the context
27         m_queue = cl::CommandQueue(m_context, m_deviceVect[
               m_nDeviceId], 0);
28
29         // read the OpenCL source file "kernels.cl"
30         std::ifstream file("kernels.cl" , std::ifstream::in);
31         std::string prog(std::istreambuf_iterator<char>(file),
32                          (std::istreambuf_iterator<char>()));
33         cl::Program::Sources source(1, std::make_pair(prog.
               c_str(), prog.length()+1));
34
35         // create cl::Program object
36         m_program = cl::Program(m_context, source);
37
38         // compile the program for the selected devices
39         m_program.build(m_deviceVect, sBuildOptions);
40 }
41 catch(cl::Error &e)
42 {
```

```
43          // error handling
44          char sBuildError[16384];
45          fprintf(stderr, "Exception thrown(%d): %s\n", e.err(),
                e.what());
46          if(e.err() == -11)
47          {
48                  // build error
49                  clGetProgramBuildInfo(m_program(),
                        m_deviceVect[0](), CL_PROGRAM_BUILD_LOG,
                        16384, sBuildError, NULL);
50                  // output OpenCL compile-time error
51                  fprintf(stderr, "Build error: %s\n",
                        sBuildError);
52          }
53  }
```

Step 1 corresponds to finding of all OpenCL SDK's installed on the computer system. The situation where there are more than one OpenCL platforms installed is not uncommon. This usually happens when there are more than one OpenCL capable device on the system and they are provided from different manufacturers. One of the main requirements for an OpenCL implementation is that it should be able to find any additional implementations on the computer at runtime. It is implemented in lines 11—14. This sample code always chooses the first found platform on the system.

In step 2 we detect all the computing devices associated to the same platform. Example of such situation might be a computer system with two different graphic cards from the same vendor. We might also need the computing capabilities of each device. This is useful if we intend to use OpenCL features which are not part of the core implementation but are rather provided as extensions. It is done by the getDevices() method on line 19.

In step 3 we select the devices we intend to use for our computations and create a *context* object which will later be used for communication between the host and this group of devices. This step is implemented on lines 20—24. In this particular example we assume that the first device has the computational capabilities that we want.

Step 4 is creating the so called command queue associated with the previously created context. All the requests to the devices are done through command queues. Command queues also provide the basic synchronization mechanisms. Commands issued through one queue are guarantied to execute in the same order as requested. In our example we create only one queue. This is done by the CommandQueue() call.

Step 5 is the last step before we start the computation is the actual OpenCL code compilation. The build of the source code is done for each selected device by call to the build() method. This way the binaries are optimized for each of the devices by their own compiler. It is possible that the build is successful for some of the devices but not for all of them.

The memory management on the host's side in C++ environment is done with the help of the cl::Buffer objects. They allow us to create memory buffers on the computing devices side, to specify their size and properties together with the type of memory they represent. Also the API allows us to move data between the host and the computing devices.

After successful initialization and memory allocation we are ready to request computation operations via the command queues. This is achieved by using the enqueueNDRangeKernel() function.

B.1.2. OpenCL language

The OpenCL language allows us to write code which to be executed by a computing device side. The code is organized in OpenCL *programs*. Each program consists of one or more functions contained in one or more source files. The functions that are directly callable from the host side via the enqueueNDRangeKernel() are called *kernels*. Every program needs to have at least one kernel. This is done via the modifier *__kernel* in front of the function definition. The language is based on the *C*99 standard with some limitations and additions. Some of the most notable differences are listed below

— Recursion is not allowed

– No pointers to functions

– No dynamic memory allocation

+ Vectorized versions of the primitive data types— int2, float2, etc

+ New primitive data types— half, etc

+ Explicit distinction between memory regions via the use of the keywords __global, __local, __constant, and __private.

+ Additional keywords

IO operations are not necessarily available on all accelerators. That is why for error-checking and debugging of OpenCL code, the language relies on vendor–supplied *IO* functions and debugging. The standard printf() function is available via cl_amd_printf extension on AMD supplied devices.

B.2. OpenCL code example

As we mentioned in §4.5 most of the expensive operations in our studies are based on matrix multiplication. Here we demonstrate OpenCL source file which contains two approaches to matrix multiplication. Those matrix multiplication algorithms are described in great detail in [63]. We make some brief comments on the source code

```
1  // kernels.cl
2
3  #ifdef  cl_khr_fp64
4  #pragma OPENCL EXTENSION cl_khr_fp64 : enable
5  #else
6  #error  "double-precision floating point arithmetic is not
       available on the selected device"
7  #endif
8
9  #if !defined(nDim)
10 #error "undefined symbol nDim. Must be specified as compiler
       option -D nDim=<integer> "
11 #endif
12
```

```
13 // Naive implementation of matrix multiplication
14 // Each element of the result is computed in separate thread
15 __kernel void MatrixMult_naive(__global double2 *A, __global
       double2 *B,
16     __global double2 *C)
17 {
18     int nCol = get_global_id(0);
19     int nRow = get_global_id(1);
20     double2 z = (double2)(0,0);
21
22     for(int k = 0; k < nDim; k++)
23     {
24         z.x += A[nRow + nDim * k].x * B[k + nDim * nCol].x -
25             A[nRow + nDim * k].y * B[k + nDim * nCol].y;
26         z.y += A[nRow + nDim * k].x * B[k + nDim * nCol].y +
27             A[nRow + nDim * k].y * B[k + nDim * nCol].x;
28     }
29     C[nRow + nDim * nCol] = z;
30
31 }
32
33 // Matrix multiplication implementation which takes advantage
       of the use of local memory buffers
34 // Each thread computes one column of the result
35 __kernel void MatrixMult_local_mem(__global const double2 *A,
       __global const double2 *B, __global double2 *C,
36     __local double2 *Awrk)
37 {
38     int nLocSize = get_local_size(0);
39     int nLocID = get_local_id(0);
40     int nCol = get_global_id(0);
41     double2 Bwrk[nDim];
42     int k, nRow;
43     double2 z;
44
45     for(k = 0; k < nDim; k++)
46     {
47         Bwrk[k] = B[k + nDim * nCol];
48     }
49     for(nRow = 0; nRow < nDim; nRow++)
50     {
```

```
51          z = (double2)(0, 0);
52          for(k = nLocID; k < nDim; k = k + nLocSize)
53          {
54              Awrk[k] = A[nRow + nDim * k];
55          }
56          barrier(CLK_LOCAL_MEM_FENCE);
57          for(k = 0; k < nDim; k++)
58          {
59              z.x += Awrk[nRow + nDim * k].x * Bwrk[k].x - Awrk[
                    nRow + nDim * k].y * Bwrk[k].y;
60              z.y += Awrk[nRow + nDim * k].x * Bwrk[k].y + Awrk[
                    nRow + nDim * k].y * Bwrk[k].x;
61          }
62          C[nRow + nDim * nCol] = z;
63      }
64  }
```

OpenCL supports a wide range of devices with different hardware specifications and thus different computation capabilities. This is the reason why some of the features are not part of the core OpenCL implementation but are rather implemented as extensions. Both the OpenCL host–side API and the language provide mechanisms for detection of the available extensions on a device. On the host–side the list of available extensions could be queried by clGetDeviceInfo() call. On the device side each extension adds its name to the list of the known preprocessor macros of the compiler. As double-precision floating point arithmetic is not supported on all OpenCL devices, its support is provided by the cl_khr_fp64 extension. Without this extension we cannot define variables of type double. The preprocessor code in lines 3—8 checks if the extension is available and enables it. Otherwise it causes compile time error via the #error macro.

As OpenCL does not support dynamic arrays sometimes we need to know the size of some memory blocks in compile-time of the OpenCL code but in runtime of the of the host application. Such situation occurs with regard to the symbol nDim. We want our OpenCL code to be able to handle matrices of arbitrary size thus we need nDim to be parameter. On the other hand on line 45 we define an array of size nDim. The solution is to specify the value of nDim as option to the OpenCL compiler. In lines 13—15 we check if nDim has been defined as compiler option and return error if it hasn't.

The rest of the file contains two methods for computing the matrix multiplication $C = A.B$. The first (naive) method computes only one value of the matrix C per thread. Thus we need N^2 calls to the kernel MatrixMult_naive() in order to compute the result. The second method which is implemented in MatrixMult_local_mem() uses local memory to store the data it needs for its computations and computes a whole column of C. We need to execute N instances of this kernel. The local memory is faster and usually all of the data is cashed so we expect the second algorithm to be faster. However we note that for the matrix sizes we were interested in ($N \sim 100$) the naive matrix multiplication performed as well as the more complicated algorithm.

Bibliography

[1] G. Alexanian, A.P. Balachandran, G. Immirzi, and B. Ydri. Fuzzy $\mathbb{CP}^2$. *J.Geom.Phys.*, 42:28–53, 2002.

[2] Jan Ambjorn, K.N. Anagnostopoulos, Wolfgang Bietenholz, T. Hotta, and J. Nishimura. Simulating simplified versions of the IKKT matrix model. *Nucl.Phys.Proc.Suppl.*, 94:685–688, 2001.

[3] D.J. Amit. *Field Theory, the Renormalization Group, and Critical Phenomena*. World Scientific, Singapore, 1978.

[4] K.N. Anagnostopoulos, J. Nishimura, and P. Olesen. Noncommutative string world sheets from matrix models. *JHEP*, 0104:024, 2001.

[5] Takehiro Azuma, Subrata Bal, Keiichi Nagao, and Jun Nishimura. Nonperturbative studies of fuzzy spheres in a matrix model with the Chern-Simons term. *JHEP*, 0405:005, 2004.

[6] Takehiro Azuma, Subrata Bal, and Jun Nishimura. Dynamical generation of gauge groups in the massive Yang-Mills-Chern-Simons matrix model. *Phys.Rev.*, D72:066005, 2005.

[7] Takehiro Azuma, Satoshi Iso, Hikaru Kawai, and Yuhi Ohwashi. Supermatrix models. *Nucl.Phys.*, B610:251–279, 2001.

[8] Takehiro Azuma and Hikaru Kawai. Matrix model with manifest general coordinate invariance. *Phys.Lett.*, B538:393–405, 2002.

[9] Matthias Bach, Volker Lindenstruth, Owe Philipsen, and Christopher Pinke. Lattice QCD based on OpenCL. *Comput.Phys.Commun.*, 184:2042–2052, 2013.

[10] A.P. Balachandran, Brian P. Dolan, Joo-Han Lee, X. Martin, and Denjoe O'Connor. Fuzzy complex projective spaces and their star products. *J.Geom.Phys.*, 43:184–204, 2002.

[11] A.P. Balachandran, T.R. Govindarajan, and B. Ydri. Fermion doubling problem and noncommutative geometry. *hep-th/0006216*, 2000.

[12] A.P. Balachandran, T.R. Govindarajan, and B. Ydri. The Fermion doubling problem and noncommutative geometry. *Mod.Phys.Lett.*, A15:1279, 2000.

[13] Carl M. Bender and Philip D. Mannheim. No-ghost theorem for the fourth-order derivative Pais-Uhlenbeck oscillator model. *Phys.Rev.Lett.*, 100:110402, 2008.

[14] David E. Berenstein, Masanori Hanada, and Sean A. Hartnoll. Multi-matrix models and emergent geometry. *JHEP*, 0902:010, 2009.

[15] Edmond L. Berger. Developments in the Phenomenology of Two to Three Particle Reactions. *Conf.Proc.*, C7507141:193, 1975.

[16] Pavel Bleher and Alexander Its. Double scaling limit in the random matrix model: The Riemann-Hilbert approach. *math-ph/0201003*, 2002.

[17] A.J. Bray and M.A. Moore. Critical temperature shifts for finite slabs in the ϵ-expansion. *J. Phys*, A11:715, 1978.

[18] D. M. Brink and G. R. Satchler. *Angular Momentum.* Clarendon press, Oxford, 1968.

[19] Andrea Cappelli and Ivan D. Rodriguez. Matrix Effective Theories of the Fractional Quantum Hall effect. *J.Phys.*, A42:304006, 2009.

[20] Ursula Carow-Watamura and Satoshi Watamura. Chirality and Dirac operator on noncommutative sphere. *Commun.Math.Phys.*, 183:365–382, 1997.

[21] Murty S.S. Challa, D.P. Landau, and K. Binder. Finite size effects at temperature driven first order transitions. *Phys.Rev.*, B34:1841–1852, 1986.

[22] Alain Connes. *Noncommutative geometry.* Academic Press, California, 1994.

[23] Alain Connes. A Short survey of noncommutative geometry. *J.Math.Phys.*,

41:3832–3866, 2000.

[24] Rodrigo Delgadillo-Blando and Denjoe O'Connor. Matrix geometries and Matrix Models. *JHEP*, 1211:057, 2012.

[25] Rodrigo Delgadillo-Blando, Denjoe O'Connor, and Badis Ydri. Geometry in Transition: A Model of Emergent Geometry. *Phys.Rev.Lett.*, 100:201601, 2008.

[26] Rodrigo Delgadillo-Blando, Denjoe O'Connor, and Badis Ydri. Matrix Models, Gauge Theory and Emergent Geometry. *JHEP*, 0905:049, 2009.

[27] P. Di Francesco, Paul H. Ginsparg, and Jean Zinn-Justin. 2-D Gravity and random matrices. *Phys.Rept.*, 254:1–133, 1995.

[28] S. Digal, T.R. Govindarajan, Kumar S. Gupta, and X. Martin. Phase structure of fuzzy black holes. *JHEP*, 1201:027, 2012.

[29] Brian P. Dolan, Idrish Huet, Sean Murray, and Denjoe O'Connor. Noncommutative vector bundles over fuzzy $\mathbb{CP}^N$ and their covariant derivatives. *JHEP*, 0707:007, 2007.

[30] Brian P. Dolan and Denjoe O'Connor. A Fuzzy three sphere and fuzzy tori. *JHEP*, 0310:060, 2003.

[31] Brian P. Dolan, Denjoe O'Connor, and P. Presnajder. Matrix ϕ^4 models on the fuzzy sphere and their continuum limits. *JHEP*, 0203:013, 2002.

[32] Brian P. Dolan, Denjoe O'Connor, and Peter Presnajder. Matrix models on the fuzzy sphere. *hep-th/0204219*, 2002.

[33] C. Domb and J.L. Lebowitz. *Phase transitions and critical phenomena. Vol. 8.* Academic press, California, 1987.

[34] Michael R. Douglas and Nikita A. Nekrasov. Noncommutative field theory. *Rev.Mod.Phys.*, 73:977–1029, 2001.

[35] S. Duane, A.D. Kennedy, B.J. Pendleton, and D. Roweth. Hybrid Monte Carlo. *Phys.Lett.*, B195:216–222, 1987.

[36] Fröhlich, Jörg, Krzysztof and Gawedzki. Conformal field theory and geome-

try of strings. *hep-th/9310187*, 1993.

[37] J. Fuchs and C. Schweigert. *Symmetries, Lie algebras and representations: A graduate course for physicists*. University Press, Cambridge, 1997.

[38] William Fulton and Joe Harris. *Representation Theory: A First Course 1991*. Springer-Verlag, New-York, 1991.

[39] Fernando Garcia Flores, Xavier Martin, and Denjoe O'Connor. Simulation of a scalar field on a fuzzy sphere. *Int.J.Mod.Phys.*, A24:3917–3944, 2009.

[40] Howard Georgi. *Lie algebras in particle physics*. Benjamin Cummings, 1999.

[41] N. Goldenfeld. *Lectures on phase transitions and the renormalization group*. Addison-Wesley, 1992.

[42] T.R. Govindarajan, Pramod Padmanabhan, and T. Shreecharan. Beyond fuzzy spheres. *J.Phys.*, A43:205203, 2010.

[43] H. Grosse, C. Klimcik, and P. Presnajder. N=2 superalgebra and noncommutative geometry. *hep-th/9603071*, 1996.

[44] H. Grosse and A. Strohmaier. Towards a nonperturbative covariant regularization in 4-D quantum field theory. *Lett.Math.Phys.*, 48:163–179, 1999.

[45] G. H. Hardy and S. Ramanujan. Asymptotic formulae in combinatory analysis. *Proc. Lond. Math. Soc.*, 17:75–115, 1918.

[46] Jens Hoppe and Shing-Tung Yau. Some properties of matrix harmonics on S2. *Commun. Math. Phys.*, 195:067, 1998.

[47] Wung-Hong Huang. Thermodynamics of ideal gas on the kaluza-klein spacetime with extra fuzzy geometry. *JHEP*, 0908:102, 2009.

[48] Jesus A. Izaguirre and Scott S. Hampton. Shadow Hybrid Monte Carlo: An Efficient Propagator in phase space of macromolecules. *Journal of Computational Physics*, 200:581–604, 2004.

[49] R.A. Janik and J. Wosiek. Towards the matrix model of M theory on a lattice. *Acta Phys.Polon.*, B32:2143–2154, 2001.

[50] A. Kirillov. *Representation theory and noncommutative harmonic analysis*.

VINITI, Moscow, 1990.

[51] J.M. Kosterlitz and D.J. Thouless. Ordering, metastability and phase transitions in two-dimensional systems. *J.Phys.*, C6:1181–1203, 1973.

[52] Giovanni Landi. An Introduction to noncommutative spaces and their geometry. *hep-th/9701078*, 1997.

[53] Will Loinaz and R.S. Willey. Monte Carlo simulation calculation of critical coupling constant for continuum ϕ^4 in two-dimensions. *Phys.Rev.*, D58:076003, 1998.

[54] J. Madore. The Fuzzy sphere. *Class.Quant.Grav.*, 9:69–88, 1992.

[55] A. Marshakov. Integrable structures in matrix models and physics of 2-d gravity. *Int.J.Mod.Phys.*, A8:3831–3882, 1993.

[56] Xavier Martin. A Matrix phase for the ϕ^4 scalar field on the fuzzy sphere. *JHEP*, 0404:077, 2004.

[57] Julieta Medina, Wolfgang Bietenholz, and Denjoe O'Connor. Probing the fuzzy sphere regularisation in simulations of the 3d $\lambda\phi^4$ model. *JHEP*, 0804:041, 2008.

[58] Julieta Medina, Idrish Huet, Denjoe O'Connor, and Brian P. Dolan. Scalar and Spinor Field Actions on Fuzzy S^4: fuzzy $\mathbb{CP}^3$ as a S^2_F bundle over S^4_F. *JHEP*, 1208:070, 2012.

[59] Julieta Medina and Denjoe O'Connor. Scalar field theory on fuzzy S^4. *JHEP*, 0311:051, 2003.

[60] Wen Mei and W Hwu. *GPU computing gems— Emerald Edition*. University of Illinois, 2011.

[61] Istvan Montvay and Gernot Munster. *Quantum fields on a lattice*. Cambridge University Press, 1994.

[62] Bogdan Morariu and Alexios P. Polychronakos. Fractional quantum Hall effect on the two-sphere: A Matrix model proposal. *Phys.Rev.*, D72:125002, 2005.

[63] A. Munshi, T. Mattson, B. Gaster, and D. Ginsburg. *OpenCL programming guide*. Stanford University, California, 2012.

[64] Denjoe O'Connor, Brian P. Dolan, and Martin Vachovski. Critical Behaviour of the Fuzzy Sphere. *JHEP*, 2013:85, 2013.

[65] Denjoe O'Connor and Veselin G. Filev. Near commuting multi-matrix models. *JHEP*, 04:144, 2013.

[66] Denjoe O'Connor and Badis Ydri. Monte Carlo Simulation of a NC Gauge Theory on The Fuzzy Sphere. *JHEP*, 0611:016, 2006.

[67] P. Olesen. Towards matrix models of IIB superstrings. *hep-th/9708070*, 1997.

[68] Andrea Pelissetto and Ettore Vicari. Critical phenomena and renormalization group theory. *Phys.Rept.*, 368:549–727, 2002.

[69] A.M. Perelomov. Coherent states for arbitrary lie groups. *Commun.Math.Phys.*, 26:222–236, 1972.

[70] A.M. Perelomov. *Generalized coherent states and their applications*. Springer-Verlag, Berlin, 1986.

[71] Alexios P. Polychronakos. Quantum Hall states as matrix Chern-Simons theory. *JHEP*, 0104:011, 2001.

[72] William H. Press, Saul A. Teukolsky, William T Vetterling, and Brian P. Flannery. *Numerical Recipes in C*. Cambridge University Press, 1988.

[73] Stefan Schaefer. *Simulations with the Hybrid Monte Carlo algorithm: Implementation and data analysis*, 2009.

[74] Stefan Schaefer. Status and challenges of simulations with dynamical fermions. *PoS*, LATTICE2012:001, 2012.

[75] Hartland S. Snyder. Quantized space-time. *Phys.Rev.*, 71:38–41, 1947.

[76] H. Eugene Stanley. Scaling, universality, and renormalization: Three pillars of modern critical phenomena. *Rev.Mod.Phys.*, 71:S358–S366, 1999.

[77] Harold Steinacker. Quantized gauge theory on the fuzzy sphere as random matrix model. *Nucl.Phys.*, B679:66–98, 2004.

[78] Raul Toral and Amitabha Chakrabarti. Numerical determination of the phase diagram for the $c\phi^4$ model in two dimensions. *Phys.Rev.*, B42:2445–2454, 1990.

[79] Raul Toral and A.L. Ferreira. Generalized hybrid Monte Carlo. *hep-lat/9409014*, 1994.

[80] D.A. Varshalovich, A.N. Moskalev, and V.K. Khersonsky. *Quantum theory of angular momentum: irreducible tensors, spherical harmonics, vector coupling coefficients, 3nj symbols*. Nauka, 1988.

[81] B. Widom. The critical point and scaling theory. *Physica*, 73:107–118, 1974.

[82] E. Wigner. *Group theory and its applications to the quantum mechanics of atomic spectra*. Academic Press, New York, 1988.

[83] K. G. Wilson and J. Kogut. The renormalization group and the ϵ expansion. *Phys. Reports. Math. Soc.*, 75, 1974.

[84] Badis Ydri. Noncommutative geometry as a regulator. *Phys.Rev.*, D63:025004, 2001.